

การดูดซับของแก๊สขนาดเล็กบนไทเทเนียมไดออกไซด์และโลหะที่มีไทเทเนียมไดออกไซด์
เป็นตัวรองรับ

นางสาวไรรณา หวันพะหยอ

วิทยานิพนธ์นี้เป็นส่วนหนึ่งของการศึกษาตามหลักสูตรปริญญาวิทยาศาสตรดุษฎีบัณฑิต
สาขาวิชาเคมี ภาควิชาเคมี
คณะวิทยาศาสตร์ จุฬาลงกรณ์มหาวิทยาลัย
ปีการศึกษา 2553
ลิขสิทธิ์ของจุฬาลงกรณ์มหาวิทยาลัย



5 0 7 3 8 6 5 0 2 3

ADSORPTION OF SMALL GASES ON TiO₂ AND TiO₂-SUPPORTED METAL

Miss Raina Wanbayor

A Dissertation Submitted in Partial Fulfillment of the Requirements
for the Degree of Doctor of Philosophy Program in Chemistry
Department of Chemistry
Faculty of Science
Chulalongkorn University
Academic Year 2010
Copyright of Chulalongkorn University

Thesis Title ADSORPTION OF SMALL GASES ON TiO₂ AND TiO₂-
SUPPORTED METAL
By Miss Raina Wanbayor
Field of Study Chemistry
Thesis Advisor Associate Professor Vithaya Ruangpornvisuti, Dr. rer. nat.

Accepted by the Faculty of Science, Chulalongkorn University in Partial
Fulfillment of the Requirements for the Doctoral Degree

..... Dean of the Faculty of Science
(Professor Supot Hannongbua, Dr. rer. nat.)

THESIS COMMITTEE

..... Chairman
(Assistant Professor Warinthorn Chavasiri, Ph. D.)

..... Thesis Advisor
(Associate Professor Vithaya Ruangpornvisuti, Dr. rer. nat.)

..... Examiner
(Associate Professor Thammarat Aree, Ph. D.)

..... Examiner
(Associate Professor Nongnuj Muangsin, Ph. D.)

..... External Examiner
(Professor Kritsana Sagarik, Dr. rer. nat.)

ไรนา หวันบะหยอ : การดูดซับของแก๊สขนาดเล็กบนไทเทเนียมไดออกไซด์และโลหะที่มีไทเทเนียมไดออกไซด์เป็นตัวรองรับ. (ADSORPTION OF SMALL GASES ON TiO_2 AND TiO_2 -SUPPORTED METAL) อ. ที่ปรึกษาวิทยานิพนธ์หลัก: รศ.ดร. วิทยา เรืองพรวิสุทธิ์, 112 หน้า.

ทฤษฎีเค้นชิตีฟังก์ชัน (DFT) ได้ใช้เพื่อศึกษาการดูดซับของแก๊สอะตอมคู่ แก๊สอะตอมสาม และแก๊สหลายอะตอม บนผิวอะนาเทส (001) และ (101), รูไทล์ (001) และ (110) ของไทเทเนียมไดออกไซด์ (TiO_2) การคำนวณใช้โมเดลแบบคลัสเตอร์และระยะขอบเขตเงื่อนไขเพื่อศึกษารายละเอียดของพลังงานและโครงสร้างการดูดซับ พบว่าโครงสร้างที่โดดเด่นที่สุดสอดคล้องกับการดูดซับของแก๊สโดยตรงไปยังตำแหน่ง Ti_{5c} ของผิวเหล่านี้ ผลของอันตรกิริยาระหว่างตัวถูกดูดซับและตัวดูดซับสำหรับผิวอะนาเทสเกิดการดูดซับที่อ่อนกว่าผิวรูไทล์ ศึกษาการเปลี่ยน CO เป็น CO_2 จากการช่วยเหลือของโซล การดูดซับและการเปลี่ยน N_2O เป็น N_2 บนผิวอะนาเทส (101) โดยใช้หลักการคำนวณเริ่มต้น การแสดงตนของประจุบวกบนผิวอะนาเทส (101) เพิ่มพลังงานการดูดซับของ CO ช่วยให้เกิดการเปลี่ยนเป็น CO_2 ทำให้เกิดเป็นช่องว่างออกซิเจน พบว่า CO เป็นตัวรีดิวซ์ที่ดีสำหรับ N_2O ซึ่ง CO ถูกออกซิไดซ์ เป็น CO_2 และ N_2O ถูกรีดิวซ์เป็น N_2 ภายใต้การกระตุ้นด้วยแสง ดังนั้นผลการคำนวณแสดงการออกซิเดชันของ CO และรีดักชันของ N_2O บนผิวอะนาเทส (101) อาจเป็นกระบวนการโฟโตคะตะไลติกที่มีประสิทธิภาพ ได้ขยายการตรวจสอบเพื่อศึกษาบทบาทของโลหะแพลทินัมที่มีไทเทเนียมไดออกไซด์เป็นตัวรองรับ (Pt/TiO_2) ของผิวอะนาเทส (101) และการดูดซับกับ CO , N_2 , CO_2 และ N_2O พบว่าอันตรกิริยาที่แข็งแกร่งระหว่างอะตอมแพลทินัมและผิวอะนาเทส (101) อาจรับผิดชอบต่อการเกิดปฏิกิริยาการดูดซับที่เพิ่มขึ้นของ CO และ CO_2

ภาควิชา.....เคมี.....

ลายมือชื่อ.....

สาขาวิชา.....เคมี.....

ลายมือชื่อ อ.ที่ปรึกษาวิทยานิพนธ์.....

ปีการศึกษา.....2553.....

5073865023 : MAJOR CHEMISTRY

KEYWORDS : DFT / Adsorption / Gases / Co-adsorption / anatase TiO₂ (001) and (101) / Rutile TiO₂ (001) and (110) / Photocatalysis / Periodic DFT / TiO₂-supported Pt /

RAINA WANBAYOR: ADSORPTION OF SMALL GASES ON TiO₂ AND TiO₂-SUPPORTED METAL. ADVISOR: ASSOC. PROF. VITHAYA RUANGPORNVISUTI, Dr. rer. nat., 112 pp.

Density functional theory (DFT) calculations have been performed to study the adsorption of di-, tri-, and polyatomic gases on the anatase (001) and (101), rutile (001) and (110) surfaces of TiO₂. The calculations employing model clusters and periodic boundary conditions to detailed study the adsorption energies and adsorption geometries. It was found that the most remarkable geometry corresponds to the adsorption of gases directly onto the Ti_{5C} site of these surfaces. The interaction between adsorbate and substrate for the anatase surface resulted weaker than that for the rutile. The hole-assisted conversion of CO to CO₂, the adsorption and conversion of N₂O to N₂ on anatase TiO₂ (101) surface have been studied using first-principles calculations. The presence of the positive charge on the anatase (101) surface increases the adsorption energy of CO, allowing the it conversion of CO to CO₂ and leaving an oxygen vacancy behind. CO is found to be a good reducing agent for N₂O, in which CO is oxidized to CO₂ and N₂O is reduced to N₂ under photo-excitation. Therefore, the results indicate that the oxidation of CO and the reduction of N₂O on the anatase (101) surface could be an efficient photocatalytic process. The investigation was extended to study the role of TiO₂-supported Pt of the anatase (101) surface (Pt/TiO₂) on the adsorption of CO, N₂, CO₂ and N₂O. It was found that the strong interaction between Pt atom and anatase (101) surface could be responsible for the enhanced adsorption of CO and CO₂.

Department : Chemistry Student's Signature

Field of Study : Chemistry Advisor's Signature

Academic Year : 2010

ACKNOWLEDGMENTS

The success of this dissertation is due to my interest in research of computational chemistry. In this time, I would like to acknowledge several people who have helped me to achieve my goals for this study.

First of all, I would like to thank my advisor, Assoc. Prof. Dr. Vithaya Ruangpornvisuti, for the kindness and support. I deeply thank him for his valuable suggestion and comments to research and study in the Ph. D. program. I was able to overcome research problems and achieve the quality of my work.

I am very grateful to the Thailand Research Fund (TRF) for full financial support through the Royal Golden Jubilee (RGJ) grant scholarship and Center for Petroleum, Petrochemicals and Advanced Materials for partially support. I deeply thank to Dr. Peter Deák, my foreign co–advisor, for his helpful comments excellent explanation and valuable knowledge as well as planning all the accommodations during my visit to Bremen Center for Computational Material Science (BCCMS), University Bremen, Germany. I also would like to thank Prof. Dr. Thomas Frauenheim and his wife for their hospitality. Special thank would be encouraged to the people in the BCCMS groups. I have gotten many great opportunities to improve myself, along with the support from my beloved friend who take care of me and help me when I was in Germany.

I would like to give special thanks to Assist. Prof. Dr. Warinthorn Chavasiri, Assoc. Prof. Dr. Thammarat Aree, Assoc. Prof. Dr. Nongnuj Muangsin and Prof. Dr. Kritsana Sagarik for their valuable suggestion and comments in my examination.

In addition, I would like to thank the lovely people in Supramolecular Chemistry Research Unit (SCRU) at Chulalongkorn University are also being encouraged and appreciated.

Finally, I would like to express my gratitude to my beloved family and my friends for their endless love and for always supporting and believing in me throughout my study.

CONTENTS

	Page
ABSTRACT IN THAI	iv
ABSTRACT IN ENGLISH	v
ACKNOWLEDEMENTS	vi
CONTENTS	vii
LIST OF TABLES	xi
LIST OF FIGURES	xii
LIST OF ABBREVIATIONS	xvi
CHAPTER I – INTRODUCTION	1
1.1 Research background and research rationale	2
1.1.1 Crystal structures.....	2
1.1.2 Structural surfaces of anatase and rutile.....	4
1.1.3 Photocatalytic process of TiO ₂	5
1.1.4 Research rationale.....	6
1.2 Objectives.....	8
1.3 Scope of this dissertation.....	8
1.4 Expected results.....	9
CHAPTER II – ADSORPTION OF DI-, TRI- AND POLYATOMIC GASES ON THE ANATASE TiO₂ (001) AND (101) SURFACES AND THEIR ADSORPTION ABILITIES	11
2.1 Abstract.....	12
2.2 Introduction.....	12
2.3 Computational methods.....	13
2. 4 Results and discussion	15
2.4.1 Adsorption of diatomic gases on the anatase TiO ₂	17
2.4.2 Adsorption of triatomic gases on the anatase TiO ₂	20
2.4.3 Adsorption of polyatomic gases on the anatase TiO ₂	21
2.5 Conclusions.....	23

	Page
CHAPTER III – ADSORPTION OF CO, H₂, N₂O, NH₃ AND CH₄ ON THE ANATASE TiO₂ (001) AND (101) SURFACES AND THEIR COMPITITIVE ADSORPTION PREDICTED BY PERIODIC DFT CALCULATIONS.....	24
3.1 Abstract.....	25
3.2 Introduction.....	25
3.3 Computational methods.....	27
3.4 Results and discussion	29
3.4.1 Adsorptions of CO, H ₂ , N ₂ O, NH ₃ and CH ₄ gases on the anatase TiO ₂	29
3.4.2 Co-adsorption on the anatase TiO ₂	36
2.5 Conclusions.....	39
CHAPTER IV – PERIODIC DENSITY-FUNCTIONAL THEORY STUDY OF CO, H₂, N₂O, H₂O, NH₃ AND CH₄ ADSORBED ON THE RUTILE TiO₂ (001) AND (110) SURFACES.....	40
4.1 Abstract.....	41
4.2 Introduction.....	41
4.3 Computational methods.....	42
4.4 Results and discussion	44
4.5 Conclusions.....	49
CHAPTER V – FIRST-PRINCIPLE THEORETICAL STUDY OF HOLE-ASSISTED CONVERSION OF CO TO CO₂ ON THE ANATASE TiO₂ (101) SURFACE.....	50
5.1 Abstract.....	51
5.2 Introduction.....	51
5.3 Computational methods.....	53
5.4 Results and discussion	55
5.4.1 Adsorption of CO on the anatase TiO ₂ (101) surface.....	56
5.4.2 Oxidation of CO on the anatase TiO ₂ (101) surface.....	57
5.4.3 Dissociation of CO ₂ from the anatase TiO ₂ (101) surface.....	59

	Page
5.5 Conclusions.....	62
CHAPTER VI – ELECTRON–ASSISTED ADSORPTION OF N₂O ON ANATASE TiO₂ (101) SURFACE: A THEORETICAL STUDY.....	63
6.1 Abstract.....	64
6.2 Introduction.....	64
6.3 Computational methods.....	66
6.4 Results and discussion	67
6.4.1 Adsorption of N ₂ O molecule on neutral surface of anatase TiO ₂ (101)	67
6.4.2 Adsorption of N ₂ O molecule on negative surface of anatase TiO ₂ (101).....	70
6.4.3 Conversion of N ₂ O to N ₂ by CO on anatase TiO ₂ (101) surface.....	72
6.5 Conclusions.....	76
CHAPTER VII – FIRST–PRINCIPLES THEORETICAL STUDY OF Pt ATOM SUPPORTED ON ANATASE TiO₂ (101) SURFACE AND THEIR INTERACTION WITH CO, N₂, CO₂ AND N₂O.....	77
7.1 Abstract.....	78
7.2 Introduction.....	78
7.3 Computational methods.....	79
7. 4 Results and discussion	81
7.4.1 Adsorption of CO.....	82
7.4.2 Adsorption of N ₂	84
7.4.3 Adsorption of CO ₂	85
7.4.4 Adsorption of N ₂ O.....	86
7.5 Conclusions.....	89
CHAPTER VIII – CONCLUSIONS.....	90
8.1 Conclusions.....	90
8.2 Research limitations.....	92
8.3 Suggestions for future work.....	92

	Page
REFERENCES	93
APPENDIX	110
VITAE	112

LIST OF TABLES

Table	Page
1.1 Structural parameters of anatase and rutile TiO ₂	4
2.1 The adsorption energies of the di-, tri- and polyatomic gases adsorbed on the anatase TiO ₂ (001) and (101) surfaces.....	16
3.1 Observed and computed lattice parameters of the anatase TiO ₂ , with space group <i>I4₁/amd</i>	30
3.2 Selected parameters of optimized structures for CO, H ₂ , N ₂ O, NH ₃ and CH ₄ gases adsorbed on the anatase TiO ₂ (001) and (101) surfaces, distances and angles given in Å and degrees, respectively...	32
3.3 Adsorption energies (in kcal/mol) for the CO, H ₂ , N ₂ O, NH ₃ and CH ₄ adsorbed on the anatase TiO ₂ (001) and (101) surfaces.....	33
3.4 Selected atomic charges (in e) of optimized structures for CO, H ₂ , N ₂ O, NH ₃ and CH ₄ gases adsorbed on the anatase TiO ₂ (001) and (101) surfaces	35
4.1 Computed and experimental lattice parameters of the rutile TiO ₂ , with space group <i>P4₂/mnm</i>	43
4.2 Selected parameters of optimized structures for CO, H ₂ , N ₂ O, H ₂ O, NH ₃ and CH ₄ gases adsorbed on the rutile TiO ₂ (001) and (110) surfaces, distances and angles given in Å and degrees, respectively...	46
4.3 Adsorption energies for the CO, H ₂ , N ₂ O, H ₂ O, NH ₃ and CH ₄ adsorbed on the rutile TiO ₂ (001) and (110) surfaces.....	48
5.1 Adsorption energies and geometry parameters for CO adsorption at a Ti _{5C} site on the anatase TiO ₂ (101) surface. For comparison, results of periodic B3LYP calculations with localized basis sets on the same (1×2) (a) [25] and on a (1×1) slab (b) [29] are given in parentheses....	57
6.1 Adsorption energies and geometrical parameters for N ₂ O adsorption at a Ti _{5C} site on the anatase TiO ₂ (101) surfaces.....	69
7.1 Adsorption energies and geometrical parameters for CO, N ₂ , CO ₂ and N ₂ O adsorption on the anatase TiO ₂ (101) surface with and without Pt atom	83

LIST OF FIGURES

Figure		Page
1.1	Structures of (a) anatase and (b) rutile TiO ₂	3
1.2	Structures of (a) anatase (001), (b) anatase (101), (c) rutile (001) and (d) rutile (110) surfaces.....	5
2.1	The anatase TiO ₂ (a) (001) and (b) (101) surfaces modeled as Ti ₉ O ₃₃ H ₃₀ and Ti ₉ O ₃₃ H ₄₂ clusters, respectively	15
2.2	The adsorption structures of diatomic gases (a) O ₂ (triplet state), (b) N ₂ , (c) H ₂ , (d, e) CO and (f) NO, adsorbed on the anatase TiO ₂ (001) (left) and (101) (right) surfaces. Hydrogen bond distances are in Å...	19
2.3	The adsorption structures of triatomic gases (a) H ₂ O, (b) H ₂ S, (c) N ₂ O, (d) CO ₂ , (e) NO ₂ and (f) SO ₂ on the anatase TiO ₂ (001) (left) and (101) (right) surfaces. Hydrogen bond distances are in Å.....	21
2.4	The adsorption structures of polyatomic gases (a) NH ₃ , (b) C ₂ H ₂ , (c) C ₂ H ₄ and (d) CH ₄ , adsorbed on the anatase TiO ₂ (001) (left) and (101) (right) surfaces. Hydrogen bond distances are in Å.....	22
2.5	Plot for comparisons of the adsorption energies of small hydrocarbon molecules on the anatase TiO ₂ (001) and (101) surfaces.	23
3.1	The TiO ₂ (001) (left) and (101) (right) surface slabs of the full optimized crystal.....	29
3.2	Adsorption structures of (a) CO, (b) H ₂ , (c) N ₂ O, (d) NH ₃ and (e) CH ₄ , adsorbed on anatase TiO ₂ (001) surface. Bond distances are in Å.....	32
3.3	Adsorption structures of (a) CO, (b) N ₂ O, (c) NH ₃ and (d) CH ₄ , adsorbed on the anatase TiO ₂ (101) surface. Bond distances are in Å.	33
3.4	Adsorption structures of (a) CO, (b) N ₂ O, (c) NH ₃ and (d) CH ₄ , adsorbed on the anatase TiO ₂ (101) surface. Bond distances are in Å..	36
3.5	Adsorption energies of CO, N ₂ O, NH ₃ and CH ₄ on the anatase TiO ₂ (001) and (101) surfaces, based on the strategy I.....	37
3.6	Adsorption configurations of CO and N ₂ O co-adsorbed on the anatase-TiO ₂ (001) surface as (a) [CO···O=N=N], configuration I and (b) [N=N=O/CO], configuration II. Bond distances are in Å.....	38

Figure	Page
3.7 Co-adsorption configurations of (a) CO and N ₂ O on the anatase TiO ₂ (001) surface and (b) its proposed transition-state structure...	39
4.1 The rutile TiO ₂ (a) (001) and (b) (110) surface slabs of the full optimized crystal.....	43
4.2 Adsorption structures of (a) CO, (b) H ₂ , (c) N ₂ O, (d) H ₂ O (e) NH ₃ and (f) CH ₄ , adsorbed on the rutile TiO ₂ (001) surface. Bond distances are in Å.....	45
4.3 Adsorption structures of (a) CO, (b) H ₂ , (c) N ₂ O, (d) H ₂ O (e) NH ₃ and (f) CH ₄ , adsorbed on the rutile TiO ₂ (110) surface. Bond distances are in Å.....	47
4.4 Adsorption energies of CO, H ₂ , N ₂ O, H ₂ O, NH ₃ and CH ₄ on the rutile TiO ₂ (001) and (110) surfaces.....	48
5.1 The optimized structure of the (1 × 2) slab model for the anatase TiO ₂ (101) surface. Five- and sixfold coordinated titanium, and two- and threefold coordinated oxygen surface atoms are labeled as Ti _{5C} , Ti _{6C} , O _{2C} , and O _{3C} , respectively.....	54
5.2 Scheme of photo-oxidation/reduction processes (POP/PRP) upon UV excitation of a TiO ₂ crystal in the presence of acceptor (A) and donor (D) molecules in the vicinity of the surface.....	56
5.3 Adsorption of CO on the anatase TiO ₂ (101) surface with the C (a) and the O atom (b) towards the surface. The geometry data for the neutral and the positive case are given in Table 5.1.....	57
5.4 The [CO ₂ /TiO ₂ + V _O] ⁺ configuration, arising upon interaction of the adsorbed CO molecule with a nearby O _{2C} site. Bond distances are in Å	58
5.5 Total energy profile for CO adsorption at the O _{2C} site of the positive anatase (101) surface. The insets show the starting and final configurations and the barrier state. At the starting position the carbon end of CO is 2.5 Å above the O _{2C} site, while the last configuration is the one shown in Figure 5.4. The configuration coordinate expresses approximately the motion of the C atom. (In fact, it is the length of a supervector between two consecutive	

Figure	Page
which is built of the relative positions of the C and O atoms of CO, the surface atoms to which C is bonded along the path, and the first neighbors of the latter). The curve is a cubic spline fitted to the barrier region to guide the eye. The zero of the energy scale is taken to be the energy of CO + [TiO ₂] ⁺	59
5.6 Total energy profile along the [CO/TiO ₂] ⁺ to [CO ₂ /TiO ₂ +VO] ⁺ diffusion pathway. The configuration coordinate and the energy scale is defined as in Figure 5.5. The insets show the starting and final configurations and the barrier state.....	60
5.7 Total energy diagram for the oxidation of CO on the positive anatase TiO ₂ (101) surface. All energies are given in eV, with respect to the energy of free CO above the positive surface. The zero of the energy scale is taken to be the energy of CO + [TiO ₂] ⁺ ...	61
6.1 Adsorption configurations of N ₂ O on the neutral surface of anatase TiO ₂ (101) as the N ₂ O pointing (a) its nitrogen atom, (b) its oxygen atom toward the titanium atom Ti _{5C} of the surface and (c) N ₂ O bridged structure. Bond distances are in angstrom.....	68
6.2 Adsorption configurations of N ₂ O on the negative surface of anatase TiO ₂ (101) as the N ₂ O pointing (a) it nitrogen atom, (b) N ₂ O dissociated structure, (c) bridge bending structure and (d) symmetric bridge structure. Bond distances are in angstrom.....	71
6.3 Scheme of photo-oxidation and reduction processes due to UV excitation of a TiO ₂ crystal in the presence of N ₂ O acceptor and CO donor molecules in the vicinity of the surface.....	73
6.4 Structure for physisorptions of CO ₂ and N ₂ products adsorbed over the same O _{2C} atom. Top and side views are shown at above and below pictures, respectively. Bond distances are in Å.....	74
6.5 Potential energy profile (in eV) for conversion of CO + N ₂ O to CO ₂ + N ₂ on the anatase TiO ₂ (101) surface. Determination of the barrier for its conversion has been not succeeded	75
6.6 The proposed mechanism for conversion of CO + N ₂ O to CO ₂ + N ₂ on the spin-polarized anatase TiO ₂ (101) surface as (a) the barrier	

Figure	Page
state 1 (TS1), (b) the reduction process of N ₂ O to N ₂ on the CO ₂ /[TiO ₂ +VO] ⁺ via the proposed barrier state 2 (TS2) and (c) the desorption step.	76
7.1 The optimized structure of the (1×2) slab model for the anatase TiO ₂ (101) surface. Five- and sixfold coordinated titanium, and two- and threefold coordinated oxygen surface atoms are labeled as Ti _{5C} , Ti _{6C} , O _{2C} , and O _{3C} , respectively [27].....	81
7.2 The optimized configuration of TiO ₂ -supported Pt of anatase (101) surface. Bond distances are in Å.....	82
7.3 Optimized geometries of CO adsorbed on the surface of (a) Pt/TiO ₂ (101) and (b) clean TiO ₂ (101) with C-end, (c) Pt/TiO ₂ (101) and (b) clean TiO ₂ (101) with O-end. Bond distances are in Å.....	84
7.4 The optimized geometries of the adsorption of N ₂ molecule on the surface of (a) Pt/TiO ₂ (101) and (b) clean TiO ₂ (101). Bond distances are in Å.....	85
7.5 The optimized geometries of the adsorption of CO ₂ molecule on the surface of (a) Pt/TiO ₂ (101) and (b) clean TiO ₂ (101). Bond distances are in Å.....	86
7.6 The optimized geometries of the adsorption of N ₂ O molecule on the surface of (a) Pt/TiO ₂ (101) and (b) clean TiO ₂ (101), with N-end, (c) Pt/TiO ₂ (101) and (b) clean TiO ₂ (101), with O-end and (e) Pt/TiO ₂ (101) and (d) clean TiO ₂ (101), with bridge bending configuration. Bond distances are in Å.....	88

LIST OF ABBREVIATIONS AND SYMBOLS

3D	Three Dimension
A	Acceptor
AIMD	<i>Ab initio</i> molecular dynamics
Å	Angstrom
B3LYP	Beck 3 Lee–Yang–Parr
BSSE	Basis set superposition error
CPMD	Car–Parrinello molecular dynamics
D	Donor
d_{ap}	Apical Ti–O bond length
DFT	Density functional theory
DRIFTS	Diffuse reflectance infrared fourier transform spectroscopy
e^-	Electron
E	Energy
eV	Electron volt
Exp	Experiment
Eq.	Equation
GGA	Generalized gradient approximation
K	Kelvin
LEED	Low–energy electron diffraction
LH	Langmuir–Hinshewood
MD	Molecular dynamics
NEB	Nudged elastic band method
h^+	Hole
O _{2C}	Twofold–coordinated O atom
O _{3C}	Threefold–coordinated O atom
PAW	Projector augmented–wave
PBC	Periodic boundary condition
PBE	Perdew–Burke–Emzerhof
POP	Photo–oxidation process
PRP	Photo–reduction process
SCR	Selective catalytic reduction

TiO ₂	Titanium dioxide
Ti ₅ C	Fivefold-coordinated Ti atom
Ti ₆ C	Sixfold-coordinated Ti atom
TPD	Temperature-programmed desorption
UV	Ultraviolet
V _O	Oxygen vacancy
VASP	Vienna <i>ab initio</i> simulation package
XPS	X-ray photoelectron spectroscopy

CHAPTER I

INTRODCTION

Titanium dioxide (TiO_2) is one of the most investigated metal oxide materials that are widely used in many applications such as heterogeneous catalysis [1], photocatalysis [2–6], white pigment [3], gas sensors [7–11], dye-sensitized solar cells [12–15] and catalyst support [16]. It is the most appropriate material for industrial use, not only for today's industrial applications but also for future applications as well. TiO_2 is inexpensive, biologically and chemically stable and considered to be nontoxic and safe to both humans and the environment. TiO_2 is white color, therefore, no absorption in the visible region. In fact the absorption in the visible range is able to improve by doping such as nitrogen [17]. However, it is active under UV irradiation ($\lambda < 400$ nm) as a photocatalysis. There are three types of TiO_2 , anatase, rutile and brookite. All of these crystalline forms of TiO_2 occur in nature as mineral. But brookite is extremely difficult to synthesize in the laboratory, only rutile and anatase has been successfully synthesized in pure form at low temperature [18]. Both anatase and rutile forms are commonly used both experimental and theoretical studies; their structures and surfaces have been extensively investigated [19–21]. They are frequently used as a gas sensor and as a photocatalyst for various organic reactions. In order to elucidate of the molecular gases adsorbed on various surface planes of different TiO_2 forms as well as redox reactions of their molecules has been extremely studied over many years. Especially, the adsorption of transition metal atoms on TiO_2 have received a great deal of interest on TiO_2 -supported catalysts due to their good catalytic performance in many important processes [22–24]. Therefore, anatase and rutile surfaces become the rational goal of this work.

Understanding of adsorption of molecular gases on anatase and rutile TiO_2 surfaces were performed using the first-principles calculations based on the density functional theory. The cluster models and periodic boundary conditions (PBCs) of both surfaces were used as a case study. The calculations were used to develop the new catalyst for the selective catalytic reaction in the present of various small pollutant gases, the adsorption abilities of these small molecules can be utilized to discover new catalysts.

The thesis contents, based on the publications, submission and preparations, are as follows:

Chapter II: the adsorption of di-, tri- and polyatomic gases on anatase TiO_2 (101) and (001) surface based on the cluster models approach.

Chapter III: the adsorption of CO , H_2 , N_2O , NH_3 and CH_4 on the anatase TiO_2 (101) and (001) surfaces and their competitive co-adsorption based on periodic approach.

Chapter IV: the adsorption of CO , H_2 , N_2O , NH_3 and CH_4 on the rutile TiO_2 (110) and (001) surfaces based on periodic approach.

Chapter V: the adsorption of CO and the hole-assisted conversion of CO to CO_2 on the anatase TiO_2 (101) surface as a photocatalytic oxidation process based on periodic approach.

Chapter VI: the adsorption of N_2O and conversion of N_2O to N_2 by CO on the anatase TiO_2 (101) surface based on periodic approach.

Chapter VII: the role of the Pt atom supported on anatase TiO_2 (101) surface (Pt/TiO_2) and adsorption with CO , N_2 , CO_2 and N_2O based on periodic approach.

The representation of the six chapters (II–VII), in which detailed calculations, results and discussion are given in terms of research articles [25–27] in chapters II, III and V, submitted manuscript [28] in chapter IV, and preparation for publication in chapters VI, and VII. All articles are part of this dissertation in partial fulfillment of the requirements for the degree of Doctor of Philosophy in Chemistry at Chulalongkorn University.

1.1 RESEARCH BACKGROUND AND RESEARCH RATIONALE

1.1.1 Crystal structures

Both anatase and rutile have tetragonal crystal structures, in which can be described in terms of chain of TiO_6 octahedra. The two crystal structures differ by the distortion of each octahedron and by the assembly pattern of the octahedron chains. Usually, the octahedron of anatase is somewhat more distorted than that of rutile. Each Ti atom (formally in a +4 oxidation state) is surrounded by an octahedron of six O atoms (formally in a -2 oxidation state), and the O atoms are linked to three Ti

atoms [21]. Figure 1.1 shows the crystal structures of anatase (left) and rutile (right). In the anatase structure each octahedron is in contact with eight neighbors (four sharing an edge and four sharing a corner) while in rutile structure each octahedron is in contact with 10 neighbor octahedrons (two sharing edge oxygen pairs and eight sharing corner oxygen atoms) [30]. The structural parameters of anatase and rutile TiO_2 are shown in Table 1.1. Rutile is the most stable for large particles, but anatase becomes more stable than rutile only when the particle size decreases below *ca.* 14 nm [34]. These differences in lattice structures cause different mass densities and electronic structures between the two forms of TiO_2 . Mass density of the anatase phase is lower than rutile and the band gap of anatase is somewhat wider, which affects on the activity of photocatalytic process [21]. However, there are many studies have reported the structure and reactivity of the different low-index anatase and rutile surfaces. The TiO_2 nanoparticles have predominantly anatase (101) and rutile (110) [21] majority surfaces, together with minority anatase (001) [35] and rutile (001) surfaces [36].

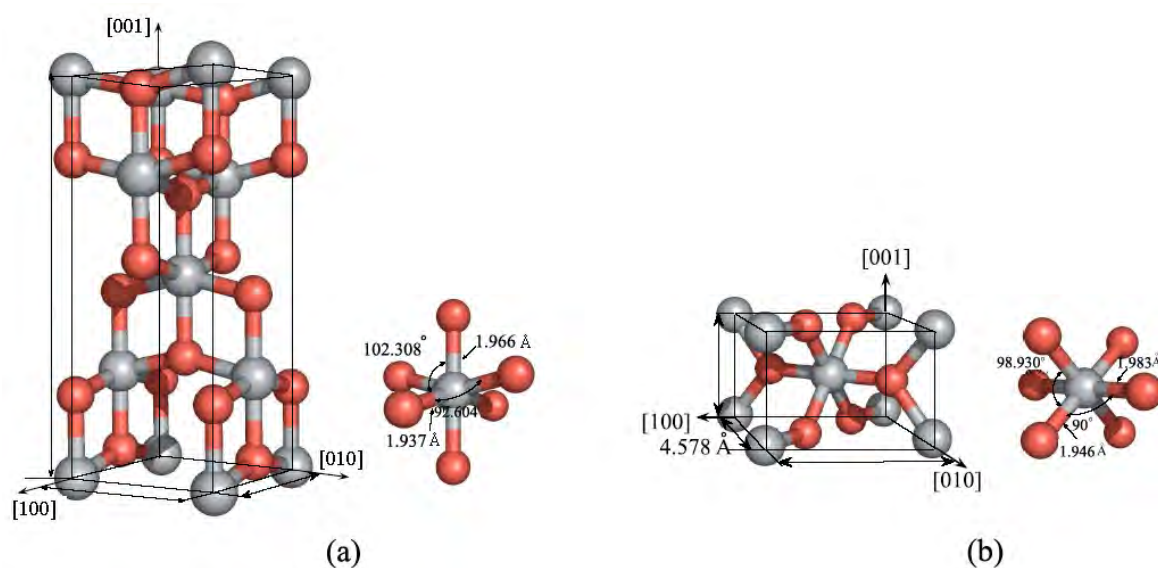


Figure 1.1 Structures of (a) anatase and (b) rutile TiO_2 [29].

Table 1.1 Structural parameters of anatase and rutile TiO₂.

	Anatase	Rutile
Bravias lattice	Body-centered tetragonal	Primitive tetragonal
Space group	No. 141 <i>I</i> 4 ₁ /amd	No. 136 <i>P</i> 4 ₂ /mnm
Lattice parameters [Å] ^a		
<i>a</i>	3.782	4.586
<i>b</i>	3.782	4.586
<i>c</i>	9.502	2.954
Energy gap [eV]	3.2 ^b	3.0 ^c
Density [g/cm ³] ^d	3.894	4.250

^a Ref. [31]^b Ref. [32]^c Ref. [33]^d Ref. [30]

1.1.2 Surface structures of anatase and rutile

The structures of the anatase (001) and (101), rutile (001) and (110) surfaces are shown in Figure 1.2. All surfaces consist of two-fold coordinated O atoms, marked as (O_{2C}), these O_{2C} atoms are called bridging O atoms, and three-fold coordinated O atoms, marked as (O_{3C}), these atoms are called in-plane oxygen atoms. Above the plane of the surface contain of five-fold coordinated Ti atoms, marked as (Ti_{5C}), and six-fold coordinated Ti atoms are located in the surface, marked as (Ti_{6C}).

The low surface energy of anatase is (101), the rutile is (110) surface [21], in which the most stable phases. Anatase also exposed potentially more reactive (001) surface [37]. Recently less stable surface rutile (001) has been also explored to find new physicochemical properties [20] and found to induce unique reactions [38]. The structural and electronic interactions between TiO₂ substrates and adsorbates are of particular interest because of their importance in the photocatalysis process. Stable adsorption configurations of several small molecules on anatase and rutile surface were found in many studies. Thus, the adsorption sites and the reactive dynamics on different surfaces are considered.

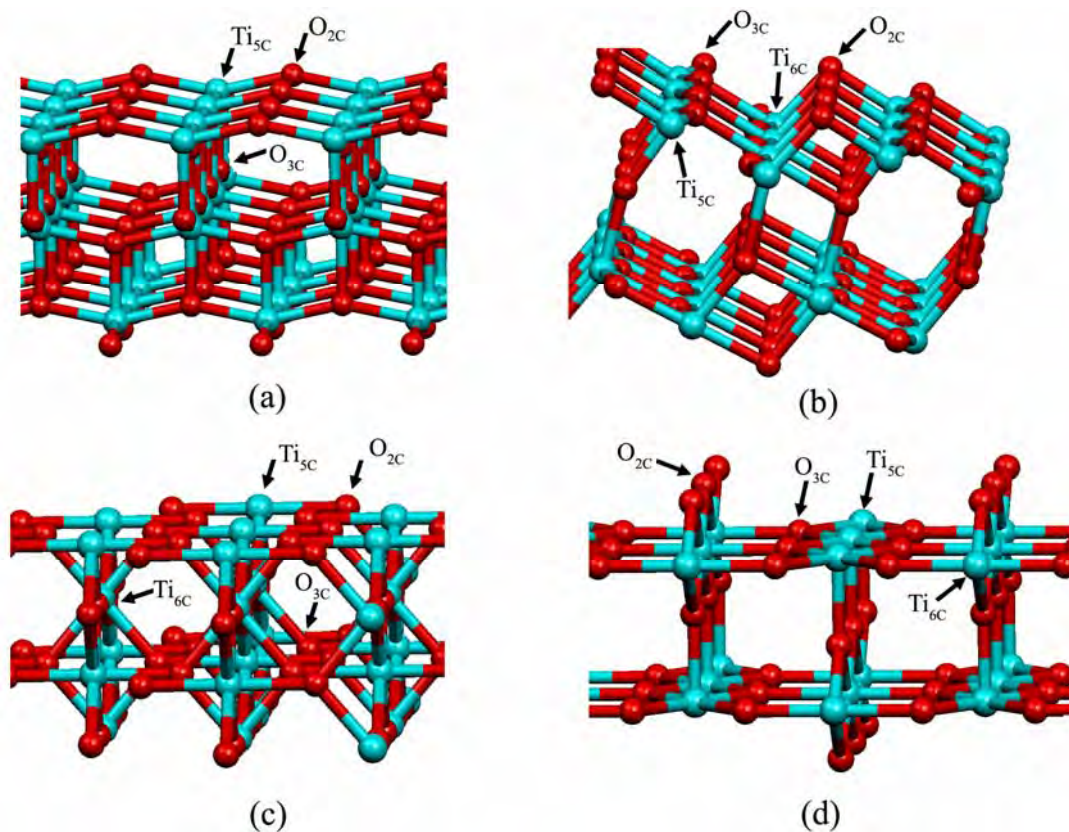
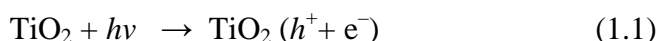


Figure 1.2 Structures of (a) anatase (001), (b) anatase (101), (c) rutile (001) and (d) rutile (110) surfaces.

1.1.3 Photocatalytic process of TiO_2

The TiO_2 -based photocatalysis has been received a great consideration in the fact that it allows the degradation of the organic compound to simple molecules, e.g. H_2O and CO_2 . This approach is based on the photocatalytic reactions occurring at the surface of a catalyst after an initial photoexcitation with a suitable wavelength. Due to the band gap of semiconductors is located within the top of the filled valence band (VB) and the bottom of the vacant conduction band (CB). The VB is located at energy level E_v and is fully occupied and the CB with higher energy E_c is empty. Electronic states between VB and CB are forbidden. The energy of the band gap E_g is the difference between the CB and VB energies, $E_g = E_c - E_v$. However, the TiO_2 can be a good semiconductor photocatalyst since its valence-band hole is sufficiently positive for the hole to act as an acceptor and conduction-band electron is sufficiently negative for the electron to act as a donor. The band-gap of TiO_2 is rather large 3.0–

3.2 eV, corresponding to the UV region. The photocatalysis over the TiO₂ is initiated by the absorption of a photon with energy equal to or greater than the band gap of the TiO₂ and then producing electron–hole (e^-/h^+) pairs. The band–gap excitation leads to the formation of conduction band electrons and valance band holes, which serve as the sites for photoreduction and photooxidation, respectively. The generation of electron–hole pairs and its reverse process could be represented by the following equations:



where $h\nu$ is the photo energy, e^- represents a conduction band electron and h^+ represents a hole in the valence band. Conduction band electrons can be trapped in Ti⁴⁺ ions in the bulk or at the surface which is represented by Eq. (1.3).



The separated electron and hole could follow several possible pathways. Migration of electrons and holes to TiO₂ surface is followed by transfer of photoinduced electrons to adsorbed molecules or solvents [30].

1.1.4 Research rationale

Adsorption energies of the small molecules such di-, tri- and tetraatomic gases are very useful information for reaction prediction on the TiO₂ surfaces due to their co-adsorptions [39]. There have been numerous experimental and theoretical studies on adsorptions of small molecules on various surface planes of different TiO₂ phases. Therefore, to develop new solid–state gas sensors, the adsorption abilities of various gases on the solid surface lead to the discovery of gas sensors. The application of gas sensor at high temperatures for the detection of H₂, O₂, [7] CH₄ and CO [11] is explored.

Nevertheless, both anatase and rutile have been widely used as a photocatalyst and catalytic support in heterogeneous catalysis. Many experimental studies have been investigated the role of rutile TiO₂ surface. Interestingly, anatase is known to

exhibit higher photocatalytic efficiency compared with rutile [40]. As the photocatalytic activity of TiO_2 is mainly due to the oxidation power of photo-generated holes in its valence band, hole transfer to a molecule adsorbed on the TiO_2 surface initiates the oxidation reaction and the oxidized molecule changes into a final product through sequential chemical events [41]. The photoinduced electrons were trapped in the bulk or scavenged at the surface, e.g., by oxygen molecules. Consequently, it is desirable to better define behavior of photocatalytic reaction of electron acceptor molecule by donor molecule and the roles of electron and hole during photocatalysis [42]. The majority of studies concern either calculations on small cluster models or calculations with periodic boundary conditions. Due to the interaction between TiO_2 and the adsorbed molecule plays a very important role to remove a pollutant from the environment. Therefore, there are several researches have been extensively studied the adsorption of molecular gases on different of TiO_2 surfaces such as CO, CO_2 , H_2 and H_2O [45], N_2 , O_2 , and CO [44], NH_3 [45–46], NO [47–48], NO_2 [49] and N_2O [50]. To our knowledge, the adsorption of gases on the electron-excited of neutral, negatively or positively charged surfaces of the TiO_2 modeled as the photocatalyst has never been studied. The model as a photocatalytic reaction is the interaction between photo-induced electrons and holes on the TiO_2 surface with molecular gases. To better understand the photocatalytic reaction on the TiO_2 photocatalyst, the adsorption of gases on different charged surfaces of the TiO_2 should be investigated using spin-polarized calculations.

Furthermore, transition metals deposited on TiO_2 surface are known to act as promoters of catalytic reactions. The addition of platinum (Pt) to a TiO_2 (Pt/ TiO_2) system can modify its chemical reactivity and therefore enhance its catalytic performance in the photodecomposition rate of organic compounds such as trichloroethylene [49]. The interaction of molecular gases with Pt/ TiO_2 as well as clean TiO_2 surface has also been investigated.

The main purpose of this thesis is to emphasize the important differences in the surface behavior of anatase (001) and (101), rutile (001) and (110) as a gas sensor application. While anatase, in the course of photocatalytic reactions is advantage over rutile [40]. Therefore, we studied only photocatalytic reactions of anatase as a photocatalysis application.

1.2 OBJECTIVES

In this study, several computational methods based on DFT calculations were used to investigate the adsorption of molecular gases on the anatase (001) and (101), rutile (001) and (110) surfaces and TiO₂-supported Pt of anatase (101) surface (Pt/TiO₂). The aims of these calculations were;

1. To study and provide detailed information about the adsorption abilities and adsorption energies of di-, tri- and polyatomic gases on cluster models of anatase TiO₂ (001) and (101) surfaces.
2. To study the adsorption of CO, H₂, N₂O, NH₃ and CH₄ gases including their competitive co-adsorption on the anatase TiO₂ (001) and (101) surfaces.
3. To study the adsorption of CO, H₂, N₂O, NH₃ and CH₄ gases on the rutile TiO₂ (001) and (110) surfaces.
4. To investigate the adsorption of CO and predict the efficiency of photocatalytic oxidation of CO into CO₂ on anatase TiO₂ (101) surface.
5. To investigate the adsorption of N₂O and predict the photocatalytic reduction of N₂O into N₂ by CO on anatase TiO₂ (101) surface.
6. To study the Pt atom supported on anatase (101) surface (Pt/TiO₂) and its adsorption with CO, N₂, CO₂, and N₂O.

1.3 SCOPE OF THE DISSERTATION

This dissertation was carried out in order to investigate the adsorption of molecular gases on anatase- and rutile-TiO₂ surfaces by using computational approach. The attention is focused both on the optimized geometries of the molecules and the surfaces, and on the energies involved in the adsorption. The scope of this study is one-by-one corresponding to the research objectives:

1. The adsorption abilities and adsorption energies of diatomic (O₂, N₂, H₂, CO and NO), triatomic (H₂O, H₂S, N₂O, CO₂, NO₂ and SO₂) and polyatomic (NH₃, C₂H₂, C₂H₄ and CH₄) gases on cluster models of anatase TiO₂ (001) and (101) surfaces were studied using the B3LYP/6-

- 31G(d). All calculations were performed with the GAUSSIAN 03 program.
2. The adsorption of CO, H₂, N₂O, NH₃ and CH₄ gases including their competitive co-adsorption on the anatase TiO₂ (001) and (101) surfaces were studied using periodic boundary condition. All DFT calculations of two-dimensionally periodic slab model have been carried out using the CRYSTAL06 computational code, based on the expansion of the crystalline orbitals as a linear combination of a basis set consisting of atom centered Gaussian orbitals.
 3. The adsorption of CO, H₂, N₂O, NH₃ and CH₄ gases on the rutile TiO₂ (001) and (110) surfaces were studied using two-dimensionally periodic slab model with CRYSTAL06 computational code.
 4. The adsorption of CO and the efficiency of photocatalytic oxidation of CO into CO₂ on anatase TiO₂ (101) surface were calculated using spin-polarization and standard plane wave expansions within the generalized gradient approximation (GGA) with the Vienna *ab initio* simulation package (VASP). The dissociation of CO₂ was performed by using molecular dynamics (MD) calculations.
 5. The adsorption of N₂O and photocatalytic reduction of N₂O to N₂ by CO on anatase TiO₂ (101) surface were calculated using spin-polarization and standard plane wave expansions within the GGA with VASP code.
 6. The adsorption CO, CO₂, N₂O, N₂ gases on Pt/TiO₂ of anatase (101) surface were calculated using GGA calculations with VASP code.

1.4 EXPECTED RESULTS

TiO₂ has important surface-related applications in the field of gas sensors and photocatalysis due to its high ability to adsorb and wide band-gap energy. Therefore, the study of molecular gases adsorption on the TiO₂ surfaces to basic knowledge is a useful technology. TiO₂-based photocatalysis for destruction of organic compounds in polluted air and waste water has been improved. Anatase and rutil forms of TiO₂ usually exhibit different surface structure arrangements thus different surface reactivity. However, the different surface is reflected in the adsorption and desorption

behavior of adsorbates, and their adsorption behavior on these surfaces is well understood as a gas sensor and photocatalysis applications. This work is intended to be the starting point of a comprehensive theoretical investigation of the differences between anatase and rutile surfaces. We believe that a detailed study of the surface properties of anatase- and rutile-TiO₂ will serve as a good starting point for more specific investigations. Especially, knowledge of the efficient photocatalytic reaction of toxic gases is one of the most desirable in the research of the development of environmentally friendly catalysts.

CHAPTER II

ADSORPTION OF DI-, TRI- AND POLYATOMIC GASES ON THE ANATASE TiO₂ (001) AND (101) SURFACES AND THEIR ADSORPTION ABILITIES

Raina Wanbayor, Vithaya Ruangpornvisuti

*Department of Chemistry, Faculty of Science, Chulalongkorn University, Bangkok
10330, Thailand*

**This article has been published in Journal of Molecular Structure: THEOCHEM
Page: 103–108. Volume: 952. Year: 2010.**

2.1 ABSTRACT

The adsorption energies ΔE_{ads} of diatomic (O_2 , N_2 , H_2 , CO and NO), triatomic (H_2O , H_2S , N_2O , CO_2 , NO_2 and SO_2) and polyatomic (NH_3 , C_2H_2 , C_2H_4 and CH_4) gases on the anatase TiO_2 (001) and (101) surfaces were obtained by density functional method. The strongest adsorption energies, computed using the B3LYP/6-31G(d) with BSSE correction, of diatomic, triatomic and polyatomic gases on the anatase TiO_2 are $\Delta E_{\text{ads}}(\text{CO}) = -8.69$, $\Delta E_{\text{ads}}(\text{H}_2\text{O}) = -9.77$ and $\Delta E_{\text{ads}}(\text{NH}_3) = -21.19$ kcal/mol for (001) surface and $\Delta E_{\text{ads}}(\text{O}_2) = -99.71$, $\Delta E_{\text{ads}}(\text{S}_2\text{O}) = -27.59$ and $\Delta E_{\text{ads}}(\text{NH}_3) = -30.78$ kcal/mol for (101) surface, respectively. All the adsorptions of studied gases on the anatase TiO_2 (001) and (101) surfaces compared with experiments and other methods are reported.

2.2 INTRODUCTION

Titanium dioxide was most widely used for various applications such as photocatalysis [2, 50, 51], heterogeneous catalysis [1], gas sensors [7–10, 52–57], dye-sensitized solar cells [58–60, 15, 61, 62] and electro-chromic devices [63–66]. Adsorption energies of the small molecules such di-, tri- and tetraatomic gases are very useful information for reaction prediction on the TiO_2 surfaces due to their co-adsorption [40, 67]. In the environmental field, in order to develop the new catalyst for the selective catalytic reduction (SCR) of NO_x [45] in presence of various small pollutant gases, the adsorption abilities of these small molecules can be utilized to success of new catalyst discovery. Nevertheless, developing new solid-state gas sensors, the adsorption abilities of various gases on the solid surface lead to the discovery of gas sensors.

There have been many experimental and theoretical researches for the adsorption of small molecules on various surface planes of different TiO_2 phases. Theoretical researches of the adsorption of H_2O and NH_3 on the anatase TiO_2 (101) and (001) surfaces as cluster models using density functional theory (DFT) [68], the CO oxidation on stoichiometric anatase TiO_2 (001) surface by ab initio calculations [69], H_2O and O_2 on the anatase TiO_2 (100) [70] and H_2O on the anatase TiO_2 (100), (010) and (001) surfaces using semiempirical MSINDO method [71] were studied.

The adsorption of H₂O on the anatase TiO₂ (101) surface using many cluster models was investigated using *ab initio* molecular orbital theory and DFT [72] and CO₂ on the anatase TiO₂ (010), (001), and (101) surfaces using small TiO₂ clusters was studied by DFT calculations [73]. The structural, electronic and vibrational properties of intermediates of the O₂ photoreduction [74] at the anatase TiO₂ (101) surface and water molecules in contact with the anatase TiO₂ (101) surface [75] were investigated by performing DFT calculations and *ab initio* molecular dynamics (AIMD) simulations. Theoretical simulations of the adsorption behaviors of thin water overlayers on the anatase TiO₂ (101) surface using Car–Parrinello molecular dynamics (CPMD) simulations [76] and molecular dynamics simulations [77] were carried out. The experiments of the adsorption of water on the anatase TiO₂ (001) surface using synchrotron radiation–excited core level photoelectron spectroscopy [78], adsorption of NH₃ and ND₃ on the anatase phase of TiO₂ using laser Raman spectroscopy [79], adsorption of CO₂ and NH₃ on anatase and rutile TiO₂ using infrared spectrometry [80] and the interaction of water and methanol with the anatase TiO₂ (101) surface using low–energy electron diffraction (LEED), temperature–programmed desorption (TPD) and X–ray photoelectron spectroscopy (XPS) [81] were carried out. Although, there are many theoretical studies of adsorptions of these small gases on the anatase TiO₂, several interesting gases adsorbed on the various surface planes of the anatase TiO₂ have been studied using different methods. In this paper, adsorptions of diatomic (O₂, N₂, H₂, CO and NO), triatomic (H₂O, H₂S, N₂O, CO₂, NO₂ and SO₂) and polyatomic (NH₃, C₂H₂, C₂H₄ and CH₄) gases on the anatase TiO₂ (001) and (101) surfaces which are the most common surfaces for anatase TiO₂ [3] have been comprehensively studied using density functional calculations. Adsorption abilities, in terms of adsorption energy of all studied gases have been analyzed.

2.3 COMPUTATIONAL METHODS

All structures of adsorbate gases, modeled clusters for the anatase TiO₂ (001) and (101) surfaces and their adsorption complexes were optimized using density functional theory (DFT) method. DFT calculations have been performed with the Becke’s three parameter hybrid functional [82] with the non–local correlation

functional of Lee–Yang–Parr [83], B3LYP method [84] with 6–31G(d) basis set [85,86]. All studied structures were computed with the restricted B3LYP except the triplet–state structure for of oxygen adsorbed on TiO₂ (001) and (101) surfaces, the spin–unrestricted B3LYP/6–31G(d) being employed. All calculations were performed with the GAUSSIAN 03 program [87].

The anatase TiO₂ (001) and (101) surfaces were modeled as Ti₉O₃₃H₃₀ and Ti₉O₃₃H₄₂ clusters, respectively. Structures of the Ti₉O₃₃H₃₀ and Ti₉O₃₃H₄₂ clusters were obtained from the partial optimization of the molecular geometry of hydrogen–terminated structures of clusters modified from the X–ray crystallographic structures of anatase TiO₂ [88]. The dangling bonds of the hydrogen–terminated structures were restrained based on the orientation of their bonds. The B3LYP/6–31G(d) optimized structures of the Ti₉O₃₃H₃₀ and Ti₉O₃₃H₄₂ clusters are shown in Figure 2.1 Partial optimizations of adsorption complex between adsorbate gas and adsorbent surface whose structure was treated as rigid cluster were carried out.

The adsorption energy ΔE_{ads} of adsorbate gases on the TiO₂ surface which is modeled as the rigid cluster were computed from the total energies of the cluster–adsorbate complex $E_{\text{cluster–adsorbate}}$, the cluster E_{cluster} and isolated adsorbate $E_{\text{adsorbate}}$ as shown in the following equation:

$$\Delta E = E_{\text{cluster–adsorbate}} - (E_{\text{cluster}} + E_{\text{adsorbate}}) \quad (2.1)$$

The adsorption energies of oxygen molecule adsorbed on TiO₂ (001) and (101) surfaces were computed from the following equation:

$$\Delta E = E_{\text{cluster–O}_2(\text{triplet})} - (E_{\text{cluster}} + E_{\text{O}_2(\text{triplet})}) \quad (2.2)$$

To estimate the basis set superposition error (BSSE) for the energies of adsorption complexes at the B3LYP/6–31G(d) level, counterpoise (CP) calculations were performed using the Boys–Bernardi’s CP scheme [89]; $\Delta E_{\text{ads}}^{\text{BSSE}}$ has been referred for the B3LYP/6–31G(d) calculation with BSSE corrections. The adsorption energies of adsorbate gases computed at the B3LYP/6–31G(d) level have been reported throughout the paper, unless otherwise specified.

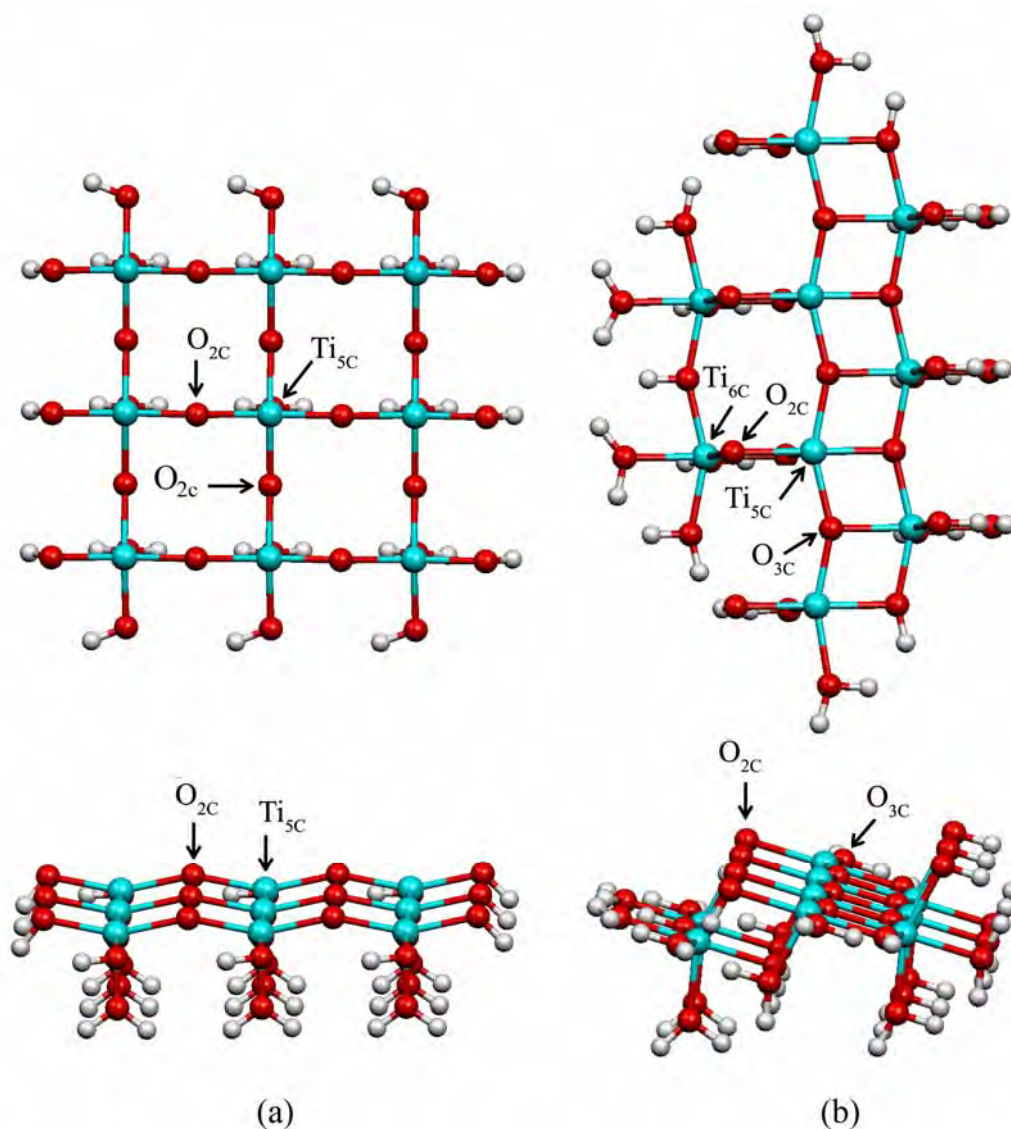


Figure 2.1 The anatase TiO_2 (a) (001) and (b) (101) surfaces modeled as $\text{Ti}_9\text{O}_{33}\text{H}_{30}$ and $\text{Ti}_9\text{O}_{33}\text{H}_{42}$ clusters, respectively.

2.4 RESULTS AND DISCUSSION

The structures of the $\text{Ti}_9\text{O}_{33}\text{H}_{30}$ and $\text{Ti}_9\text{O}_{33}\text{H}_{42}$ clusters, representing for the anatase TiO_2 (001) and (101) surfaces, obtained from the partial optimization at the B3LYP/6-31G(d) level are shown in Figure 2.1. The coordinate of anatase TiO_2 surface atoms are composed of 2-coordinate oxygen atom ($\text{O}_{2\text{C}}$) and $\text{Ti}_{5\text{C}}$ atoms for the (001) plane and $\text{O}_{2\text{C}}$, $\text{O}_{3\text{C}}$, $\text{Ti}_{5\text{C}}$ and $\text{Ti}_{6\text{C}}$ atoms as shown in Figure 2.1(a) and (b), respectively. The adsorption energies of the di-, tri-, and polyatomic gases adsorbed

on the anatase TiO₂ (001) and (101) surfaces are listed in Table 2.1. The optimized structures of all adsorption complexes are shown in Figures 2.2–2.4. Adsorption of the adsorbate gases on the Ti₉O₃₃H₃₀ and Ti₉O₃₃H₄₂ modeled clusters are separately described depending on their sizes.

Table 2.1 The adsorption energies of the di-, tri- and polyatomic gases adsorbed on the anatase TiO₂ (001) and (101) surfaces.

Adsorbate gases	(001) Ti ₉ O ₃₃ H ₃₀ ^a			(101) Ti ₉ O ₃₃ H ₄₂ ^b		
	$\Delta E_{\text{ads}}^{\text{c,d}}$	$\Delta E_{\text{ads}}^{\text{c,e}}$	$\Delta E_{\text{ads}}^{\text{BSSEC,f}}$	$\Delta E_{\text{ads}}^{\text{c,d}}$	$\Delta E_{\text{ads}}^{\text{c,e}}$	$\Delta E_{\text{ads}}^{\text{BSSEC,f}}$
<i>Diatomic</i>						
O ₂ (triplet)	-9.19	-3.10	-2.44	-107.27	-111.97	-99.71
N ₂	-8.15	-3.44	-3.77	-11.97	-12.09	-6.66
H ₂	-3.49	-3.17	-2.15	-3.18	-8.44	-1.63
CO ^g	-14.80	-10.03	-8.69	-19.75	-20.70	-12.73
CO ^h	-6.77, -5.30 ⁱ	-3.15	-2.48	-10.05	-10.77	-4.55
NO	-11.09	-8.20	- ^j	-103.66	-77.41	- ^j
<i>Triatomic</i>						
H ₂ O	-16.39, -35.63 ^k	-13.03	-9.77	-35.86, -28.97 ^h	-37.00	-23.50
	-18.68 ^l			-17.30 ^{p,q}		
	-13.6 ^m			-27.10 ^r		
	-23.46 ⁿ			-22.96 ^s		
	-17.69 ^o			-27.44 ^t		
H ₂ S	-12.49	-8.42	-8.10	-19.33, -11.30 ^v	-23.01	-13.24
N ₂ O	-11.97	-8.58	-7.42	-13.69	-15.42	-9.03
CO ₂	-11.27	-8.09	-6.05	-12.79	-12.89	-6.63
NO ₂	-8.24	-5.61	- ⁱ	-125.56	-129.03	- ⁱ
SO ₂	-7.39	-4.97	-1.36	-34.79	-41.08	-27.59
<i>Polyatomic</i>						
NH ₃	-29.19, -23.72 ⁿ	-26.20	-21.19	-33.03, -30.78 ⁿ	-39.29	-30.78
C ₂ H ₂	-11.26	-8.13	-6.80	-17.12	-19.19	-14.09
C ₂ H ₄	-10.11	-8.11	-2.40	-16.06	-18.06	-9.77
CH ₄	-5.52	-4.68	-1.16	-4.31	-8.68	-2.21

^a Its total energies at the B3LYP/6–31G(d) and B3LYP/6–311G(d,p)/B3LYP/6–31G(d) levels are -10146.37479510 a.u. and -10147.6820240 a.u., respectively.

^b Its total energies at the B3LYP/6–31G(d) and B3LYP/6–311G(d,p)//B3LYP/6–31G(d) levels are –10152.68020140 a.u. and –10154.048498100 a.u., respectively.

^c In kcal/mol.

^d Computed at the B3LYP/6–31G(d) level.

^e Computed at the B3LYP/6–311G(d,p)//B3LYP/6–31G(d) level.

^f Computed at the B3LYP/6–31G(d) level with BSSE corrections.

^g Configuration of the adsorbed CO by pointing its carbon atom towards titanium atom of TiO₂.

^h Configuration of the adsorbed CO by pointing its oxygen atom towards titanium atom of TiO₂.

ⁱ The (001) slab, computed with the VASP–GGA method, taken from ref. [69]

^j No BSSE calculation carried out.

^k The (001) 2×2×3 cluster, computed with, taken from ref. [90]

^l Computed with MD simulation, taken from ref. [94]

^m The Ti₆O₁₉H₁₂ cluster, computed with the DFT/VWN(BP86) method, taken from ref. [95]

ⁿ The TiO₂O₉H₁₀ cluster, computed with the B3LYP/6–31G(d,p) method, taken from ref. [68]

^o The Ti₂₁O₅₈H₃₂ cluster, computed with the MSINDO method, taken from ref. [71]

^p Computed with MD simulation, taken from ref. [96]

^q XPS method, taken from ref. [81]

^r The Ti₆O₂H₂₀ cluster, computed with the B3LYP/6–31G(d)//HF/6–31G(d) method, taken from ref. [72]

^s The (101) slab, computed with the DFT–GGA(PW91) VASP method, taken from ref. [97]

^t The Ti₈O₂₈H₂₄ cluster, computed with the DFT/GGA(RPBE)DZVP method, taken from ref. [98]

^u Computed with the DFT/GGA method, taken from ref. [99]

^v Computed with MD simulation, taken from ref. [96]

2.4.1 Adsorption of diatomic gases on the anatase TiO₂

Configurational structures of the adsorption complexes of diatomic gases on the anatase TiO₂ (001) and (101) surfaces are shown in Figure. 2.2. Table 1 shows that the CO can be adsorbed either on the TiO₂ (001) or (101) surfaces as two configurations and the stronger one is the configuration of CO–carbon atom pointing towards the Ti atom of the surface. The CO adsorbed on the (001) surface is the strongest adsorption which is stronger than the O₂ adsorption by 5.61 kcal/mol; all energies presented in the paper were computed at the B3LYP/6–31G(d) level unless otherwise specified. The adsorption abilities of diatomic gases on the anatase TiO₂ (001) and (101) surfaces are in the orders: CO > NO > O₂ > N₂ > H₂ and O₂ > NO >> CO > N₂ > H₂, respectively. The first and second strongest adsorption gases (CO and

NO) on the TiO_2 (001) surface, computed at either the B3LYP/6-31G(d) or B3LYP/6-311G(d,p)//B3LYP/6-31G(d) level are in the same sequence. Adsorption energies of O_2 , N_2 and H_2 on the anatase TiO_2 (001) surface computed at the B3LYP/6-31G(d) level are reasonably different but their B3LYP/6-311G(d,p)//B3LYP/6-31G(d) and BSSE corrected B3LYP/6-31G(d) values are very low and in the same order. This may be caused by (i) using polarized basis set as 6-311G(d,p) for low polar diatomic gases adsorbed on low polar TiO_2 (001) surface and (ii) underestimation of BSSE calculations on interaction between low polar diatomic gas and low polar TiO_2 (001) atoms. Therefore, the B3LYP/6-311G(d,p)//B3LYP/6-31G(d) and BSSE corrected B3LYP/6-31G(d) methods are inaccurate method for calculation of interaction of low polar diatomic gas and low polar TiO_2 (001) surface atoms. Nevertheless, sizes of clusters as $\text{Ti}_9\text{O}_{33}\text{H}_{30}$ and $\text{Ti}_9\text{O}_{33}\text{H}_{42}$ should not be the main cause of these inaccurate results.

The adsorption on the TiO_2 (101) surface, the adsorption sequences obtained from either the B3LYP/6-31G(d) or B3LYP/6-311G(d,p)//B3LYP/6-31G(d) or BSSE corrected B3LYP/6-31G(d) calculations are in the same sequence except the BSSE corrected B3LYP/6-31G(d) adsorption energy of NO which could not be obtained because no convergence of its calculation is found.

Two types of adsorption configurations of CO on the TiO_2 (001) and (101) surfaces were found. The first type is the configuration of CO pointing its carbon atom towards titanium atom of TiO_2 and the second type is the configuration of CO pointing its oxygen atom towards titanium atom of TiO_2 . The adsorption energies of the first configuration type of CO adsorbed on the TiO_2 (001) and (101) surfaces are higher than those of the second type. The adsorption energies of the most favorable configuration (the first type) for CO adsorbed on the TiO_2 (001) and (101) surfaces are -14.80 and -109.75 kcal/mol, respectively, and more stable than that of the second configuration type by 8.03 and 9.70 kcal/mol, respectively.

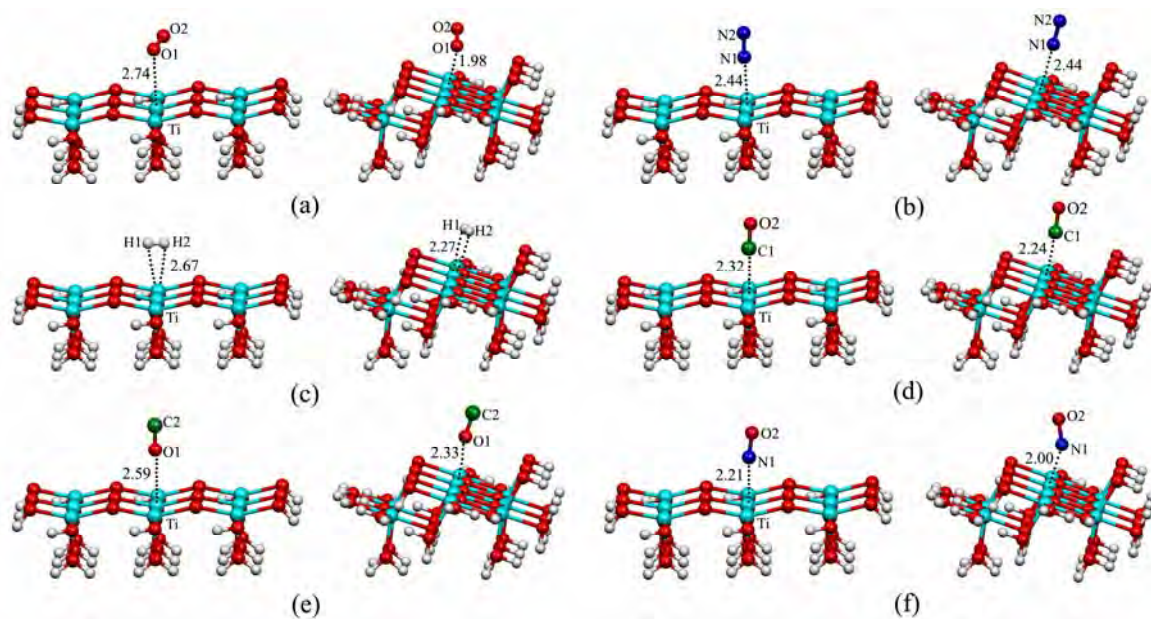


Figure 2.2 The adsorption structures of diatomic gases (a) O₂ (triplet state), (b) N₂, (c) H₂, (d, e) CO and (f) NO, adsorbed on the anatase TiO₂ (001) (left) and (101) (right) surfaces. Hydrogen bond distances are in Å.

The bond distances between CO–carbon atom and surface–Ti atom for the adsorptions of CO on the TiO₂ (001) surface as C··Ti = 2.32 Å and (101) surface as C··Ti = 2.24 Å are shorter than those between CO–oxygen atom and surface–Ti atom for the TiO₂ (001) and (101) surfaces by 0.27 and 0.09 Å, respectively.

The O₂ adsorbed on the TiO₂ (101) surface is the strongest adsorption of which adsorption energy is –107.27 kcal/mol and much stronger than the adsorption on the (001) surface by 98.08 kcal/mol. As many experiments and theoretical calculations have shown that O₂ cannot bind to perfect TiO₂ (110) surface [91–93], the TiO₂ (101) is the most favorable surface for the O₂ adsorption. The bond distances between O₂–oxygen atom and surface–Ti atom for the adsorptions of O₂ on the TiO₂ (0 0 1) surface as O··Ti = 2.74 Å and (101) surface as O··Ti = 1.97 Å correspond to their adsorption energies as mentioned above.

The adsorption of the NO on the TiO₂ (101) surface is stronger than that on the (001) surface by 92.57 kcal/mol at the B3LYP/6–31G(d) level and 69.21 kcal/mol at the B3LYP/6-311G(d,p)//B3LYP/6–31G(d) level. The bond distances between

NO–nitrogen atom and surface–Ti atom for the adsorptions of NO on the TiO₂ (001) surface as N...Ti = 2.21 Å and TiO₂ (101) surface as N...Ti = 2.00 Å were found.

The adsorption energies of N₂ adsorbed on the TiO₂ (001) and (101) surfaces are –8.15 and –11.97 kcal/mol, respectively. The adsorption of H₂ on the TiO₂ (001) and (101) surfaces are very weak of which the adsorption energies are –3.49 and –3.18 kcal/mol, respectively.

2.4.2 Adsorption of triatomic gases on the anatase TiO₂

Configurational structures of the adsorption complexes of triatomic gases on the anatase TiO₂ (001) and (101) surfaces are shown in Figure 2.3. Due to the B3LYP/6–31G(d) adsorption energies, the adsorption abilities for triatomic gases adsorbed on the TiO₂ (001) and (101) surfaces are in orders: H₂O > H₂S ≈ N₂O ≈ CO₂ > NO₂ ≈ SO₂ and NO₂ ≈ H₂O ≈ SO₂ > H₂S > N₂O ≈ CO₂, respectively. Nevertheless, the adsorption energies of these gases on the TiO₂ (001) and (101) surfaces obtained from the B3LYP/6–311G(d,p)//B3LYP/6–31G(d) or BSSE corrected B3LYP/6–31G(d) calculations result reasonable orders of adsorption abilities compared with the order obtained from the B3LYP/6–31G(d) computations. The H₂O adsorbed on the TiO₂ (001) surface is the strongest adsorption and its adsorption energy (ΔE_{ads} is –16.39 kcal/mol) is the reasonable value compared with the values obtained from the other works [68, 71, 93–95]. The adsorption energy of H₂O adsorbed on the TiO₂ (101) surface (ΔE_{ads} is –35.86 kcal/mol) is stronger than the adsorption on the TiO₂ (001) by 17.47 kcal/mol. The B3LYP/6–31G(d) adsorption energy of the H₂O adsorbed on the TiO₂ (001) surface is overestimate value but the BSSE corrected B3LYP/6–31G(d) adsorption energy ($\Delta E_{\text{ads}}^{\text{BSSE}} = -23.50$ kcal/mol) is more reasonable as compared with the values taken from the other works [68, 72, 82, 96–99].

The adsorption energies of H₂S, N₂O and CO₂ adsorbed on the TiO₂ (001) and (101) surfaces are not much different except the H₂S adsorbed on the TiO₂ (101) being stronger than on the (001) surface by 6.84 kcal/mol. The NO₂ and SO₂ adsorbed on the TiO₂ (001) surface is weak but on the TiO₂ (101) surface are very strong. The NO₂ adsorption on the TiO₂ (101) surface (ΔE_{ads} is –125.56 kcal/mol) is the most stable adsorption on the TiO₂ (101) surface and much stronger than on the (001) surface by 117.32 kcal/mol. The bond distances between NO₂–nitrogen atom and

surface–Ti atom, the N···Ti bond distance for the TiO₂ (001) surface is long (N···Ti = 2.62 Å) and longer than for the (101) surface (N···Ti = 2.14 Å) by 0.68 Å. The NO₂ adsorption on either the TiO₂ (001) or (101) surface, the NO₂ molecule points its nitrogen atom towards the surface–Ti atom, see and Figure 2.3(e). The SO₂ adsorption on the TiO₂ (101) surface (ΔE_{ads} is –34.79 kcal/mol) is pretty strong and much stronger than on the (001) surface by 27.40 kcal/mol. The SO₂ molecule adsorbed on the TiO₂ (001) surface points its sulfur atom towards the surface–Ti atom but point its oxygen atom towards the surface–Ti atom, see Figure 2.3(f).

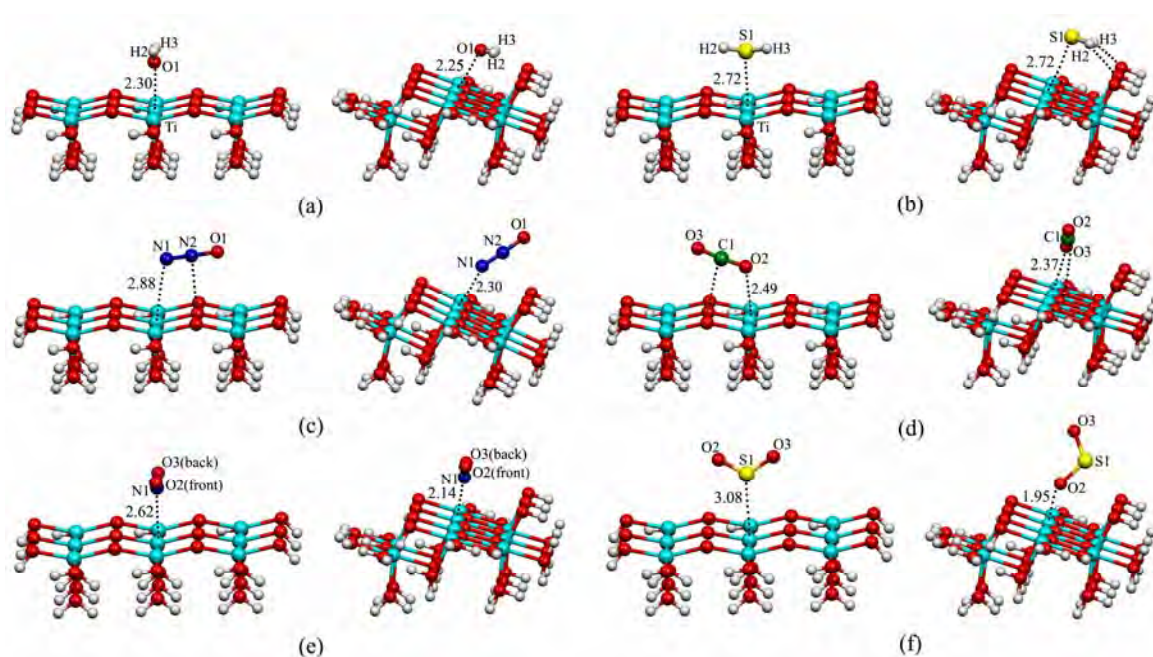


Figure 2.3 The adsorption structures of triatomic gases (a) H₂O, (b) H₂S, (c) N₂O, (d) CO₂, (e) NO₂ and (f) SO₂, adsorbed on the anatase TiO₂ (001) (left) and (101) (right) surfaces. Hydrogen bond distances are in Å.

2.4. 3. Adsorption of polyatomic gases on the anatase TiO₂

Structures of the adsorption complexes of polyatomic gases on the anatase TiO₂ (001) and (101) surfaces are shown in Figure 2.4. The adsorption abilities for polyatomic gases on either the TiO₂ (001) or (101) surface computed at either the B3LYP/6–31G(d) or B3LYP/6–311G(d,p)//B3LYP/6–31G(d) or BSSE corrected B3LYP/6–31G(d) level, are in the same order: NH₃ >> C₂H₂ > C₂H₄ >> CH₄.

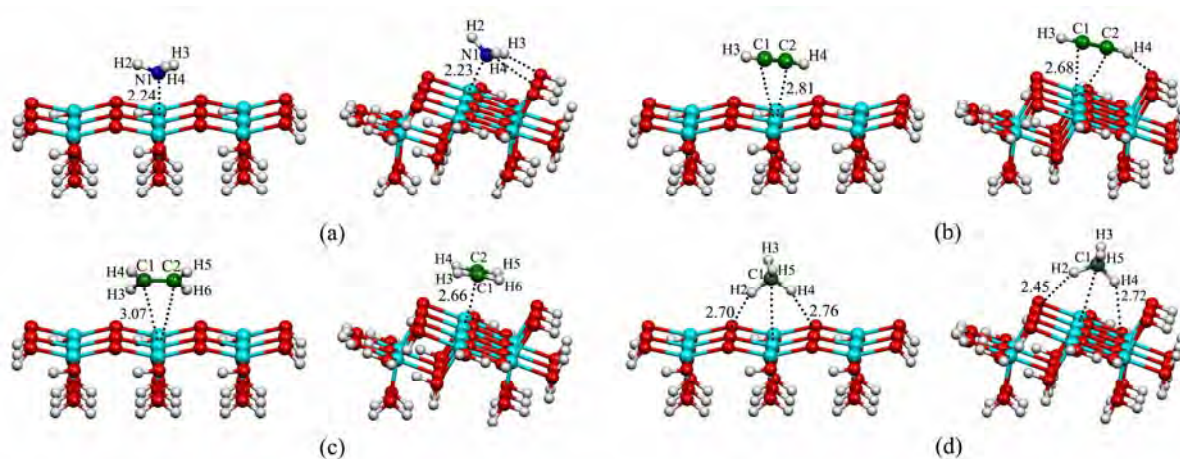


Figure 2.4 The adsorption structures of polyatomic gases (a) NH_3 , (b) C_2H_2 , (c) C_2H_4 and (d) CH_4 , adsorbed on the anatase TiO_2 (001) (left) and (101) (right) surfaces. Hydrogen bond distances are in Å.

Adsorptions of NH_3 on either the TiO_2 (001) or (101) surface are very strong and stronger than others (C_2H_2 , C_2H_4 and CH_4) by more than 10 kcal/mol. The adsorption energy of NH_3 on the TiO_2 (001) ($\Delta E_{\text{ads}} = -29.91$ kcal/mol) and (101) ($\Delta E_{\text{ads}} = -39.25$ kcal/mol) surfaces are close to the values reported in Ref. [68]. The bond distances between NH_3 -nitrogen atom and surface-Ti atom, the $\text{N}\cdots\text{Ti}$ bond distance for the TiO_2 (001) surface ($\text{N}\cdots\text{Ti} = 2.24$ Å) and the (101) surface ($\text{N}\cdots\text{Ti} = 2.23$ Å) are hardly different. For the adsorption of NH_3 on either the TiO_2 (001) or (101) surface, the NH_3 molecule pointing its nitrogen atom towards the surface-Ti atom was found as shown in Figure 2.4(a).

The adsorption energies of C_2H_2 and C_2H_4 adsorbed on the TiO_2 (001) and (101) surfaces are -8.15 and -11.97 kcal/mol, respectively. Plot for comparison of the adsorption energies of C_2H_2 , C_2H_4 and CH_4 adsorbed on the anatase TiO_2 (001) and (101) surfaces is shown in Figure 2.5. It shows small different adsorption energies of CH_4 adsorbed on the TiO_2 (001) and (101) surfaces but the adsorption of C_2H_2 , C_2H_4 on the TiO_2 (101) are stronger than on the TiO_2 (001) by 5.86 and 5.95 kcal/mol, respectively.

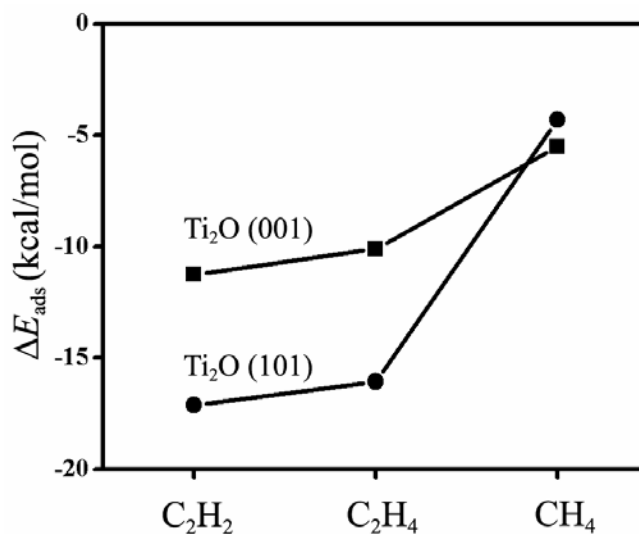


Figure 2.5 Plot for comparisons of the adsorption energies of small hydrocarbon molecules on the anatase TiO₂ (001) and (101) surfaces.

2.5 CONCLUSIONS

The adsorption energies of di-, tri- and polyatomic gases adsorbed on anatase TiO₂ (001) and (101) surfaces which are modeled as the Ti₉O₃₃H₃₀ and Ti₉O₃₃H₄₂ clusters were obtained using the B3LYP/6-31G(d), B3LYP/6-311G(d,p)//B3LYP/6-31G(d) and BSSE corrected B3LYP/6-31G(d) calculations. The adsorption abilities for all the studied gases on the anatase TiO₂ (001) and (101) surfaces are in the orders: NH₃ >> H₂O > CO > H₂S ≈ N₂O > CO₂ ≈ C₂H₂ ≈ NO ≈ C₂H₄ > O₂ > NO₂ ≈ N₂ > SO₂ > CH₄ > H₂ and NO₂ > O₂ ≈ NO ≈ H₂O > SO₂ > NH₃ >> CO ≈ H₂S > C₂H₂ > C₂H₄ > N₂O > CO₂ > N₂ > CH₄ > H₂, respectively.

The adsorptions of all studied gases on the anatase TiO₂ can be summarized that the TiO₂ (001) surface greatly prefers to adsorb NH₃ and H₂O, and the TiO₂ (101) surface prefers to adsorb NO and O₂. The TiO₂ (101) surface may probably be expected to be a catalyst for NO_x conversion reaction.

CHAPTER III

ADSORPTION OF CO, H₂, N₂O, NH₃ AND CH₄ ON THE ANATASE TiO₂ (001) AND (101) SURFACES AND THEIR COMPETITIVE ADSORPTION PREDICTED BY PERIODIC DFT CALCULATIONS

Raina Wanbayor and Vithaya Ruangpornvisuti

*Department of Chemistry, Faculty of Science, Chulalongkorn University, Bangkok
10330, Thailand*

This article has been published in Materials Chemistry and Physics

Page: 720–725. Volume: 124. Year: 2011.

3.1 ABSTRACT

The adsorption of CO, H₂, N₂O, NH₃ and CH₄ gases on the anatase TiO₂ (001) and (101) surfaces were investigated by two-dimensionally periodic slab model DFT calculation. The most energetically favorable positions of these gases on the anatase TiO₂ surface computed using two different optimization models were obtained. The relative adsorption energies of these gases on the anatase TiO₂ (001) and (101) surfaces are in orders: NH₃ ($\Delta E_{\text{ads}} = -26.6$ kcal/mol) \gg CO ($\Delta E_{\text{ads}} = -9.7$ kcal/mol) \gg H₂ \approx CH₄ \approx N₂O and NH₃ ($\Delta E_{\text{ads}} = -24.3$ kcal/mol) \gg CO ($\Delta E_{\text{ads}} = -6.8$ kcal/mol) \approx N₂O $>$ CH₄, respectively. The N₂O energetically likes better to adsorb on the TiO₂ (101) than the (001) surface. The H₂ dislike to adsorb on the TiO₂ (101) but weakly adsorb on the TiO₂ (001) surface. The CH₄ weakly adsorbs on the TiO₂ (001) surface but very weakly adsorbs on the TiO₂ (101). Two configurations for co-adsorption of N₂O and CO as [O=N=N \cdots CO] and [CO \cdots O=N=N] were found.

3.2 INTRODUCTION

As the titanium dioxide (TiO₂) has been widely employed in many industrial fields, such as photocatalysis [2,3], heterogeneous catalysis [1] and gas-sensor applications [7, 101], its structures and surfaces have been widely studied [19, 20]. Adsorption energies of the small molecules such di-, tri- and tetraatomic gases are very useful information for reaction prediction on the TiO₂ surfaces due to their co-adsorption [40, 39, 67]. For example, in the environmental field, in order to develop the new catalyst for the selective catalytic reduction (SCR) of NO_x [45] in the presence of various small pollutant gases, the adsorption abilities of these small molecules can be utilized to success of new catalyst discovery. Nevertheless, developing new solid-state gas sensors, the adsorption abilities of various gases on the solid surface lead to the discovery of gas sensors.

There have been many experimental and theoretical studies on adsorptions of small molecules on various surface planes of different TiO₂ phases. Theoretical researches of the adsorption of H₂O and NH₃ on the anatase TiO₂ (101) and (001) surfaces as cluster models using density functional theory (DFT) [68], the CO oxidation on stoichiometric anatase TiO₂ (001) surface by *ab initio* calculations [69],

H₂O and O₂ on the anatase TiO₂ (100) [70] and H₂O on the anatase TiO₂ (100), (010) and (001) surfaces using semiempirical MSINDO method [71] were studied. The adsorption of H₂O on the anatase TiO₂ (101) surface using many cluster models was investigated using *ab initio* molecular orbital theory and DFT [72] and CO₂ on the anatase TiO₂ (010), (001), and (101) surfaces using small TiO₂ clusters was studied by DFT calculations [73]. The structural, electronic, and vibrational properties of intermediates of the O₂ photoreduction [74] at the anatase TiO₂ (101) surface and water molecules in contact with the anatase TiO₂ (101) surface [75] were investigated by performing DFT calculations and *ab initio* molecular dynamics (AIMD) simulations. Theoretical simulations of the adsorption behaviors of thin water overlayers on the anatase TiO₂ (101) surface using Car–Parrinello molecular dynamics (CPMD) simulations [76] and molecular dynamics simulations [77] were carried out.

The experiments of the adsorption of water on the anatase TiO₂ (001) surface using synchrotron radiation–excited core level photoelectron spectroscopy [78], adsorption of NH₃ and ND₃ on the anatase phase of TiO₂ using laser Raman spectroscopy [79], adsorption of CO₂ and NH₃ on anatase and rutile TiO₂ using infrared spectrometry [80] and the interaction of water and methanol with the anatase–TiO₂ (101) surface using low–energy electron diffraction (LEED), temperature–programmed desorption (TPD), and X–ray photoelectron spectroscopy (XPS) [81] were carried out.

Even though, there are many theoretical studies of adsorptions of the small gases on the various surface planes of anatase TiO₂, several interesting gases adsorbed on the various plane surfaces of the anatase TiO₂ have not been extensively and comparatively studied using the same or similar methods. The purpose of this work is an examination of the adsorption of CO, H₂, N₂O, NH₃ and CH₄ gases including their competitive co–adsorption on the most stable surfaces of the anatase TiO₂ (001) and (101). The anatase (001) and (101) which are the most common surfaces for anatase [3] have been investigated using density functional theory (DFT) and two–dimensionally periodic slab model [101–103]. Adsorption abilities, in terms of binding and interaction energies of the studied gases have been analyzed and reported.

3.3 COMPUTATIONAL METHODS

All DFT calculations of two-dimensionally periodic slab model have been carried out using the CRYSTAL06 computational code [104], based on the expansion of the crystalline orbitals as a linear combination of a basis set consisting of atom centred Gaussian orbitals. The Kohn–Sham orbitals as Gaussian–type–orbital basis sets of doublezeta quality as an 86–51G(3d) and an 8–411G contraction scheme have been respectively employed for the titanium and oxygen atoms on TiO₂ (001) [105] and (101) surfaces [106]. Basis set for carbon, oxygen, hydrogen and nitrogen atoms of adsorbates employed in this calculations are a 631d1G [107], an 8411dG [108], 31p1G [109] and a 631dG [109], respectively except for carbon atom of methane adsorbed on the TiO₂ (001) surface, the 6311d11G [108] being used. The hybrid functional, B3LYP including Becke’s three parameter exchange [83] and Lee–Yang–Parr correlation [84], has been employed.

The TiO₂ (001) and (101) slabs created using the lattice parameters taken from the X–ray ($a = 3.793$, $c = 9.510$ and $u = 0.208$) [110] (strategy I), and the full geometry optimization ($a = 3.7365$, $c = 9.9811$ and $u = 0.202$) (strategy II) are given in Table 3.1 The Monkhorst–Pack scheme for 8×8×8 k–point mesh in the Brillouin zone was applied for anatase TiO₂ crystal. In geometry optimizations of two-dimensionally periodic slab, the lattice constants were fixed at these values while the positions of all Ti and O atoms were allowed to vary.

The anatase TiO₂ (001) and (101) surfaces are respectively modeled as (1×1) with two Ti layers and (1×1) with four Ti layers as shown in Figure 3.1 The tolerances for geometry optimization convergence have been set to the default values [104] and the Coulomb–exchange screening tolerances were set to (7, 7, 7, 7, 12) and (7, 7, 7, 7, 14) for TiO₂ (001) and (101) surfaces, respectively. All slab calculations have been performed with a Monkhorst–Pack [111] k–point grid with shrinking factors (8, 8).

There are two adsorption sites for the TiO₂ (001) surface: twofold–coordinate O atom (O_{2C}) and fivefold–coordinate Ti atom (Ti_{5C}) and four adsorption sites for the TiO₂ (101) surface: twofold–coordinate O atom (O_{2C}), threefold–coordinate O atom (O_{3C}), fivefold–coordinate Ti atom (Ti_{5C}), and sixfold–coordinate Ti atom (Ti_{6C}).

The adsorption energy (E_{ads}) is computed for adsorbate on the clean surface as follows:

$$\Delta E_{\text{ads}} = E_{\text{adsorbat/surface}} - (E_{\text{adsorbat}} + E_{\text{surface}}) \quad (3.1)$$

where $E_{\text{adsorbat/surface}}$ is the energy of adsorbate on the TiO_2 surface, E_{adsorbat} and E_{surface} are an isolated molecule of adsorbate and a clean TiO_2 surface, respectively.

As the competitive adsorption between two adsorbates and the TiO_2 (001) surface, the Eley–Rideal type has been proposed in this work. Therefore, the first adsorption energy (ΔE_{ads}^1) and the second adsorption energy (ΔE_{ads}^2) are defined as the stepwise adsorption energies for adsorption of the adsorbing gas and non-adsorbing gas, respectively and their energies are written as the Eqs. (3.2) and (3.3).

$$\Delta E_{\text{ads}}^1 = E_{\text{A/TiO}_2} - (E_{\text{A}} + E_{\text{TiO}_2}) \quad (3.2)$$

$$\Delta E_{\text{ads}}^2 = E_{\text{B/A/TiO}_2} - (E_{\text{B}} + E_{\text{A/TiO}_2}) \quad (3.3)$$

Where A and B are adsorbing and non-adsorbing gases, respectively. The overall adsorption energy ($\Delta E_{\text{ads}}^{\text{overall}}$) is therefore defined in Eq. (3.4).

$$\Delta E_{\text{ads}}^{\text{overall}} = \Delta E_{\text{ads}}^1 + \Delta E_{\text{ads}}^2 \quad (3.4)$$

Coverage of adsorbate on the TiO_2 surfaces in terms of the coverage fraction (θ) can be computed as the ratio between the numbers of adsorbate molecules and titanium active atoms in the two-dimensionally periodic slab model. The coverage fraction of adsorbate on the TiO_2 surfaces modeled as (1×1) primitive and (1×1) supercell structures using in the computations are $\theta = 0.25$ and $\theta = 1$ for, respectively.

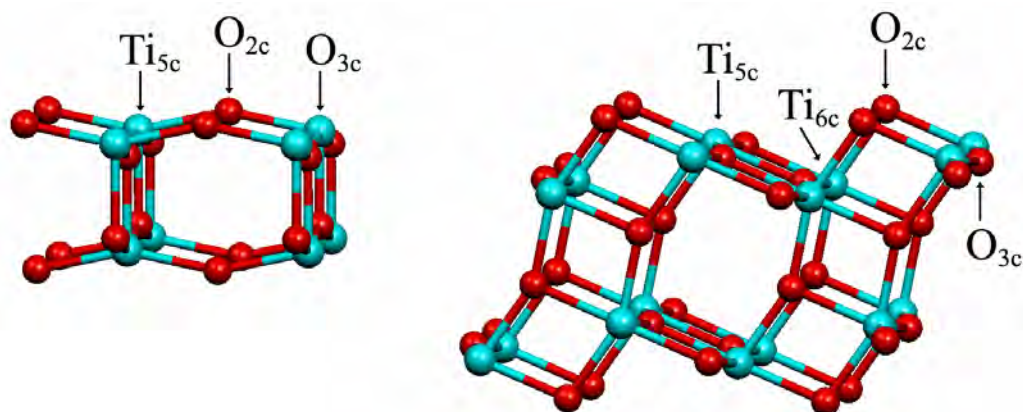


Figure 3.1 The TiO₂ (001) (left) and (101) (right) surface slabs of the full optimized crystal.

3.4 RESULTS AND DISCUSSION

3.4.1 Adsorptions of CO, H₂, N₂O, NH₃ and CH₄ gases on the anatase TiO₂

The adsorption structures of the CO, H₂, N₂O, NH₃ and CH₄ gases on the anatase TiO₂ (001) and (101) surfaces are shown in Figures 3.2 and 3.3, respectively. Bulk parameters of anatase TiO₂ compared with X-ray crystallographic data and other computational works are shown in Table 3.1. In this work, the TiO₂ (001) and (101) surfaces of the slab of X-ray crystal structure ($a = 3.793$, $c = 9.510$ and $u = 0.208$) [110], and of the fully optimized geometry ($a = 3.7365$, $c = 9.9811$ and $u = 0.202$) were termed as the strategy I and strategy II, respectively. The X-ray bulk parameters used in this work were used in many previous works and their results seem to be more accurate than our optimized parameters. On the TiO₂ (001) surface, the atoms O_{2c} and Ti_{5c}, are able to interact with adsorbate. Even though, the TiO₂ (101) surface atoms are different coordinate atoms as O_{2c}, O_{3c}, Ti_{5c} and Ti_{6c}, only the O_{2c}, O_{3c} and Ti_{5c} atoms interact with adsorbate molecules whose interaction cause the physical adsorption.

Table 3.1 Observed and computed lattice parameters of the anatase TiO₂, with space group $I4_1/amd$.

Parameter ^a	DFT ^b	DFT ^c	DFT ^d	Exp ^e	Exp ^f	Exp ^g	Exp ^h	Exp ⁱ	Exp ^j
a	3.737	3.741	3.822	3.793	3.784	3.782	3.7845	3.872	3.783
c	9.981	9.964	9.690	9.510	9.515	9.502	9.5143	9.616	9.513
u^k	0.202	0.202	–	0.208	0.208	0.208	0.2081	0.208	–
α	0	3.741	0	0	0	0	0	0	0
β	0	5.641	0	0	0	0	0	0	0
γ	90	109.4	90	90	90	90	90	90	90

^a The lattice constants (a , c) are in Å.

^b This work, a full optimization at constant volume.

^c Ref. [112]

^d Ref. [113]

^e Ref. [110]

^f Ref. [88]

^g Neutron powder diffraction, Ref. [31]

^h Ref. [114]

ⁱ Nano-crystalline Ref. [115]

^j Nano-crystalline Ref. [116]

^k A fraction of a lattice constant, $u = d_{ap}/c$, where d_{ap} is the apical Ti–O bond length, Ref. [117]

Selected parameters of optimized structures of adsorption CO, H₂, N₂O, NH₃ and CH₄ gases onto the anatase TiO₂ (001) and (101) surfaces are shown in Table 3.2. The CO adsorption on TiO₂, its C atom pointing toward the titanium atom of (001) surface ($C-Ti_{5C} = 2.537$) is longer than the (101) surface by 0.34 Å and but its adsorption energy on the (001) surface is more stable than on the (101) surface by 3 kcal/mol. At high coverage ($\theta = 1$) for the CO adsorbed either on the TiO₂ (001) or (101) surface, the CO points its C atom down on top of the Ti atom and its C=O bond orientation points toward surface titanium atom with small slope, see Figures 3.2 and 3.3.

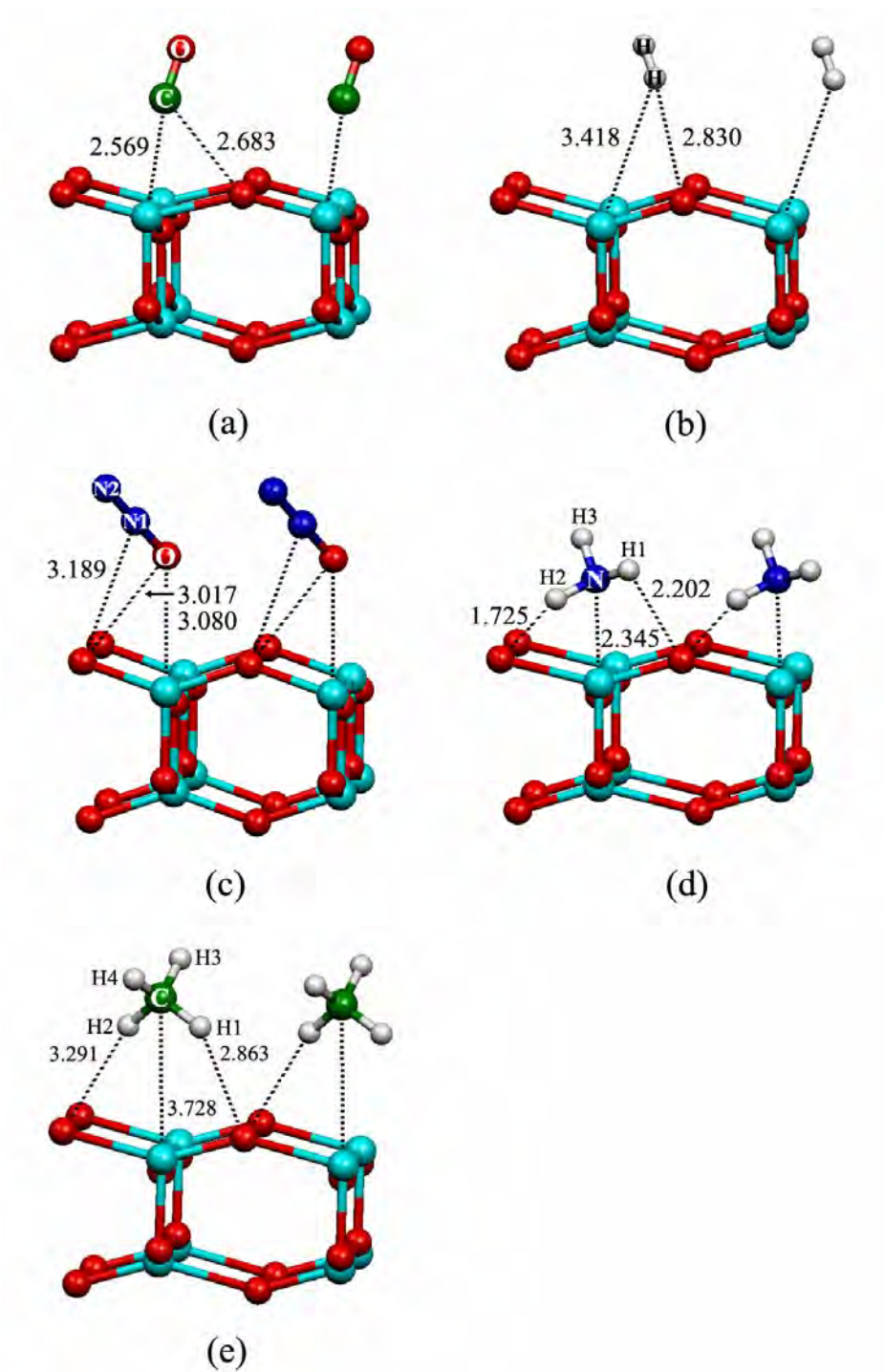


Figure 3.2 Adsorption structures of (a) CO, (b) H_2 , (c) N_2O , (d) NH_3 and (e) CH_4 , adsorbed on anatase TiO_2 (001) surface. Bond distances are in Å.

Table 3.2 Selected parameters of optimized structures for CO, H₂, N₂O, NH₃ and CH₄ gases adsorbed on the anatase TiO₂ (001) and (101) surfaces, distances and angles given in Å and degrees, respectively.

Adsorbate/TiO ₂ parameters	TiO ₂ (001) ^{a,b}	Adsorbate/TiO ₂ parameters	TiO ₂ (101) ^{b,c}
<i>CO adsorbate</i>			
C–Ti _{5C}	2.568	C–Ti _{5C}	2.443
C–O _{2C}	2.683	C–O _{2C}	2.862
O–C–Ti _{5C}	170.0	O–C–Ti _{5C}	175.0
<i>H₂ adsorbate</i>			
H–Ti _{5C}	3.418	H–Ti _{5C}	-
H–H–Ti _{5C}	2.830	H–H–Ti _{5C}	-
H–H–Ti _{5C}	143.0	H–H–Ti _{5C}	-
<i>N₂O adsorbate</i>			
O–Ti _{5C}	3.079	O–Ti _{5C}	2.506
O–O _{2C}	3.016	O–O _{2C}	2.842
N1–O _{2C}	3.187	N1–O _{2C}	2.900
N1–O–Ti _{5C}	111.9	N1–O–Ti _{5C}	113.3
<i>NH₃ adsorbate</i>			
N–Ti _{5C}	2.336	N–Ti _{5C}	2.384
H1–O _{2C}	2.383	H1–O _{2C}	2.250
H1–N–Ti _{5C}	92.5	H1–N–Ti _{5C}	96.9
<i>CH₄ adsorbate</i>			
C–Ti _{5C}	3.741	C–Ti _{5C}	3.494
H1–O _{2C} ^d	2.860	H1–O _{2C}	2.698
H2–O _{2C} ^d	3.155	H2–O _{2C}	3.717
H1–C–Ti _{5C}	49.7	H1–C–Ti _{5C}	50.83

^a (1×1) with two Ti layers.

^b Based on the strategy II.

^c (1×1) with four Ti layers.

^d They are not the same atom.

Table 3.3 Adsorption energies (in kcal/mol) for the CO, H₂, N₂O, NH₃ and CH₄ adsorbed on the anatase TiO₂ (001) and (101) surfaces.

Adsorbate	TiO ₂ (001) ^a			TiO ₂ (101) ^b		
	ΔE_{ads}^1 (I) ^c	ΔE_{ads}^2 ^d		ΔE_{ads}^1 ^c	ΔE_{ads}^2 ^d	
CO	-9.73	-8.49	-5.30 ^e	-6.78	-3.12	-5.70 ^f
H ₂	-3.15	-1.77		- ^g	- ^g	
N ₂ O	-2.41	-2.21		-5.00	-5.44	
NH ₃	-26.58	-24.11	-23.72 ^h	-24.34	-24.41	-30.78 ^h ; -27.5 ⁱ
CH ₄	-2.93	-1.21		-0.65	-0.37	

^a (1×1) with two Ti layers.

^b (1×1) with four Ti layers.

^c Based on the strategy I.

^d Based on the strategy II.

^e The (001) surface, computed with the VASP–GGA method, Ref. [69]

^f The (2×2) slab, computed with the periodic DFT method, Ref. [111]

^g No adsorption was found.

^h The TiO₉H₁₀ cluster, computed with the B3LYP/6–31G(d,p) method, Ref. [68]

ⁱ The (001) surface, computed with the VASP–GGA method, Ref. [118]

The N₂O adsorption on TiO₂, its O atom pointing toward the titanium atom of (001) surface (O–Ti_{5C} = 2.948) is longer than the (101) surface by 0.45 Å and but its adsorption energy on the (001) surface is less stable than on the (001) surface by 2.6 kcal/mol. The adsorption energies of these gases adsorbed on the anatase TiO₂ (001) and (101) surfaces are listed in Table 3.3. It shows that both of the TiO₂ (001) and (101) surfaces can strongly adsorb NH₃ and fairly adsorb CO. The H₂ can weakly be adsorbed on the TiO₂ (001) surface but not adsorbed on the TiO₂ (001) surface. Plot of their adsorption energies derived from computation of the strategy I are shown in Figure 3.4.

Selected atomic charges (in e) of all the optimized structures for CO, H₂, N₂O, NH₃ and CH₄ gases adsorbed on the anatase TiO₂ (001) and (101) surfaces are shown in Table 3.4. It shows change of partial charge of atoms of adsorbate and surface TiO₂ as isolation and adsorption state. Physically, the TiO₂ (001) surface seem to be smoother than the (001) surface as demonstrated in Figure 3.1 and number of active titanium atom per area of the (001) surface are larger than of the (101) surface.

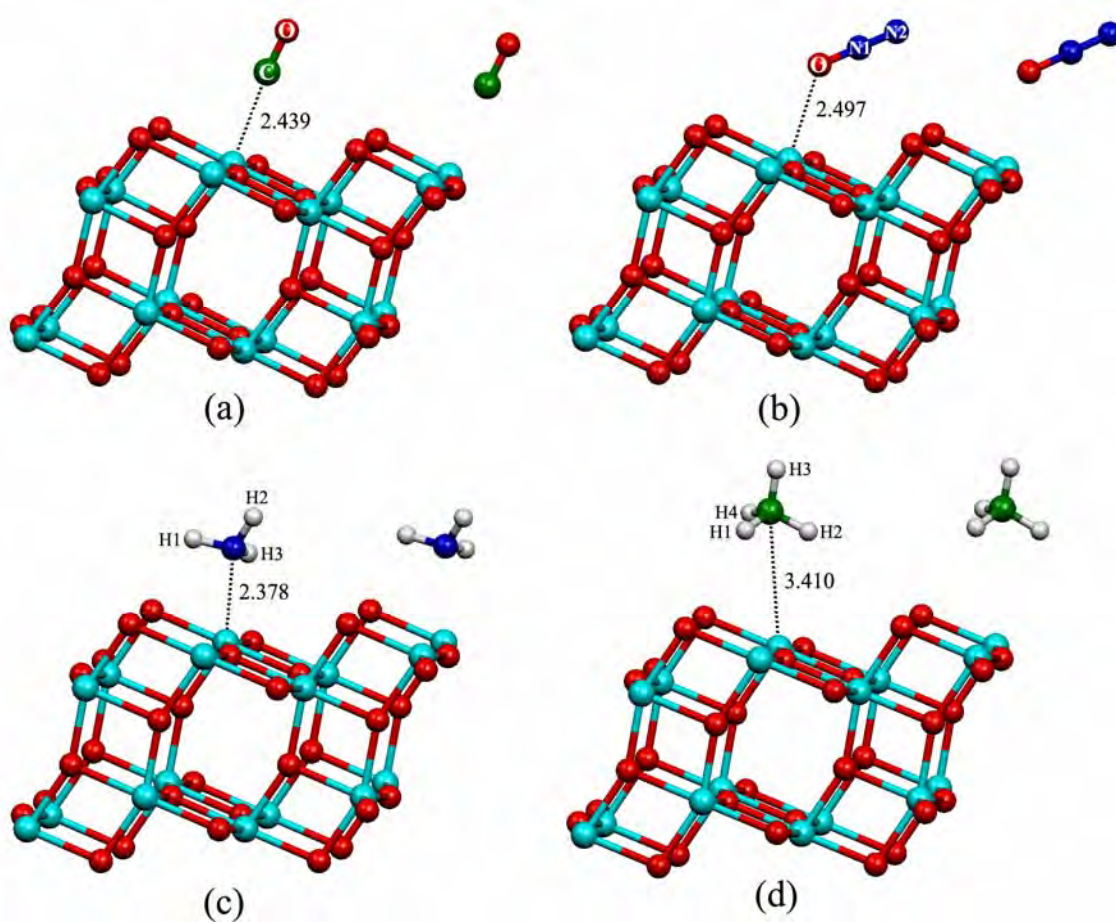


Figure 3.3 Adsorption structures of (a) CO, (b) N₂O, (c) NH₃ and (d) CH₄, adsorbed on the anatase TiO₂ (101) surface. Bond distances are in Å.

Table 3.4 Selected atomic charges (in e) of optimized structures for CO, H₂, N₂O, NH₃ and CH₄ gases adsorbed on the anatase TiO₂ (001) and (101) surfaces.

Adsorption system	TiO ₂ (001) ^{a,b}	TiO ₂ (101) ^{b,c}
<i>CO/TiO₂</i>		
TiO ₂	Ti _{5C} = 2.543, O _{2C} = -1.315, O _{3C} = -1.182	Ti _{5C} = 2.452, O _{2C} = -1.274, O _{3C} = -1.058
CO	C = 0.053	C = 0.093
CO	O = -0.106	O = -0.142
<i>H₂/TiO₂</i>		
TiO ₂	Ti _{5C} = 2.524, O _{2C} = -1.317, O _{3C} = -1.198	-
H ₂	H = 0.000	-
H ₂	H = -0.010	-
<i>N₂O/TiO₂</i>		
TiO ₂	Ti _{5C} = 2.533, O _{2C} = -1.321, O _{3C} = -1.201	Ti _{5C} = 2.446, O _{2C} = -1.283, O _{3C} = -1.079
N ₂ O	N = -0.212	N = -0.177
N ₂ O	N = 0.432	N = 0.481
N ₂ O	O = -0.232	O = -0.177
<i>NH₃/TiO₂</i>		
TiO ₂	Ti _{5C} = 2.551, O _{2C} = -1.322, O _{3C} = -1.246	Ti _{5C} = 2.462, O _{2C} = -1.333, O _{3C} = -1.094
NH ₃	N = -0.806	N = -0.835
NH ₃	H = 0.341	H = 0.338
NH ₃	H = 0.246	H = 0.299
NH ₃	H = 0.230	H = 0.233
<i>CH₄/TiO₂</i>		
TiO ₂	Ti _{5C} = 2.529, O _{2C} = -1.314, O _{3C} = -1.193	Ti _{5C} = 2.452, O _{2C} = -1.338, O _{3C} = -1.033
CH ₄	C = -0.648	C = -0.507
CH ₄	H = 0.163	H = 0.129
CH ₄	H = 0.154	H = 0.123
CH ₄	H = 0.155	H = 0.119
CH ₄	H = 0.152	H = 0.123

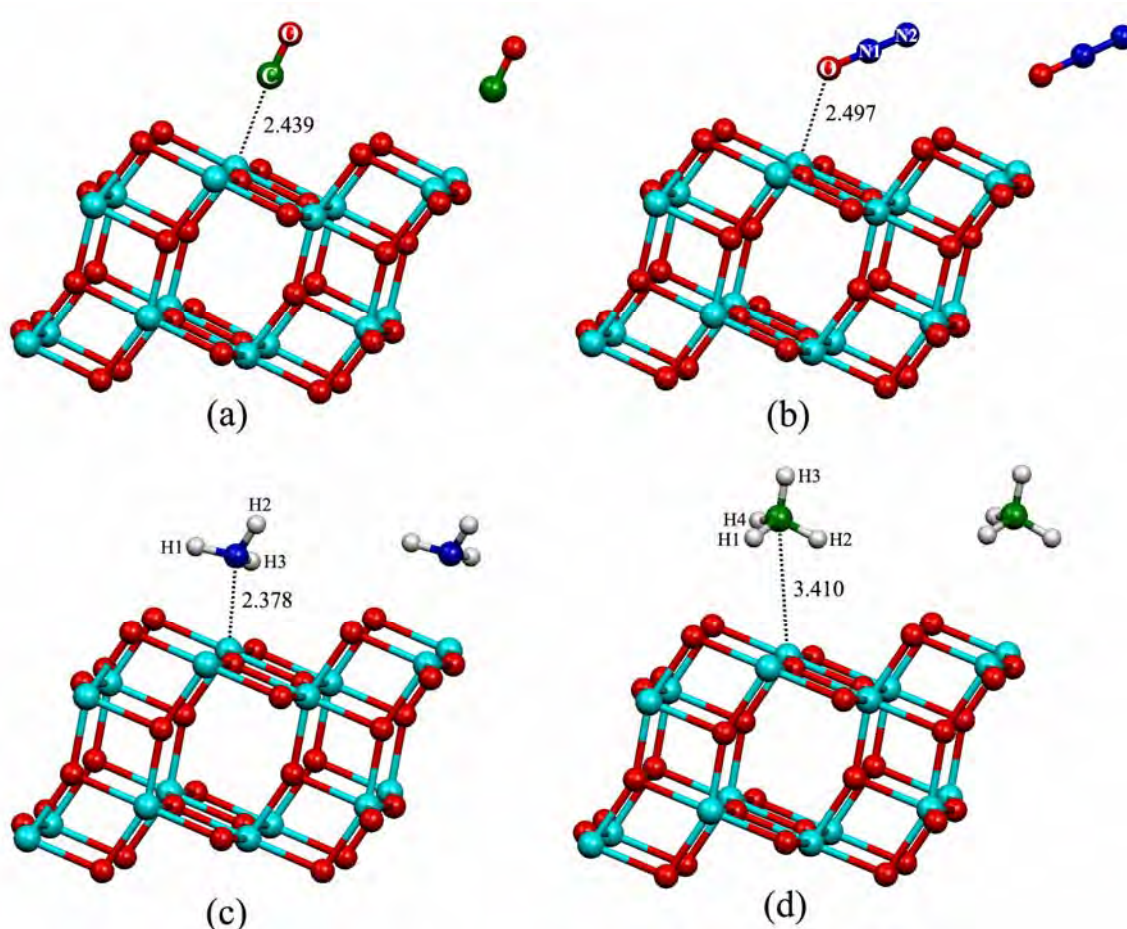


Figure 3.4 Adsorption structures of (a) CO, (b) N₂O, (c) NH₃ and (d) CH₄, adsorbed on the anatase TiO₂ (101) surface. Bond distances are in Å.

3.4.2 Co-adsorption on the anatase TiO₂

Co-adsorption configurations of three possible pairs, CO/N₂O, CO/H₂ and H₂/N₂O were studied using the partial optimization model of which the coordinates based on the TiO₂ (1×1) supercell with three Ti layers (12 Ti atoms and 24 O atoms) were frozen. It was found that the co-adsorption of these three pairs cannot take place on the anatase TiO₂ (101) surface. This may be caused by the corrugated character of the anatase TiO₂ (101) surface. Convergences of the structure optimizations of co-adsorption configuration of CO/H₂ and H₂/N₂O on the anatase TiO₂ (001) surface have been not achieved but departures of these co-adsorption CO/H₂ and H₂/N₂O from the TiO₂ (001) surface were found. It can be remarked that co-adsorption of H₂

and N₂O should not exist because the repulsion between atoms of H₂ and N₂O overcomes their adsorption whose energies are -3.15 and -2.41 kcal/mol, respectively. Desorption of H₂ and N₂O on the TiO₂ (001) surface is suggested by divergence of their co-adsorption.

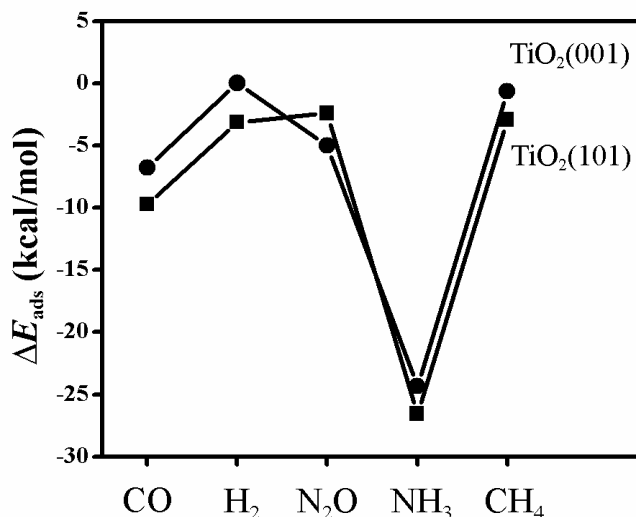
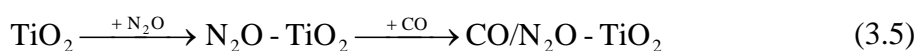


Figure 3.5 Adsorption energies of CO, N₂O, NH₃ and CH₄ on the anatase TiO₂ (001) and (101) surfaces, based on the strategy I.

There are two configurations for co-adsorption of N₂O and CO as the [CO...O=N=N] and [O=N=N...CO] which are called as configuration I and configuration II, respectively (see Figure 3. 6(a) and (b)). These two configurations were obtained from the structure optimizations using the initial configurations based on the possible adsorption structures. Only the configuration of [CO...O=N=N] (configuration I) leads to the production of CO₂ and N₂. The conversion of the N₂O and CO to the CO₂ and N₂ is likely to follow the Eley-Rideal type mechanism. Two possible stepwise reactions of the adsorption of N₂O and CO on the (001) surface are shown in the Eqs. (3.5) and (3.6).



where as $\Delta E_{\text{ads}}^1 = -9.10$, $\Delta E_{\text{ads}}^2 = -2.59$ and $\Delta E_{\text{ads}}^{\text{Overall}} = -11.69$ kcal/mol,



where as $\Delta E_{\text{ads}}^1 = -12.03$, $\Delta E_{\text{ads}}^2 = -5.05$ and $\Delta E_{\text{ads}}^{\text{Overall}} = -17.08$ kcal/mol. It was found that the stepwise reactions of Eq. (3.5) corresponds with the configuration I (Figure 3.5(a)) and the Eley–Rideal type mechanism. Namely, CO secondly adsorbs on top of N₂O as the firstly adsorbed species; this can be confirmed with the bond distances of their interactions, see Figure 3.6.

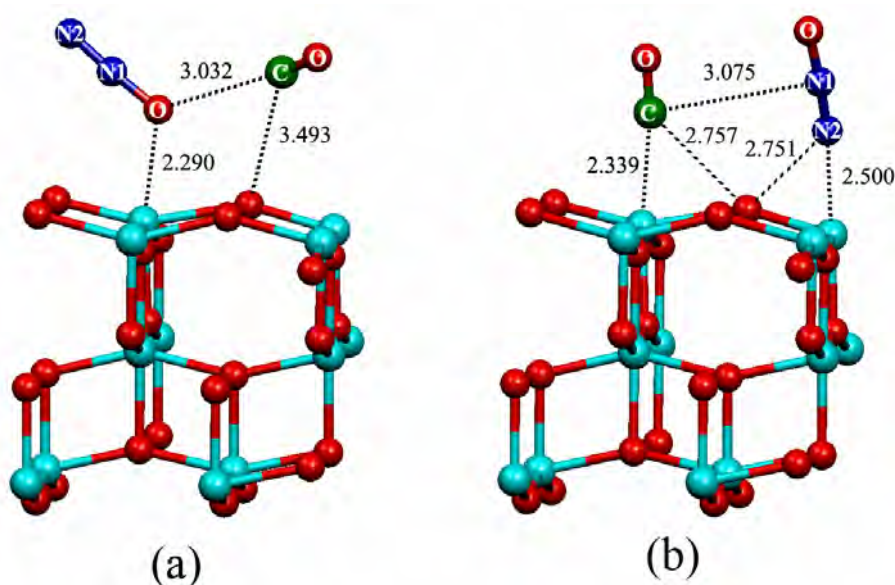


Figure 3.6 Adsorption configurations of CO and N₂O co-adsorbed on the anatase–TiO₂ (001) surface as (a) [CO···O=N=N], configuration I and (b) [N=N=O/CO], configuration II. Bond distances are in Å.

As two configurations for co-adsorption of N₂O and CO as [CO···O=N=N] and [N=N=O/CO] were found. Only the configuration I, [CO···O=N=N] leads to the production of CO₂ and N₂. The conversion of N₂O and CO to products CO₂ and N₂ is likely to follow the Eley–Rideal type mechanism. To forward this conversion reaction, the reactants N₂O and CO adsorbed on the anatase–TiO₂ (001) surface have to form transition–state whose the proposed structure can be given as shown in Figure 3.7. The co-existing gases CO₂ and N₂ dislike to be adsorbed but rather desorbed on

the (001) surface. This trend was indicated by divergence of the structure optimization of co-adsorption of CO₂ and N₂ on the (001) surface.

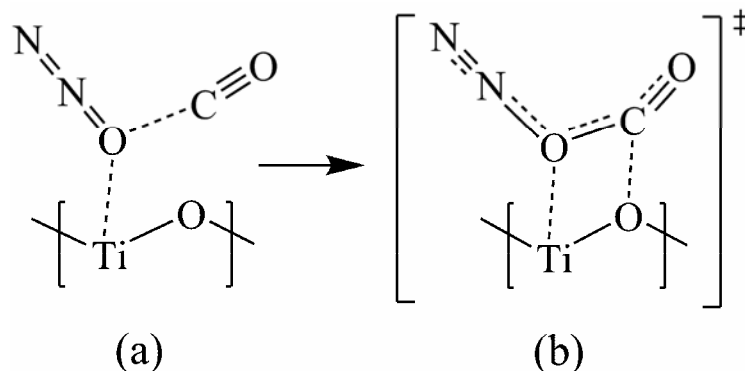


Figure 3.7 Co-adsorption configurations of (a) CO and N₂O on the anatase TiO₂ (001) surface and (b) its proposed transition-state structure.

2.5 CONCLUSIONS

The adsorption of CO, H₂, N₂O, NH₃ and CH₄ gases on the anatase TiO₂ (001) and (101) surfaces were investigated using the B3LYP calculations. The relative adsorption energies of these gases on the TiO₂ (001) and (101) surfaces are in orders: NH₃ \gg CO \gg H₂ \approx CH₄ \approx N₂O and NH₃ \gg CO \approx N₂O $>$ CH₄, respectively. Two configurations for co-adsorption of N₂O and CO on the TiO₂ (001) were found but on the (101) does not exist. It has been suggested that the configuration I of the co-adsorption of N₂O and CO on the anatase-TiO₂ (001) surface can be converted to form products CO₂ and N₂ via the transition-state.

CHAPTER IV

PERIODIC DENSITY-FUNCTIONAL THEORY STUDY OF CO, H₂, N₂O, NH₃ AND CH₄ ADSORBED ON THE RUTILE TiO₂ (001) AND (110) SURFACES

Raina Wanbayor, Vithaya Ruangpornvisuti

*Department of Chemistry, Faculty of Science, Chulalongkorn University, Bangkok
10330, Thailand*

This article has been submitted

4.1 ABSTRACT

The adsorption energies of CO, H₂, N₂O, NH₃ and CH₄ gases on the rutile TiO₂ (001) and (110) surfaces were obtained using periodic slab models density–functional method. The relative adsorption energies of these gases on the rutile TiO₂ (001) and (110) surfaces are in orders: NH₃ > N₂O > CO >> H₂ > CH₄ and NH₃ > N₂O ≈ CO >> H₂, respectively.

4.2 INTRODUCTION

Many applications of titanium oxide (TiO₂) as photocatalysis, [1–3, 5] heterogeneous catalysis [1] and gas–sensor, [7, 100] have been successful and TiO₂ surfaces have been widely studied over many years [19–20]. As these applications of the TiO₂ caused by its adsorption abilities on gases or small molecules, there have been numerous experimental and theoretical studies on adsorptions of small molecules such di–, tri– and tetraatomic gases, and also co–adsorptions [39, 67, 26] on various surface planes of different TiO₂ phases. As in nature TiO₂ exists in four polymorphs, i.e. anatase, rutile, brookite and TiO₂ (B) core [119]. Both rutile and anatase polymorphs have been extremely investigated in experimental and theoretical studies. Nevertheless, rutile is the most stable for large particles [33], but anatase becomes more stable than rutile only when the particle size decreases below *ca.* 14 nm [34]. It has been extensively studied the adsorption of di–, tri– and tetraatomic gases on different of TiO₂ surfaces such as CO, CO₂, H₂ and H₂O [120], N₂, O₂, and CO [42], NH₃ [121–122], N₂O, [49]. In previous works, we have investigated the adsorption of small gases on the anatase TiO₂ (101) and (001) surfaces [25, 26] and compared all our results with all other works. We have found that the most stable configuration takes place when the adsorbed molecular gases toward Ti_{5C} on the surface except H₂.

Nevertheless, sequences of adsorptions of the small gases on the various surface planes of rutile TiO₂ have hardly been found. In this letter we have therefore studied adsorptions of the small gases series i.e. CO, H₂, N₂O, H₂O, NH₃ and CH₄ on the rutile TiO₂ (001) and (110) surfaces using periodic slab models density–functional

method. The adsorption abilities of the rutile TiO_2 (001) and (110) surfaces on these small gases compared with all other works have been reported.

4.3 COMPUTATIONAL METHODS

All DFT calculations of two-dimensionally periodic slab model have been carried out using the CRYSTAL06 computational code [104], based on the expansion of the crystalline orbitals as a linear combination of a basis set consisting of atom centered Gaussian orbitals. The Kohn–Sham orbitals as Gaussian–type–orbital basis sets of double zeta quality as an 86–51G(3d) and an 8–411G contraction scheme have been respectively employed for the titanium and oxygen atoms on TiO_2 (001) [105] and (110) surfaces [106]. Basis set for carbon, oxygen, hydrogen and nitrogen atoms of adsorbates employed in this calculations are a 631d1G [107], an 8411dG [108], 31p1G [109], and a 631dG [109], respectively, except for carbon atom of methane adsorbed on the TiO_2 (001) surface, the 6311d11G [108] being used. The hybrid functional, B3LYP including Becke’s three–parameter exchange [83] and Lee–Yang–Parr correlation [84], has been employed.

The optimized bulk lattice parameters, are $a = 4.572 \text{ \AA}$, and $c = 2.992 \text{ \AA}$, to be compared to the experimental results of 4.586 and 2.954 \AA , respectively [31] as listed in Table 4.1. The Monkhorst–Pack scheme for $8 \times 8 \times 8$ k–point mesh in the Brillouin zone was applied for rutile TiO_2 crystal. In geometry optimizations of two-dimensionally periodic slab, the lattice constants were fixed at these values while the positions of all Ti and O atoms were allowed to relax. The rutile TiO_2 (001) and (110) surfaces are, respectively modeled as (1×1) with three Ti layers and (1×1) with two Ti layers as shown in Figure 4.1. The tolerances for geometry optimization convergence have been set to the default values [104] and the coulomb–exchange screening tolerances were set to (7, 7, 7, 7, 12). All slab calculations have been performed with a Monkhorst–Pack [111] k–point grid with shrinking factors (8, 8). There are two adsorption sites for the rutile TiO_2 (001) surface: twofold–coordinate O atom (O_{2C}) and fivefold–coordinate Ti atom (Ti_{5C}) and three adsorption sites for the rutile TiO_2 (110) surface: twofold–coordinate O atom (O_{2C}), threefold–coordinate O atom (O_{3C}) and fivefold–coordinate Ti atom (Ti_{5C}) as shown in Figure 4.1. The adsorption energy (ΔE_{ads}) is computed for adsorbate on the clean surface as follow:

$$\Delta E_{\text{ads}} = E_{\text{adsorbate/slab}} - (E_{\text{adsorbate}} + E_{\text{slab}}) \quad (4.1)$$

where $E_{\text{adsorbate/slab}}$ is the energy of adsorbate adsorbed on the TiO_2 surface, $E_{\text{adsorbate}}$ and E_{slab} are an isolated molecule of adsorbate and a clean TiO_2 surface, respectively.

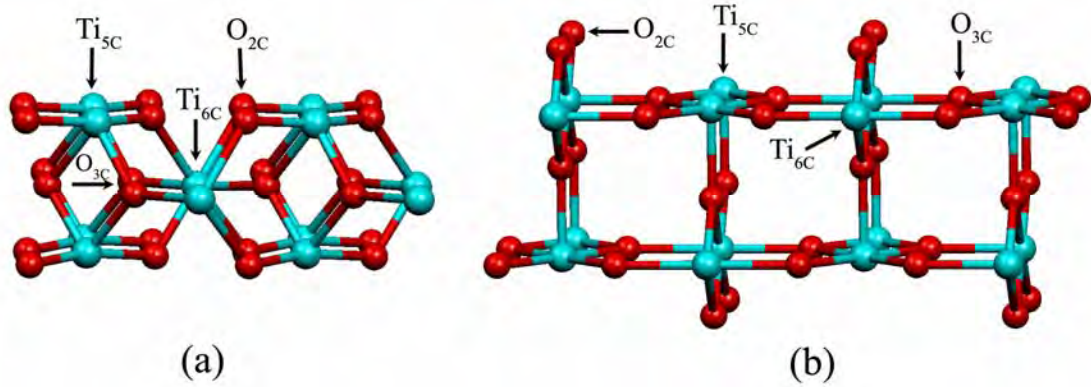


Figure 4.1 The rutile TiO_2 (a) (001) and (b) (110) surface slabs of the full optimized crystal.

Table 4.1 Computed and experimental lattice parameters of the rutile TiO_2 , with space group $P4_2/mnm$.

Parameter ^a	DFT ^b	DFT ^c	DFT ^d	DFT ^e	DFT ^f	Exp ^g	Exp ^h	Exp ⁱ
a	4.572	4.568	4.594	4.6350	4.614	4.5929	4.5937	4.586
c	2.992	2.926	2.959	2.9594	2.979	2.9591	2.5987	2.954
u^j	–	–	0.03059	–	–	0.03056	–	–

^a The lattice constants (a , c) are in Å.

^b This work.

^c Ref. [123]

^d Ref. [124]

^e Ref. [125]

^f Ref. [126]

^g Ref. [128]

^h Ref. [129]

ⁱ Ref. [31]

^j fraction of a lattice constant, $u = d_{ap}/c$, where d_{ap} is the apical Ti–O bond length.

4.4 RESULTS AND DISCUSSION

The adsorption structures of the CO, H₂, N₂O, NH₃ and CH₄ gases on the rutile TiO₂ (001) and (110) surfaces are shown in Figure 4.2. Bulk and surface parameters of the rutile TiO₂ compared with x-ray crystallographic data and other computational works are shown in Table 4.1. The x-ray bulk parameters used in this work were used in many previous works and their results seem to be more accurate than our optimized parameters. On the TiO₂ (001) surface, the atoms O_{2C} and Ti, are able to interact with adsorbate. Even though, the TiO₂ (110) surface atoms are different coordinate atoms as O_{2C}, O_{3C} and Ti_{5C}, only the O_{2C} and Ti_{5C} atoms interact with adsorbate molecules whose interaction cause the physical adsorption.

Selected parameters of optimized structures for CO, H₂, N₂O, NH₃ and CH₄ gases adsorbed on the rutile TiO₂ (001) and (110) surfaces are shown in Table 4.2. The CO adsorption on TiO₂, its C atom pointing toward the titanium atom of (001) surface (C–Ti_{5C} = 2.505 Å) is shorter than the (110) surface by 0.035 Å. The adsorption of CO on the TiO₂ (001) surface is more stable than the (110) surface by 1.16 kcal/mol. The CO adsorption on the (001) surface, the CO points its C atom down on top of the Ti atom and its C=O bond orientation points toward surface titanium atom with tilt angle (see Figure 4.2) but on the (110) surface, the CO points its C atom down on top of the Ti atom with a nearly straight line (see Figure 4.3).

The H₂ adsorption either on the TiO₂ (001) or the (110) surface are very low with energies of –2.24 and –0.66 kcal/mol, respectively. The H₂ points one of its atom toward the O_{2C} of the (001) surface with distance of 2.351 Å and its orientation is nearly perpendicular to the surface. The H₂ adsorption on the (110) surface, the H₂ point one of its atoms toward the O_{2C} of the (110) surface with the nearly straight line and pointing orientation is nearly perpendicular to the surface but the projection of its molecule on the (110) surface plane is located between O_{2C} and Ti_{5C} atoms.

The N₂O adsorptions on the (001) and (110) are very similar configurations by pointing its N-end atom toward the Ti_{5C} atom of the surface with angles of 156.7° for the (001) and 152.9° for the (110).

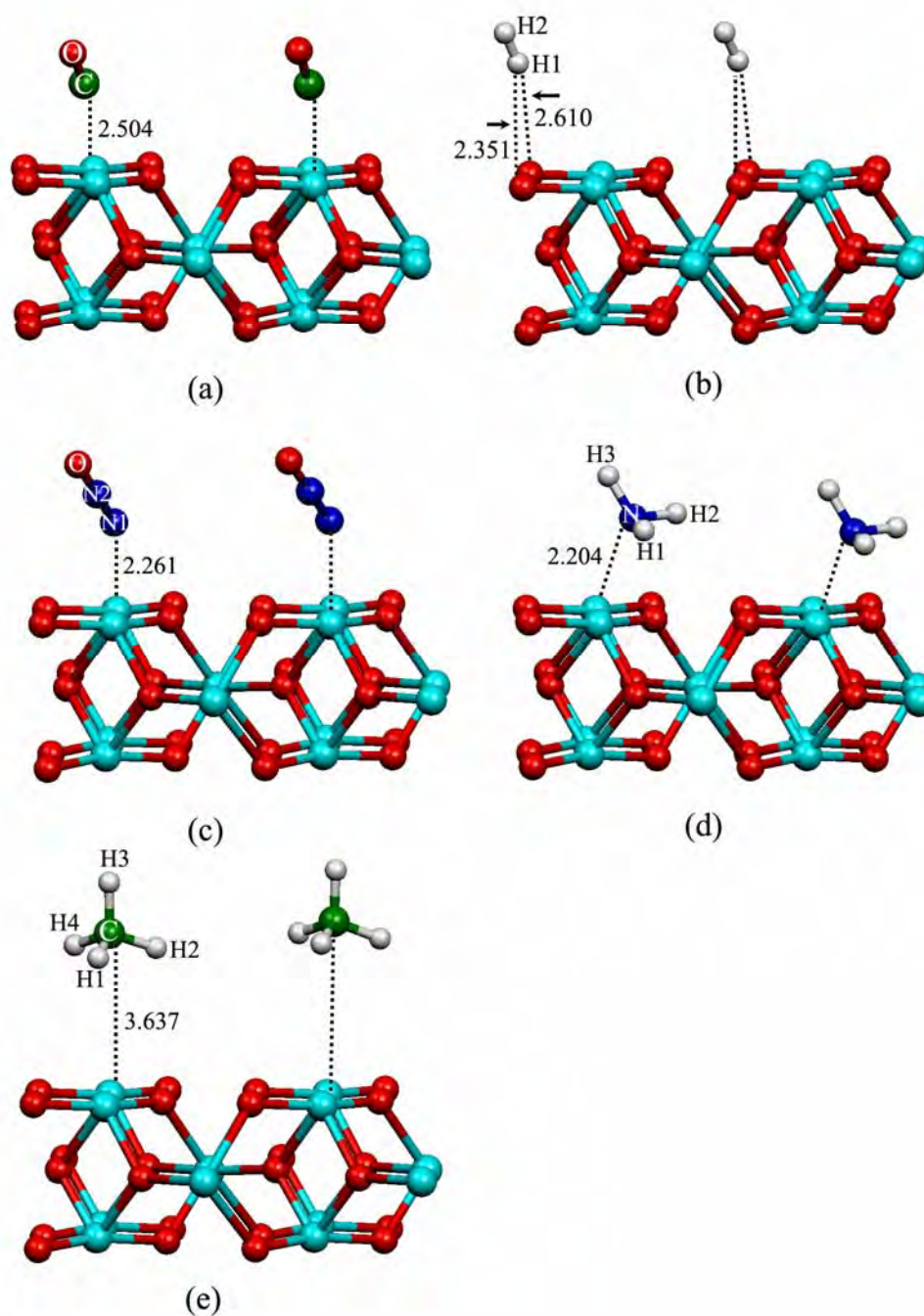


Figure 4.2 Adsorption structures of (a) CO, (b) H₂, (c) N₂O, (d) NH₃ and (e) CH₄, adsorbed on the rutile TiO₂ (001) surface. Bond distances are in Å.

Table 4.2 Selected parameters of optimized structures for CO, H₂, N₂O, NH₃ and CH₄ gases adsorbed on the rutile TiO₂ (001) and (110) surfaces, distances and angles given in Å and degrees, respectively.

Adsorbate/TiO ₂ parameters	TiO ₂ (001)	Adsorbate/TiO ₂ parameters	TiO ₂ (110)
<i>CO adsorbate:</i>			
C–Ti _{5C}	2.504	C–Ti _{5C}	2.539
C–O _{2C}	2.461	C–O _{2C}	3.348
O–C–Ti _{5C}	172.2	O–C–Ti _{5C}	179.7
<i>H₂ adsorbate:</i>			
H–Ti _{5C}	2.710	H–Ti _{5C}	3.789
H–O _{2C}	2.351	H–O _{2C}	2.778
H–H–O _{2C}	157.9	H–H–O _{2C}	175.8
H–H–Ti _{5C}	87.5	H–H–Ti _{5C}	112.0
<i>N₂O adsorbate:</i>			
N1–Ti _{5C}	2.261	N1–Ti _{5C}	2.347
N1–O _{2C}	2.937	N1–O _{2C}	3.050
N2–N1–Ti _{5C}	156.7	N2–N1–Ti _{5C}	152.9
<i>NH₃ adsorbate:</i>			
N–Ti _{5C}	2.204	N–Ti _{5C}	2.402
H1–O _{2C}	2.383	H1–O _{2C}	2.385
H1–N–Ti _{5C}	103.7	H1–N–Ti _{5C}	112.7
<i>CH₄ adsorbate:</i>			
C–Ti _{5C}	3.637	C–Ti _{5C}	– ^a
H1–O _{2C}	3.348	H1–O _{2C}	– ^a
H1–C–Ti _{5C}	81.8	H1–C–Ti _{5C}	– ^a

^a No adsorption is found.

The adsorption of NH₃ either on the (001) or (110) plane is the strongest compared with all other studied gases and the NH₃ adsorption on the (001) is more stable than on the (110) by 18.27 kcal/mol. For the NH₃ adsorption on the (001) and or (110) surfaces, the ammonia molecule points its N atom toward the Ti_{5C} atom with distances of 2.204 Å and 2.402 Å, respectively.

The methane can adsorb on the rutile TiO_2 (001) surface with very weak adsorption ($\Delta E_{\text{ads}} = -1.04$ kcal/mol) but not adsorb on the (110) surface.

The relative adsorption energies of these gases on the rutile TiO_2 (001) and (110) surfaces are in orders: $\text{NH}_3 > \text{N}_2\text{O} > \text{CO} \gg \text{H}_2 > \text{CH}_4$ and $\text{NH}_3 > \text{N}_2\text{O} \approx \text{CO} \gg \text{H}_2$, respectively. The adsorption energies of CO, H_2 , N_2O , H_2O , NH_3 and CH_4 on the rutile TiO_2 (001) and (110) surfaces are shown in Table 4.3 and comparison of their plots is shown in Figure 4.4.

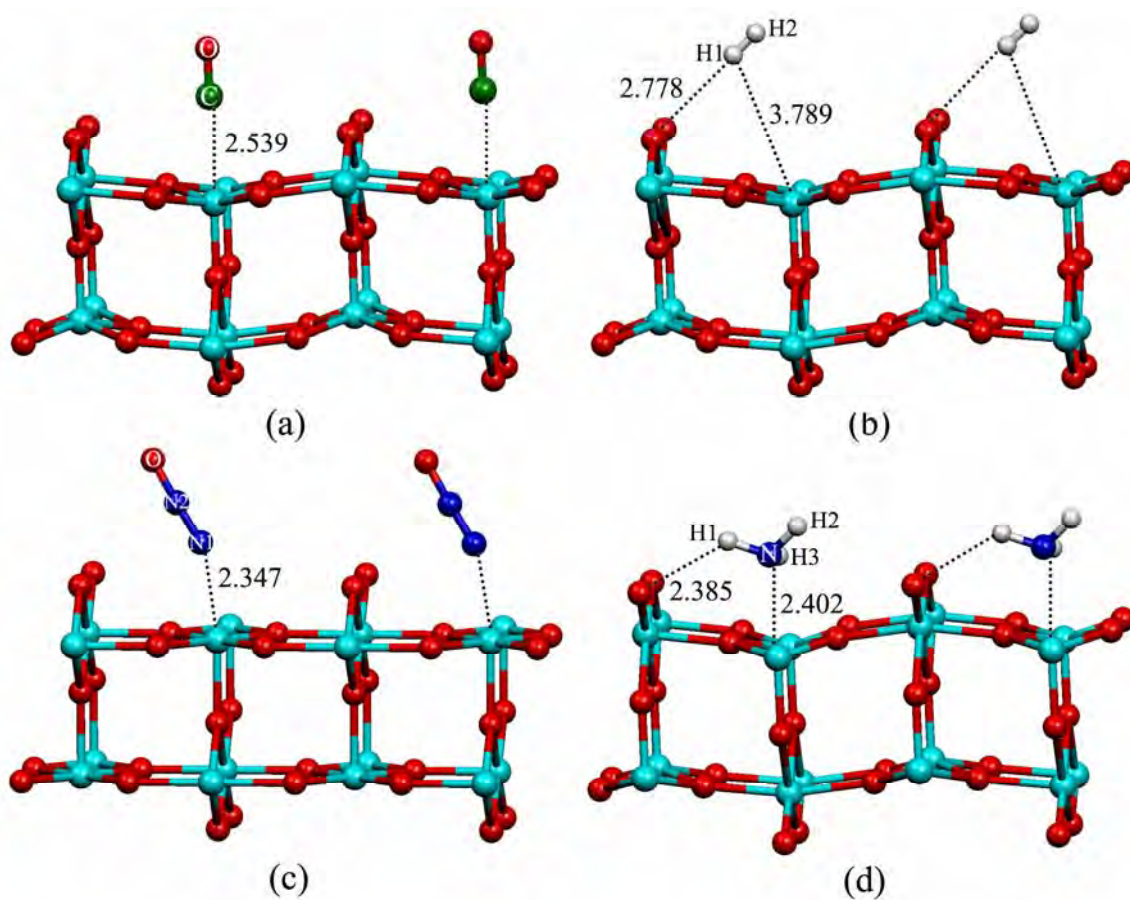


Figure 4.3 Adsorption structures of (a) CO, (b) H_2 , (c) N_2O and (d) NH_3 adsorbed on the rutile TiO_2 (110) surface. Bond distances are in Å.

Table 4.3 Adsorption energies for the CO, H₂, N₂O, NH₃ and CH₄ adsorbed on the rutile TiO₂ (001) and (110) surfaces.

Adsorbate	ΔE_{ads}	
	TiO ₂ (001) ^a	TiO ₂ (110) ^b
CO ^c	-14.77	-13.61, -18.26 ^d , -6.44 ^e
H ₂	-2.24	-0.66
N ₂ O	-18.06	-13.71, -4.2 ^f
NH ₃	-42.73	-24.46
CH ₄	-1.04	- ^g

^a (1×1) slab surface with 12 Ti atoms and 24 O atoms.

^b (1×1) slab surface with 16 Ti atoms and 32 O atoms.

^c Pointing the C-atom toward the titanium atom of surface.

^d No adsorption was found.

^e Ref. [129]

^f Ref. [130]

^g No adsorption was found.

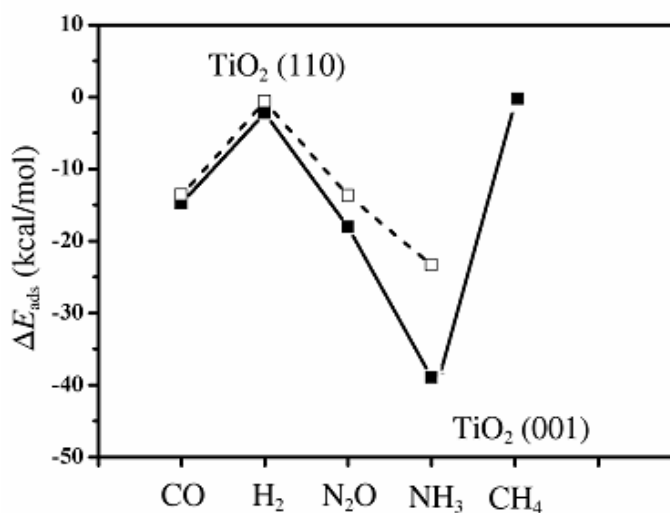


Figure 4.4 Adsorption energies of CO, H₂, N₂O, NH₃ and CH₄ on the rutile TiO₂ (001) and (110) surfaces.

4.5 CONCLUSIONS

The adsorption energies of CO, H₂, N₂O, NH₃ and CH₄ gases on the rutile TiO₂ (001) and (110) surfaces were obtained using periodic slab models density-functional method. All the studied gases can adsorb on the rutile TiO₂ (001) and (110) surfaces, except methane cannot adsorb on the (110) surface. Adsorptions of each adsorbed gases on the (001) surface are stronger than on the (110) surface. The relative adsorption energies of these gases on the rutile TiO₂ (001) and (110) surfaces are in orders: NH₃ > N₂O > CO >> H₂ > CH₄ and NH₃ > N₂O ≈ CO >> H₂, respectively.

CHAPTER V

FIRST-PRINCIPLE THEORETICAL STUDY OF HOLE-ASSISTED CONVERSION OF CO TO CO₂ ON THE ANATASE TiO₂ (101) SURFACE

Raina Wanbayor,^{1,2} Peter Deák,² Thomas Frauenheim,² and Vithaya Ruangpornvisuti¹

¹*Department of Chemistry, Faculty of Science, Chulalongkorn University, Bangkok
10330, Thailand*

²*Bremen Center for Computational Material Science, University Bremen, 28359
Bremen, Germany*

This article has been published in Journal of Chemical Physics Page: 104701-6.

Volume: 134. Year: 2011.

5.1 ABSTRACT

First principles density functional theory calculations were carried out to investigate the adsorption and oxidation of CO on the positively charged (101) surface of anatase, as well as the desorption of CO₂ from it. We find that the energy gain on adsorption covers the activation energy required for the oxidation, while the energy gain on the latter is sufficient for the desorption of CO₂, leaving an oxygen vacancy behind. Molecular dynamics simulations indicate that the process can be spontaneous at room temperature. The oxidation process described here happens only in the presence of the hole. The possibility of a photocatalytic cycle is discussed assuming electron scavenging by oxygen.

5.2 INTRODUCTION

As titanium dioxide (TiO₂) is being employed in numerous applications, such as photocatalysis [2–5], heterogeneous catalysis [1] and gas-sensors [7, 100], its structures and surfaces have been widely studied [19, 20]. Knowledge about the adsorption energies of small molecules, such as those of di-, tri- and tetraatomic gases, are very useful to predict reactions between co-adsorbed molecules [39, 40, 67]. Among the most common polymorphs [119] of TiO₂, anatase is considered the most photoactive phase [131, 132, 134].

The adsorption characteristics of CO, CO₂, H₂ and H₂O was determined by temperature-programmed desorption (TPD) from unspecified rutile surfaces with varying oxidation state between Ti⁴⁺ and Ti²⁺ [43]. These experiments indicated that CO is weakly adsorbed with low saturation coverage on the oxidized (TiO₂) surface, while the adsorption strength and the coverage slightly increase with reduction of the surface. Adsorption of CO was also studied by TPD specifically on the oxidized (non-defective) (110) surface of rutile, and compared to the case of the reduced (defective) surface [133]. The adsorption energy of CO on the non-defective surface was found to be 0.43 eV in the zero coverage limit (positive values indicate an exothermic reaction), but higher for the defective surface, when CO adsorbs in the vicinity of an oxygen vacancy (V_O). Neither CO₂ production nor oxygen exchange was observed when CO desorbed from the defective (110) rutile surface. More recent experiments

on the (110) surface of oxidized crystals resulted in 0.36 eV adsorption energy for isolated CO, diminishing to 0.20 eV at full coverage [134]. Photochemical formation of CO₂ from CO on the rutile (110) surface was found to occur, but only if O₂ was adsorbed at a V_O site [135]. The CO₂ photoproduction occurred only for above band gap light, and was correlated with the negative charging of the adsorbed oxygen. In a recent experiment it was concluded that the photocatalytic production of CO₂ is an electron-assisted process, because it is retarded by the upward band bending caused by co-adsorption of acceptor molecules [136]. Theoretical studies on the rutile (110) surface find that CO₂ formation from co-adsorbed CO and O₂ occurs if O₂ is adsorbed at a V_O site of the surface [140, 137,138]. The energy barrier for formation was found to be 0.4 eV, and after CO₂ desorption no defect was left on the surface [137]. It was also shown theoretically that the CO molecule interacts with the (110) surface mainly via its 5σ state (with C atom toward a surface Ti), and significant charge transfer is involved in the adsorption process [139].

Anatase is advantageous over rutile for photocatalysis [40]. The most stable surface of anatase is the (101) surface, which is largely free of vacancies [140]. Based on theoretical calculations it was reported that on a perfect anatase (101) surface, CO is preferentially adsorbed on the undercoordinated surface Ti atoms (Ti_{5C}), with the C atom toward the Ti_{5C} [112]. Note, that on the (001) surface this is only true for high surface coverage. When the smallest surface coverage was considered, CO could interact with both titanium and bridging oxygen (O_{2C}) atoms on the surface [141]. However, it was found that CO₂ formation on the perfect (001) anatase surface occurs only at singly coordinated terminal (O_{1C}) oxygen atoms [69]. In previous works, we have investigated the adsorption of CO on anatase TiO₂ (101) and (001) surfaces [25, 26]. In the high coverage limit we have found that the most stable configuration is when the C atom of the CO molecule interacts with Ti_{5C} on both surfaces.

Even though anatase was shown to be more reactive in photocatalysis than rutile [139], CO adsorption on it was hardly investigated experimentally, because of the lack of well defined single crystals (anatase becomes more stable than rutile only when the particle size decreases below *ca.* 14 nm) [34], and because it can be activated as a photocatalyst only by UV radiation [142]. It was shown, however, that photocatalytic oxidation of alcohols on anatase proceeds with the assistance of photo-generated holes [143].

Apparently, oxidation of CO to CO₂ on the TiO₂ surface is a photocatalytic process, which requires on the rutile (110) surface also the presence of surface oxygen vacancies. Since the most stable (101) surface of anatase is known to be free of such defects, the question arises, how a photocatalytic process can convert CO to CO₂. While the theoretical study of the charge transfer processes occurring in surface reactions upon photo-generation of electron-hole pairs is extremely difficult, one may decouple the problem and study only the effect of the hole on the reaction assuming that the electron was trapped in the bulk or scavenged at the surface, e.g., by oxygen. We have carried out CO adsorption and oxidation studies on both the neutral and the positively charged anatase (101) surface. We find that the adsorption energy is higher (−0.45 eV) on the positive surface, than on the neutral one (−0.26 eV). We will show that, in the presence of a hole, adsorption of CO on the perfect anatase surface can be followed by spontaneous oxidation to and desorption of CO₂, leaving a reduced, positively charged surface behind.

5.3 COMPUTATIONAL METHODS

Total energies and equilibrium geometries have been calculated within the first principles, generalized gradient approximation (GGA) of density functional theory (DFT), using the Perdew–Burke–Emzerhof (PBE) exchange–correlation functional [144]. Calculations have been carried out with the Vienna *ab initio* simulation package, VASP 5.2.2, using the projector augmented wave (PAW) method [145–147]. The 3*p* shell was excluded from the Ti core and the plane wave cut-off was 420 eV. Charged supercells were calculated assuming a jellium charge of opposite sign, as it is customary in modeling charged defects in semiconductors [148]. (At a thickness of 15 Å for the vacuum layer this introduces an error of ~0.01 eV in the adsorption energies.) Energy barriers have been determined by the nudged elastic band method (NEB) [149] of the VASP package. Molecular dynamics (MD) calculations were performed by heating the system from 0 K to 300 K in 500 steps at constant volume, and keeping it there for another 500 steps, with a time step of 2 fs.

The anatase TiO₂ (101) surface was modeled by a (1×2) slab of six TiO₂ layers, containing altogether 24 Ti and 48 O atoms, and a 15 Å thick vacuum layer above the slab (Figure 7.1). Periodic boundary conditions were applied in all three

dimensions, and the Brillouin-zone was sampled by a $(2 \times 2 \times 1)$ Monkhorst-Pack k -point set [111], including the zone center (Γ -point). A maximum force criterion of 0.02 eV/\AA was used for structural relaxation. Our optimized bulk lattice parameters for anatase are $a = 3.789 \text{ \AA}$ and $c = 9.607 \text{ \AA}$, to be compared to the experimental results [31] of 3.782 \AA and 9.502 \AA , respectively. The structural optimization of the slab (without and with adsorbents) was carried out by keeping the two lowest TiO_2 layers fixed at their bulk positions. There are four types of atoms on the free anatase TiO_2 (101) surface (as shown in Fig.1): two- and threefold coordinated O atoms ($\text{O}_{2\text{C}}$, and $\text{O}_{3\text{C}}$), and five- and sixfold coordinated Ti atoms ($\text{Ti}_{5\text{C}}$, $\text{Ti}_{6\text{C}}$). Based on previous work [25, 26, 112], we have investigated CO adsorption at a $\text{Ti}_{5\text{C}}$ site in various configurations, but also at an $\text{O}_{2\text{C}}$ site.

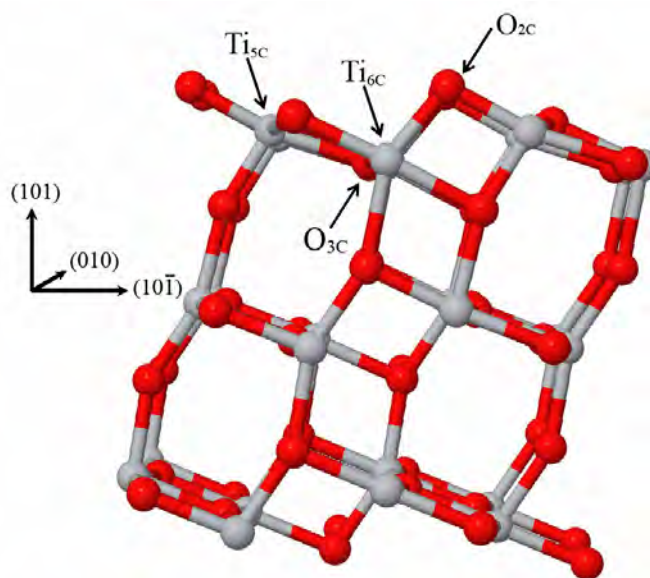


Figure 5.1 The optimized structure of the (1×2) slab model for the anatase TiO_2 (101) surface. Five- and sixfold coordinated titanium, and two- and threefold coordinated oxygen surface atoms are labeled as $\text{Ti}_{5\text{C}}$, $\text{Ti}_{6\text{C}}$, $\text{O}_{2\text{C}}$, and $\text{O}_{3\text{C}}$, respectively.

The adsorption energy of CO on the surface with charge q was computed from total energies as

$$\Delta E_{\text{ads}}^q = E_{\text{CO/slab}}^q - (E_{\text{slab}}^q + E_{\text{CO}}) \quad (5.1)$$

where $E_{\text{CO/slab}}$ and E_{slab} are the energies of the slab with and without adsorbed CO, and E_{CO} is the energy of a CO molecule, isolated in a 3D-periodic cubic unit cell of $10\text{\AA} \times 10\text{\AA} \times 10\text{\AA}$. (The desorption energy of CO_2 was calculated in a similar manner.)

Finally, we note that the self-interaction error in the GGA underestimates the localization and deepness of the hole states in bulk anatase [150], and such effects could influence our results. This error of GGA is often corrected by applying on-site Coulomb interaction terms (U) for the Ti_{3d} and O_{2p} states [151]. Such a GGA + U approach, however, may introduce uncontrolled changes in the electronic structure of the host. In the method of Lany and Zunger [152], in conjunction with a +U term, a nonlocal external potential (NLEP) ensures that the correction only affects the hole state. (Additional NLEPs are used to correct the band gap which is also underestimated in GGA.) We have checked the energy of CO adsorption on the neutral and on the positive surface with pure GGA, GGA + U (parameters of Ref. 151), and GGA + U + NLEP (parameters courtesy of S. Lany) and obtained a difference of 0.2, 0.2, and 0.3 eV, respectively, in favor of the positive charge state. This shows that the plain GGA calculation is sufficient in our case. The reason is that the surface has a localizing effect on the hole even in the GGA calculation. One also has to consider that in underestimating the energy difference between the energy of the band edge and of the hole state, GGA makes a bigger error in the position of the former than of the latter [153]. Therefore, the energy difference between the hole state and the HOMO of the CO molecule is reasonably well approximated in GGA. Therefore, the energy difference between the hole state and the HOMO of the CO molecule is reasonably well approximated in GGA.

5.4 RESULTS AND DISCUSSION

To our knowledge, the adsorption of CO on the anatase TiO_2 (101) surface under photoexcitation has never been studied. The consequences of the photogeneration of electron-hole pairs by UV light can be represented by the diagram shown in Figure 5.2. Since a CO molecule contains 10 electrons, it can be assumed that, in interaction with the TiO_2 surface, the total energy can be diminished if the molecule acts as a donor. In other words, adsorption could be promoted by the photoinduced holes, assuming that the photoinduced electrons are scavenged by

acceptor molecules in the ambient (e.g., O₂). We have modeled only the photo-oxidation process, i.e., the effect of holes on the adsorption and oxidation of CO, by investigation of its interaction with a positively charged surface.

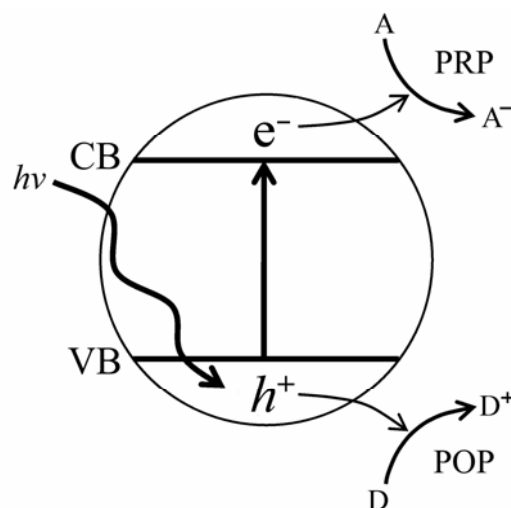


Figure 5.2 Scheme of photo-oxidation/reduction processes (POP/PRP) upon UV excitation of a TiO₂ crystal in the presence of acceptor (A) and donor (D) molecules in the vicinity of the surface.

5.4.1 Adsorption of CO on the anatase TiO₂ (101) surface

The adsorption of CO at a Ti_{5C} site on the perfect neutral and positively charged anatase (101) surfaces have been investigated for the molecule approaching the surface with the carbon or the oxygen end (Figure 5.3). The optimized bond lengths and angles, and the adsorption energies are shown in Table 5.1. CO adsorbs in a slightly tilted configuration and clearly prefers the OC··Ti orientation in both charge states in agreement with the results of previous theoretical studies [112, 25, 26]. In the positive charge state of the surface the hole is localized on the surface, and significantly increases the adsorption energy:

$$E\{[\text{CO}/\text{TiO}_2]^0\} - E\{[\text{TiO}_2]^0\} - E\{\text{CO}\} = -0.26 \text{ eV} \quad (5.2)$$

$$E\{[\text{CO}/\text{TiO}_2]^+\} - E\{[\text{TiO}_2]^+\} - E\{\text{CO}\} = -0.45 \text{ eV} \quad (5.3)$$

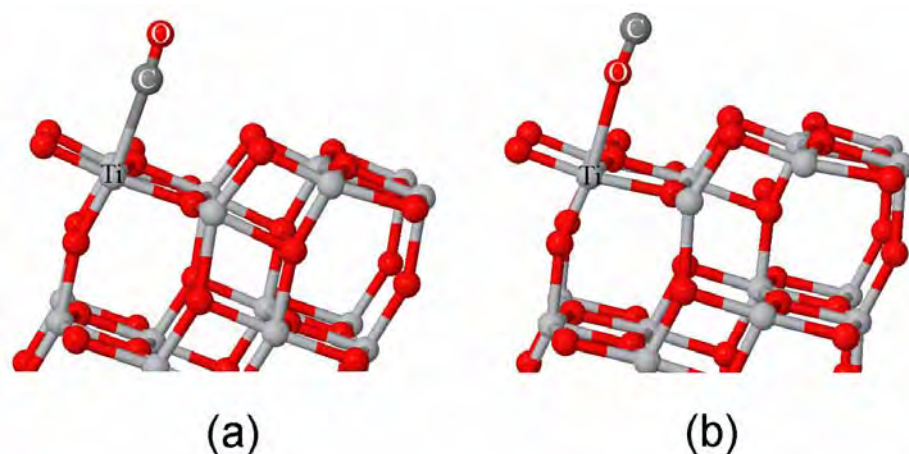


Figure 5.3 Adsorption of CO on the anatase TiO_2 (101) surface with the C (a) and the O atom (b) towards the surface. The geometry data for the neutral and the positive case are given in Table 5.1.

Table 5.1 Adsorption energies and geometry parameters for CO adsorption at a $\text{Ti}_{5\text{C}}$ site on the anatase TiO_2 (101) surface. For comparison, results of periodic B3LYP calculations with localized basis sets on the same (1×2) (a) [112] and on a (1×1) slab (b) [26] are given in parentheses.

configuration	ΔE_{ads} (eV)	distance (Å)	angle (degree)
$OC...Ti$ (neutral surface)	-0.26 (-0.14 ^a , -0.29 ^b)	C-Ti = 2.531 (2.463 ^a , 2.439 ^b) C-O = 1.139	Ti-C-O = 175.74
$OC...Ti$ (positive surface)	-0.45	C-Ti = 2.493 C-O = 1.136	Ti-C-O = 176.62
$CO...Ti$ (neutral surface)	-0.06 (-0.14 ^b)	O-Ti = 2.748 C-O = 1.143	Ti-O-C = 169.51
$CO...Ti$ (positive surface)	-0.20	O-Ti = 2.581 C-O = 1.148	Ti-O-C = 172.98

5.4.2 Oxidation of CO on the anatase TiO_2 (101) surface.

Next we have investigated the adsorption of CO at the $\text{O}_{2\text{C}}$ site. While in the neutral charge state we were not able to find an exothermic configuration, on the positively charged anatase (101) surface the one shown in Figure 5.4 was found. The bond of $\text{O}_{2\text{C}}$ to its $\text{Ti}_{6\text{C}}$ neighbor is broken, the length of its bond to the $\text{Ti}_{5\text{C}}$ neighbor

increases from 1.836 to 2.281 Å, and an O_{2C}–CO bond is formed with a bond length of 1.161 Å. In other words, a CO₂ molecule, adsorbed on a Ti_{5C} site is formed, at the price of reducing a Ti_{6C} atom to Ti_{5C} (i.e., creating a surface vacancy, V_O). The energy of this [CO₂/TiO₂+V_O]⁺ configuration with respect to the bare (positive) surface and an isolated CO molecule is

$$E\{[\text{CO}_2/\text{TiO}_2 + \text{V}_\text{O}]^+\} - E\{[\text{TiO}_2]^+\} - E\{\text{CO}\} = -2.01 \text{ eV} \quad (5.4)$$

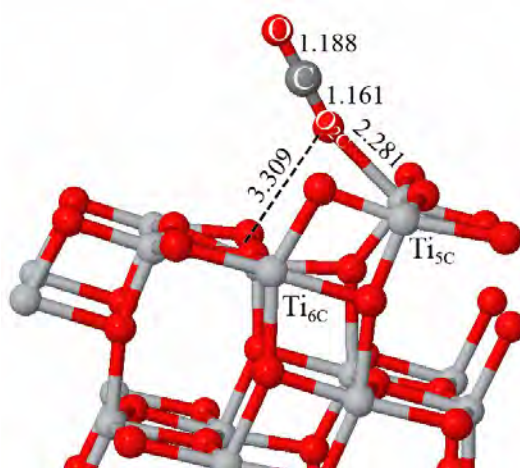


Figure 5.4 The [CO₂/TiO₂ + V_O]⁺ configuration, arising upon interaction of the adsorbed CO molecule with a nearby O_{2C} site. Bond distances are in Å.

i.e., 1.56 eV lower than the [CO/TiO₂]⁺ configuration after adsorption at the Ti_{5C} site (see Eq. 3). We emphasize, that similar [CO₂/TiO₂+V_O]⁰ configurations on the neutral surface are endothermic with respect to CO and [TiO₂]⁰. Even in the positive charge state, the [CO₂/TiO₂+V_O]⁺ configuration cannot be reached by a straight adsorption of CO at the O_{2C} site, without surmounting an energy barrier of about 0.7 eV, as shown by our NEB calculation in Figure 5.5. We find, however, that transforming the [CO/TiO₂]⁺ configuration of Fig. 3a to the [CO₂/TiO₂+V_O]⁺ configuration of Figure 5.4 requires an energy barrier of only 0.4 eV (Figure 5.6). This is smaller than the energy gain on the adsorption at the Ti_{5C} site (c.f. Fig.7).

5.4.3 Dissociation of CO₂ from the anatase TiO₂ (101) surface.

We have calculated the energy of a dissociated CO₂ molecule above the surface with the positive oxygen vacancy, with respect to that of CO above the bare positive surface to be

$$(E\{\text{CO}_2\} + E\{\text{TiO}_2 + \text{V}_\text{O}\}^+) - (E\{\text{CO}\} + E\{\text{TiO}_2\}^+) = -1.59 \text{ eV} \quad (5.5)$$

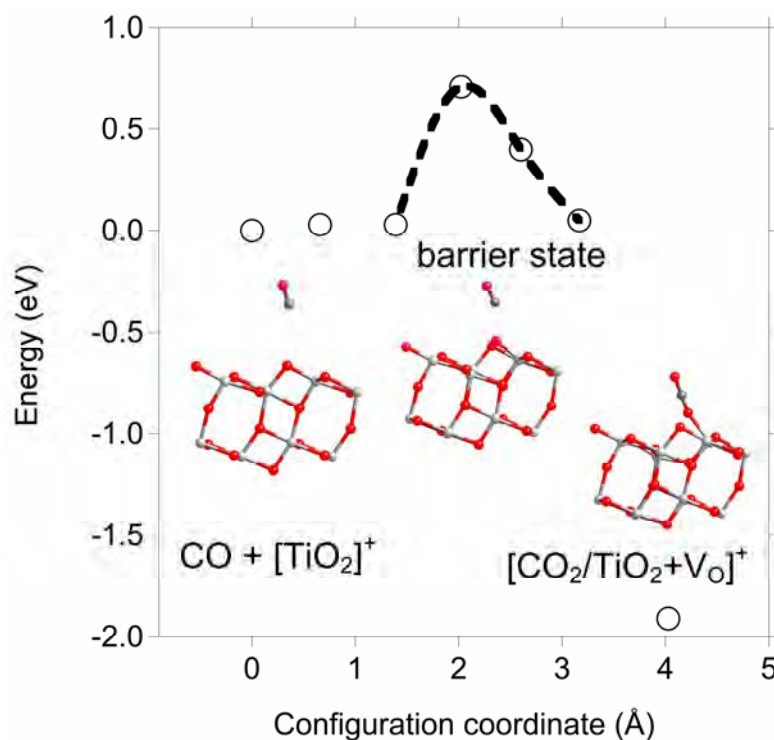


Figure 5.5 Total energy profile for CO adsorption at the O_{2C} site of the positive anatase (101) surface. The insets show the starting and final configurations and the barrier state. At the starting position the carbon end of CO is 2.5 Å above the O_{2C} site, while the last configuration is the one shown in Figure 5.4. The configuration coordinate expresses approximately the motion of the C atom. (In fact, it is the length of a supervector between two consecutive configurations which is built of the relative positions of the C and O atoms of CO, the surface atoms to which C is bonded along the path, and the first neighbors of the latter). The curve is a cubic spline fitted to the barrier region to guide the eye. The zero of the energy scale is taken to be the energy of CO + [TiO₂]⁺.

So the dissociation energy of CO_2 from $[\text{CO}_2/\text{TiO}_2+\text{V}_\text{O}]$ is only $-1.59 - (-2.01) = 0.42$ eV, and we have found no energy barrier to the dissociation in a NEB calculation. We have carried out an MD simulation at 300K for 1 ps (after a heating ramp of 1 ps), starting from the configuration of Figure 5.4. We have found that, even in this short time, the OCO–Ti distance increases from its equilibrium value (2.28 Å) to above 2.8 Å several times. Therefore, it is safe to assume, that the CO_2 molecule can spontaneously dissociate at room temperature. The dissociation leaves $[\text{TiO}_2 + \text{V}_\text{O}]^+$ behind.

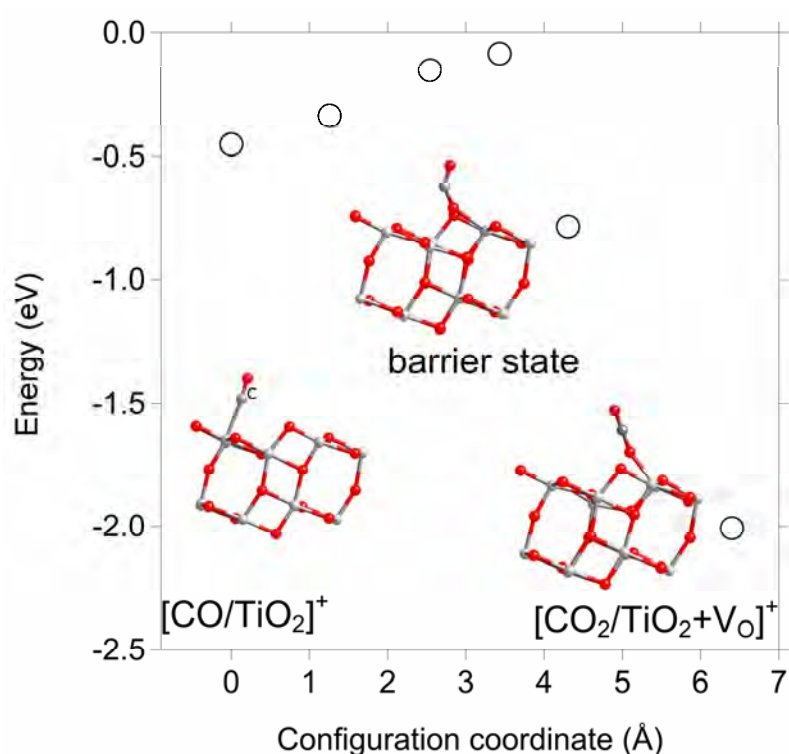


Figure 5.6 Total energy profile along the $[\text{CO}/\text{TiO}_2]^+$ to $[\text{CO}_2/\text{TiO}_2+\text{VO}]^+$ diffusion pathway. The configuration coordinate and the energy scale is defined as in Figure 5.5. The insets show the starting and final configurations and the barrier state.

Considering the energy balance of the three–step process (A–C) for the CO to CO_2 conversion in Figure 5.7, we see that – if there was no energy dissipation – the whole process could be completed spontaneously. The energy gain (0.45 eV) on the first step, $\text{CO} + [\text{TiO}_2]^+ \rightarrow [\text{CO}/\text{TiO}_2]^+$, i.e., the adsorption of CO, covers the activation energy needed in the second step for the $[\text{CO}/\text{TiO}_2]^+ \rightarrow \text{CO}_2/[\text{TiO}_2+\text{V}_\text{O}]^+$ transformation (0.4 eV). The energy gain on the latter (1.56 eV) profusely covers the

energy (0.42 eV) needed for the third, dissociation step $[\text{CO}_2/\text{TiO}_2+\text{V}_\text{O}]^+ \rightarrow \text{CO}_2 + [\text{TiO}_2+\text{V}_\text{O}]^+$ (which does not have an energy barrier). In reality, the adsorption energy can be dissipated before the second step of the process starts but, considering that our MD simulation has shown that an energy difference of 0.42 eV (needed for dissociation of CO_2) can be surmounted at room temperature, it is safe to assume, that our three-step process can be spontaneous under realistic conditions, too.

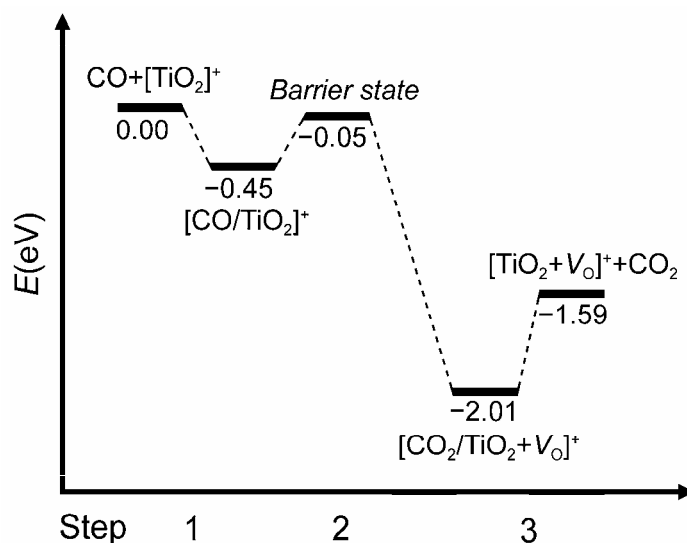


Figure 5.7 Total energy diagram for the oxidation of CO on the positive anatase $\text{TiO}_2(101)$ surface. All energies are given in eV, with respect to the energy of free CO above the positive surface. The zero of the energy scale is taken to be the energy of $\text{CO} + [\text{TiO}_2]^+$.

Unlike in the process postulated for the rutile (110) surface [135–137], neither *a priori* generation of V_O defects, nor excess oxygen is required in the proposed mechanism. Although or oxidation step does not require excess negative charge either, co-adsorption of acceptor molecules (e.g. O_2 or Cl_2) would still impair the process: note because of the band bending, [136] but because a negatively charged surface would impair the CO adsorption. In principle a hole-assisted process, similar to the one we propose here for the anatase (101) surface, could also be envisaged for the (110) surface of rutile as well. However, that surface either has donor-type V_O defects which would trap the photogenerated holes, or excess oxygen (O_2 adsorbed at V_O), leading to the known route of electron driven conversion of CO.

Finally we note, that we find the same critical barrier energy as the one found for the $\text{CO} \rightarrow \text{CO}_2$ conversion on the defective rutile (101) surface [137]. Unlike that, however, there is a good chance that the proposed conversion of CO to CO_2 on the perfect anatase (101) surface could be cyclic. It is known that oxygen molecules can act as electron scavengers in photochemical reactions on the TiO_2 surface [133]. Both experimental studies [154] and first principles molecular dynamics simulations [155] have shown that oxygen molecules can buffer electrons even without getting chemisorbed. Therefore, it is straightforward to assume that negatively charged oxygen molecules could, at the end, annihilate the positively charged oxygen vacancies created in the hole-assisted oxidation of CO. It was shown experimentally, that such an annihilation process has an important role in the interaction of oxygen with the reduced rutile (110) surface [120]. While further studies are required to clear the details in case of the anatase (101) surface, assuming electron scavenging by oxygen molecules on the one hand, and annihilation of positive oxygen vacancies in the presence of negatively charged excess oxygen on the other, appears rather plausible. That means that real photocatalytic oxidation of CO might be possible on the (101) anatase surface.

5.5 CONCLUSIONS

By first principles spin polarized GGA calculations we have shown that positive charge on the anatase (101) surface increases the adsorption energy of CO, allows its conversion to CO_2 , and the desorption of the latter with creation of a surface oxygen vacancy. This hole-assisted $\text{CO} \rightarrow \text{CO}_2$ conversion can be spontaneous. Our calculations also show that a similar CO to CO_2 conversion process would be endothermic without the presence of a hole. Holes in anatase can be produced by UV excitation. Assuming oxygen near the surface scavenging the photogenerated electrons, positively charged oxygen vacancies, produced in the conversion process, are likely to be annihilated in the presence of excess oxygen in negative charge state. Therefore, our calculations indicate that oxidation of CO on the anatase (101) surface could be an efficient photocatalytic process. While further computational studies are required to clear the details, experimental verification of the suggestion appears to be desirable.

CHAPTER VI

FIRST-PRINCIPLES THEORETICAL STUDY OF ADSORPTION OF N₂O AND CONVERSION TO N₂ BY CO ON ANATASE TiO₂ (101) SURFACE

Raina Wanbayor,^{1,2} Peter Deák,² Thomas Frauenheim,² and Vithaya Ruangpornvisuti¹

¹*Department of Chemistry, Faculty of Science, Chulalongkorn University, Bangkok
10330, Thailand*

²*Bremen Center for Computational Material Science, University Bremen, 28359
Bremen, Germany*

This article is in preparation for publication (2011).

6.1 ABSTRACT

First-principles spin-polarized density functional theory calculations in generalized gradient approximation were carried out to investigate the adsorption of N_2O on the neutral and negative surfaces of the anatase TiO_2 (101), (denoted as $[TiO_2]^0$, $[TiO_2]^-$). We have shown that the symmetric bridge configuration of adsorbed N_2O is definitively favored on both surfaces. This confirmed that the presence of electron in the conduction band could be enhanced N_2O adsorption. The highest adsorption energy has determined of -2.24 eV for N_2O adsorption on $[TiO_2]^-$ surface. In addition, the following reduction reaction of N_2O to N_2 occurs after the photocatalytic oxidation of CO and desorption of CO_2 , leading to oxygen vacancy. The oxygen atom of N_2O can heals oxygen vacancy site on the surface to form to N_2 .

6.2 INTRODUCTION

TiO_2 has been successfully applied in many application such as photocatalysis [2–5], heterogeneous catalysis [1] and gas-sensors [7, 100], its structures and surfaces have been widely studied over many years [19, 20]. The adsorptions molecular gases on various surface planes of different TiO_2 phases have been extremely reported. Among of these surfaces, anatase is considered the most stable photoreactive phase [40]. The most stable surface of anatase is the (101) surface [140]. The adsorption and dissociation of nitrous oxide (N_2O) molecule into N_2 through TiO_2 as photocatalyst have obtained attention due to this molecule is an air pollutant gas produced mainly by several industrial processes. It has been extensively studied that the adsorption of N_2O molecule on numerous different types of surface such as TiO_2 [49, 130, 156–158] ZnO [159], ZrO_2 [160], MgO [161], Cu_2O [162], Ga-ZSM-5 [163], GaN [164], Si [165], and also transition metals [166–170]. For these surfaces have shown the N_2O adsorbed both N and O atom of N_2O molecule on the surfaces, but N-bonded species show a higher photoreactivity than the O-bonded species. However, the adsorption energies of linear O and N ends over Ti atom of TiO_2 surface are relatively small when compared with bent configuration [156]. Several previous experimental and theoretical studied have been investigated the adsorption of linear molecular structure of N_2O and also bent configurations on TiO_2 , especially, rutile (110) surface [49, 130,

156, 157]. N_2O is molecularly adsorbed on the reduced TiO_2 both the N and O end configurations using UV irradiation in the range 2.1–5.0 eV. The adsorbed N_2O is photodepleted to produce adsorbed nitrogen at low coverages [49]. Shultz et al. [157] reported that the N_2O heals Ti^{3+} defects on defective TiO_2 (110), the surfaces healed by N_2O differ slightly from surfaces similarly healed by O_2 . The O_2 heals defects as O_2^- while N_2O heals defects as O^{2-} has been postulated.

Furthermore, decomposition of adsorbed N_2O to N_2 desorption on metal oxides [158, 160, 162] including metals [166,167] have been reported. The experimental study has shown the N_2O molecules are exposed to TiO_2 (110) at 90 K decompose to N_2 via either N_2 ejection from the surface and N_2O molecules bound at vacancies with the O–end of the molecule in the vacancy 170 K to liberate N_2 in the gas phase and deposit oxygen adatoms at non–defect Ti^{4+} sites [159]. In addition, Kudo and Nagayoshi [171] studied the photocatalytic reduction of N_2O on metal–supported TiO_2 powder at room temperature in the presence of H_2O and CH_3OH vapor, electrons produced by photoirradiation can site or N_2O decomposes at enhance the dissociation of N_2O through electron capture by reaction $\text{N}_2\text{O} + e^- \rightarrow \text{N}_2 + \text{O}_{(\text{ad})}^-$. On the other hand, CH_3OH is oxidized by holes on TiO_2 surfaces. The angular distribution of desorbing N_2 was studied in the decomposition of N_2O on Rh (100) at 60–140 K using temperature–programmed desorption. The dissociation to $\text{N}_{2(\text{a})} + \text{O}_{(\text{a})}$ proceeds during the geometry optimization based on DFT–GGA calculations of the lying form with both terminal atoms bonded to the adjacent bridge sites [167]. DFT reported the adsorption and the dissociation of an $\text{N}_2\text{O}_{\text{te}}$ on Cu_2O (111) surfaces. The calculations results show the dissociation reaction of N_2O molecule is $\text{N}_2\text{O} \rightarrow \text{N}_2 + \text{O}_{(\text{s})}$ [162]. The N_2O molecule was adsorbed on Pd (110) in a tilted form via the terminal N atom attached to the surface or lies horizontally on the surface. In the horizontal form applicable to inclined desorption, adsorbed N_2O is bent with its O atom pointing to the surface were reported with GGA calculation [166].

In addition, the reduction of N_2O by CO to N_2 and CO_2 has been reported [172–174]. The decomposition of N_2O accompanied by formation of adsorbed oxygen and N_2 desorption. The recent study of the kinetics of the N_2O –CO reaction on Pd (110) was performed under UHV conditions. N_2O dissociation is accordingly assumed to occur via channel $(\text{N}_2\text{O})_{\text{ad}} \rightarrow (\text{N}_2)_{\text{gas}} + \text{O}_{\text{ads}}$, following by Langmuir–

Hinshelwood (LH) reaction between adsorbed and oxygen to form CO₂: $(\text{CO})_{\text{ad}} + \text{O}_{\text{ad}} \rightarrow (\text{CO}_2)_{\text{gas}}$ [172]. The reduction of N₂O with CO on Au/TiO₂ has been investigated. The Au/TiO₂ is exhibit high catalytic activity. The reduction reaction may proceed via also a LH mechanism [174].

In previous works, we have investigated the adsorption of N₂O on anatase TiO₂ (101) and (001) surfaces [25, 26] and also co-adsorption between N₂O and CO [26]. We proposed that the possible configurations can lead to the production of CO₂ and N₂. To our knowledge, the photocatalysis of TiO₂ can be activated by UV radiation. When TiO₂ is exposed to the light of energy corresponding to the energy gap, the photo-induced holes in the valence band and photo-induced electrons in the conduction band are generated to produce electron-hole (e^-/h^+) pairs. In our previous work [27], we have reported the oxidation of CO to CO₂ on the anatase (101) surface could be an efficient photocatalytic process due to the hole-assisted. The possibility of a photocatalytic cycle is discussed assuming electron scavenging by oxygen as a acceptor molecule. During the photocatalytic reaction of the adsorbed molecule occurs due to photo-generated holes; while the majority of the electrons are trapped by acceptor molecules in the ambient (e.g. O₂ as an electrons scavenger). Consequently, it is desirable to better define behavior of photoreduction reaction of N₂O (an electron acceptor, which is known to be an efficient electron scavenger [159]) by CO as reducing agent and the roles of electron and hole during photocatalysis.

In the present work, we investigated the adsorption of N₂O on neutral and negative surfaces of anatase TiO₂ (101) as a photocatalyst using first-principle calculations based on spin-polarized density functional theory (DFT) and generalized gradient approximation (GGA). The calculations were employed slab periodic boundary conditions. The reduction of N₂O to N₂ was also studied by performing the oxidation of CO to produce CO₂ as reported in our previous work [27]. The calculated adsorption energies and geometries are presented.

6.3 COMPUTATIONAL METHODS

Our first-principles spin-polarized calculations are based on density functional theory as implemented in the VASP code. The generalized gradient corrected approximation (GGA) [82, 175] within the Perdew-Burke-Emzerhof (PBE)

exchange–correlation functional is adopted [144]. The projector augmented–wave (PAW) methods have been used [176,145], excluding also the $3p$ shell of Ti from the core. The electronic wave functions are expanded in plane waves with energy cut off of 420 eV. The slab model was adopted to investigate the interaction between the anatase TiO_2 (101) surface and N_2O molecule taken from our previous work [27]. We first checked the accuracy of the theoretical method by testing the bulk of anatase TiO_2 . The optimized bulk lattice parameters, are $a = 3.789 \text{ \AA}$, and $c = 9.607 \text{ \AA}$, to be compared to the experimental results of 3.782 and 9.502 \AA , respectively [31]. The adsorptions of N_2O initiated from several starting positions over the surface were investigated. The adsorption energy (ΔE_{ads}) of N_2O on the TiO_2 (101) surface is computed by Eq. (6.1).

$$\Delta E_{\text{ads}} = E_{\text{N}_2\text{O}/\text{surface}} - (E_{\text{N}_2\text{O}} + E_{\text{surface}}) \quad (6.1)$$

where $E_{\text{N}_2\text{O}/\text{surface}}$ is the total energy of N_2O adsorption on the TiO_2 surface system, $E_{\text{N}_2\text{O}}$ and E_{surface} are an isolated N_2O molecule and a clean TiO_2 surface, respectively. Negative adsorption energy indicates a stable adsorption process.

6.4 RESULTS AND DISCUSSION

6.4.1 Adsorption of N_2O molecule on neutral surface of anatase TiO_2 (101)

Since molecular and dissociative adsorption of N_2O on TiO_2 (110) has been examined theoretically [156]. We have identified several possible adsorption configurations of N_2O on neutral as well as on negative anatase TiO_2 (101) surfaces. Based on recently reported from Rusu and Yates [49] the N_2O can bound via the N–end and O–end of the molecule to the TiO_2 surface. Both N– and O–bonded complex formation are shown:



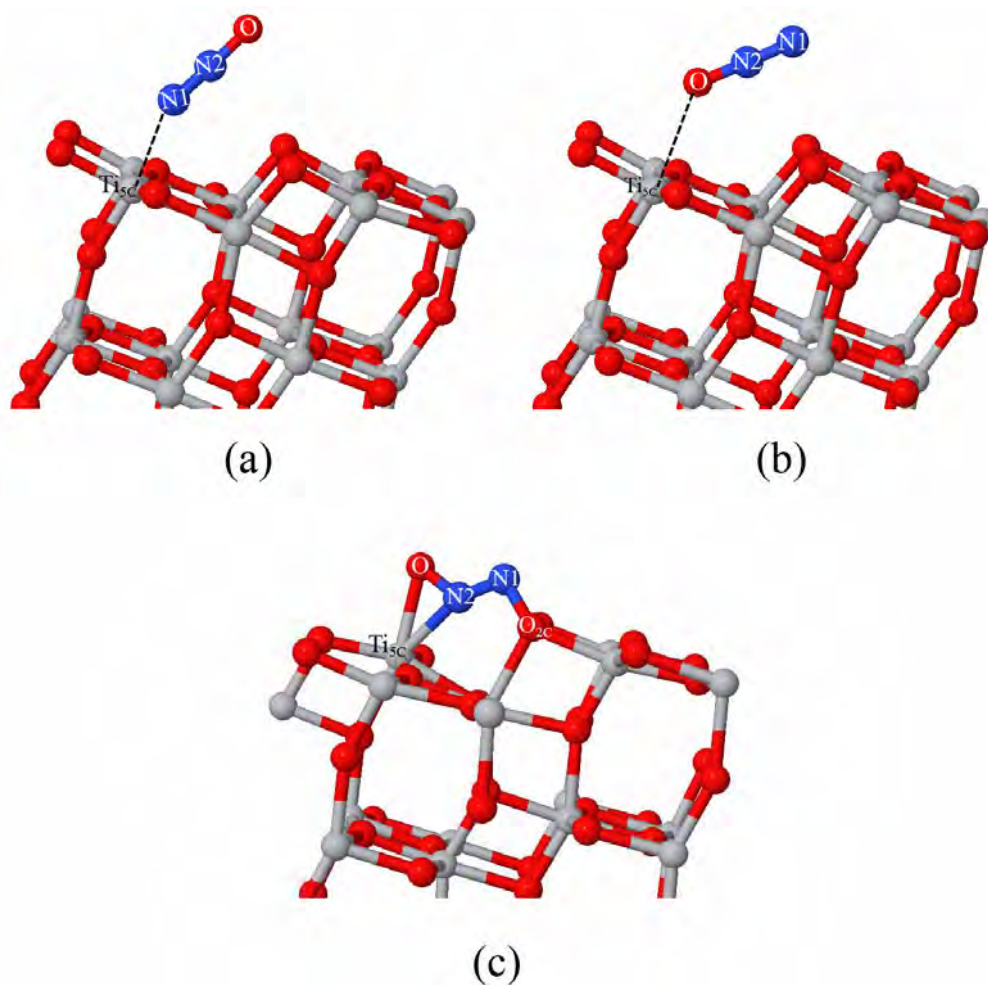


Figure 6.1 Adsorption configurations of N₂O on the neutral surface of anatase TiO₂ (101) as the N₂O pointing (a) its nitrogen atom, (b) its oxygen atom toward the titanium atom Ti_{5C} of the surface and (c) N₂O bridged structure.

We first studied adsorption of the linear N₂O molecule on neutral anatase TiO₂ (101) surface by pointing N and O atom over the Ti_{5C} site, namely, N–end and O–end, are shown in Figures 6.1 (a) and (b), respectively. The optimized bond lengths and angles, and the adsorption energies are shown in Table 6.1. The results indicate that the N₂O molecule adsorbed on TiO₂ (101) in a tilted configurations for both N–end and O–end. In the N–end the Ti_{5C}–N distance is 2.595 Å, while O–end the Ti_{5C}–O distance is 2.671 Å (Figure 6.1). The adsorption energy is larger for N–end than that O–end of 0.04 eV, indicating that N₂O prefers to adsorb N–end towards the Ti_{5C} site. Our calculated adsorption energies are found to be in agreement with the previous theoretical study [156] of the N₂O adsorption on rutile TiO₂ (110) surface. However,

N₂O can weakly adsorb on the surface in both N-end and O-end, its geometry remains linear to be within 178.90°–178.48°, respectively, which is indicative of a physisorption.

Next, we considered the adsorption for bridge configuration of N₂O on neutral surface. This configuration takes place between O_{2C} and Ti_{5C} atoms, see Figure 6.1(c). The calculated adsorption energy for bridge configuration of N₂O is –2.21 eV (Table 6.1). It was found that the N₂O is preferentially adsorbed on anatase (101) in the bridge configuration.

Table 6.1 Adsorption energies and geometrical parameters for N₂O adsorption on the anatase TiO₂ (101) surfaces.

configuration	ΔE_{ads} (eV)	distance (Å)	angle (degree)
<i>N-end</i> (TiO ₂] ⁰)	–0.17	N–Ti = 2.595 N1–N2 = 1.144 N2–O = 1.192	N1–N2–O = 178.90
<i>O-end</i> (TiO ₂] ⁰)	–0.13	O–Ti = 2.671 N1–N2 = 1.205 N2–O = 1.140	N1–N2–O = 178.48
<i>N-end</i> (TiO ₂] [–])	–0.01	N–Ti = 2.728 N1–N2 = 1.142 N2–O = 1.194	N1–N2–O = 178.24
<i>O-end</i> (TiO ₂] [–])	–1.16	O–Ti = 1.827 N1–N2 = 1.148 N2–O = 3.224	–
<i>Symmetric bridge structure</i> (TiO ₂] ⁰)	–2.21	O–Ti = 2.243 N2–Ti = 2.110 O _{2C} –N1 = 1.419 N1–N2 = 1.264 N2–O = 1.300	N1–N2–O = 124.74
<i>Bridge bending structure</i> (TiO ₂] [–])	–0.74	O–Ti = 2.159 N1–Ti = 2.264 N1–N2 = 1.189 N2–O = 1.303	N1–N2–O = 137.26
<i>Symmetric bridge structure</i> (TiO ₂] [–])	–2.24	O–Ti = 2.156 N2–Ti = 2.074 O _{2C} –N1 = 1.260 N1–N2 = 1.205 N2–O = 1.301	N1–N2–O = 126.59

6.4.2 Adsorption of N₂O molecule on negative surface of anatase TiO₂ (101)

To our knowledge, the adsorption of N₂O on the anatase TiO₂ (101) surface under photo–electron excitation has never been studied. The electron excitation from the valence band to the conduction band was initiated by UV light absorption and generation of the electron–hole pairs for photocatalysis of anatase (101). We considered the N₂O adsorbs on negative surface of anatase (101) as an electron acceptor molecule for photocatalytic reactions, assuming that direct electron transfer from the conduction band into an antibonding molecular orbital of N₂O molecule [159] after UV irradiation. Therefore, we calculated the effect of electron excitation on the adsorption and reduction, by comparing the adsorption energies between neutral and negative surfaces. All the optimized structures of N₂O adsorption on negative surface of anatase (101) are shown in Figure 6.2. The optimized bond lengths and angles, and the adsorption energies are shown in Table 6.1. As can be seen, the equilibrium Ti_{5C}–N distance is 2.728 Å versus a Ti_{5C}–N distance of 2.595 Å for the neutral surface. The adsorption energy for the N–end configuration remains very small of –0.01 eV and the adsorption energy decreases by 0.16 eV relative to neutral surface. In the case of O–end configuration is energetically favorable of –1.16 eV, similar to the early theoretical study by Sun et al. [162] of dissociation reaction of N₂O on Cu₂O (111) surface showed O–bonded with Lewis acid CU_{CUS} site and N₂ desorption with energy of –1.16 eV. We have found that the presence of an electron makes the dissociation possible and proceeds spontaneously, leading to N₂ desorption and O[–] on the surface can be bound to Ti_{5C} site of the surface in the length of 1.827 Å as shown in the Figure 6.2 (b). The photocatalytic reduction of N₂O to N₂ desorption is reasonably explained by considering the electron transfer from conduction band of anatase (101) surface to N₂O molecule during photocatalytic process. Our calculated results indicate that N₂O could be an efficient electron scavenger as electron acceptor for photocatalysis of anatase (101) surface.

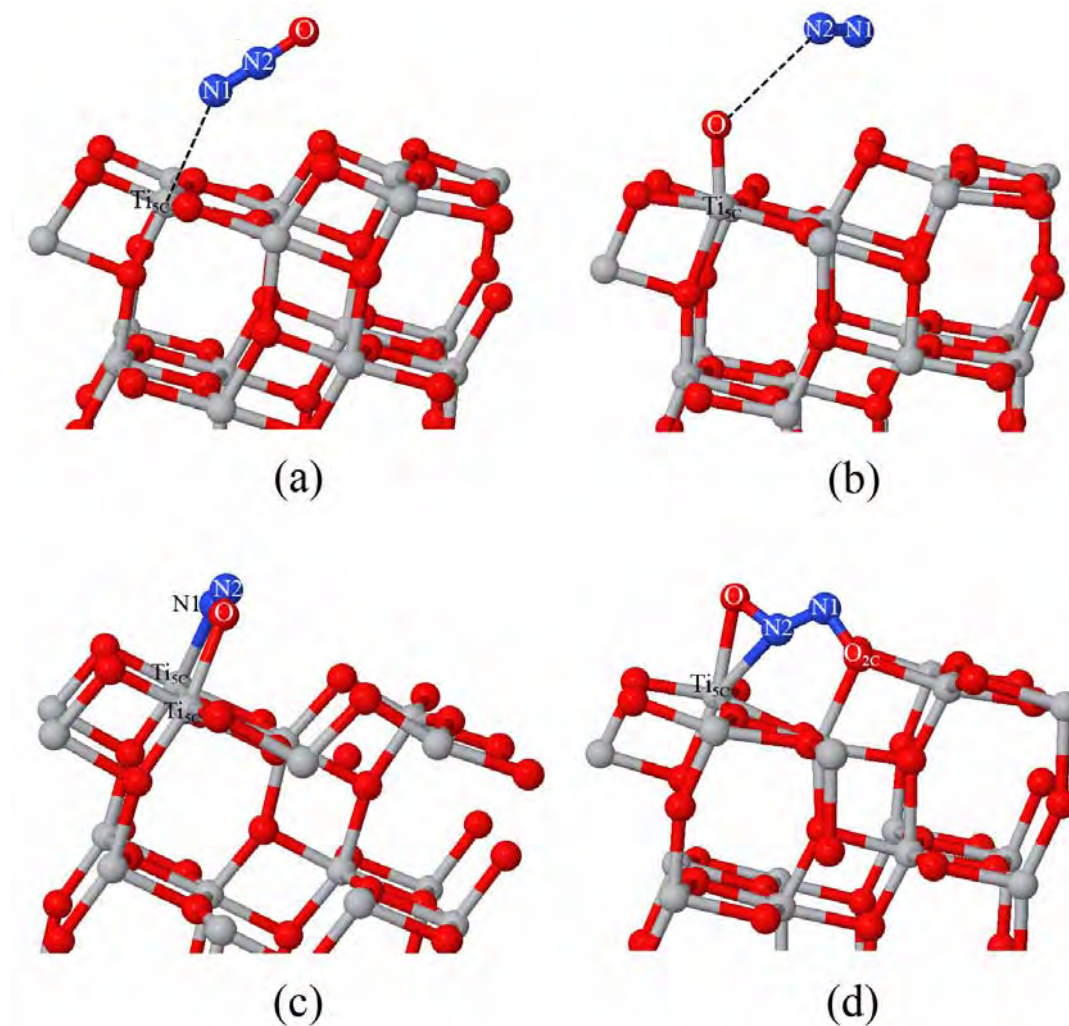


Figure 6.2 Adsorption configurations of N_2O on the negative surface of anatase TiO_2 (101) as the N_2O pointing (a) it nitrogen atom, (b) N_2O dissociated structure, (c) bridge bending structure and (d) symmetric bridge structure. Bond distances are in angstrom.

Next, we investigated the adsorption of bent structures of N_2O molecule on negative anatase TiO_2 (101) surface similar to the theoretical study from Sorescu and Yates [130] that the bent configuration occurs after N_2O molecule received some electron charge from defective rutile TiO_2 (110) surface. As the anatase TiO_2 (101) is a corrugated structure as similar as to the rutile TiO_2 (110), which is free from the vacancies [25]. Consequently, there are two bent configurations of N_2O adsorbed on negative surface have identified. The first one takes place between two neighbor $\text{Ti}_{5\text{C}}$ sites as called bridge bending structure, while the second takes place between $\text{Ti}_{5\text{C}}$ and

O_{2C} sites as called symmetric bridge structure [130]. Adsorption energies and some selected parameters for the optimized geometries are shown in Table 6.1. As can be seen from Figure 6.3 and the data in Table 6.2, the strongly adsorbed N_2O molecule of both bent structures on negative surface relative to the linear structure indicate that the presence of an electron can significantly increase the adsorption energy. As in the bridge bending structure case (Figure 6.2 (c)) we find that for the $Ti_{5C}-O$ and $Ti_{5C}-N1$ distances are 2.159 and 1.189 Å, respectively, with an adsorption energy of -0.74 eV. On the other hand, however, optimized geometry of the N_2O molecule is desorbed from two neighboring Ti_{5C} atoms of the neutral surface. This configuration the N_2O molecule remains linear structure of 179.72° . The symmetric bridge structure (Figure 6.2 (d)) is more favorable than the bridge bending structure by -1.50 eV for negative surface. It is remarkable that the most stable configuration correspond to a symmetric bridge structure of N_2O molecule with N atom bonded to Ti_{5C} , while O atom bonded to O_{2C} site.

6.4.3 Conversion of N_2O to N_2 by CO on anatase TiO_2 (101) surface

In our previous work [27], we reported the hole-assisted of conversion of CO to CO_2 on the positive surface of anatase (101) as a photocatalytic oxidation reaction. For photocatalytic reactions of anatase (101), the adsorbed molecule might be promoted by the photo-induced holes, while the photo-induced electrons are scavenged by acceptor molecules in the ambient (e.g. O_2 or N_2O as an oxidizing agent). In the present study, we investigate the reduction of N_2O by CO molecule as reducing agent therefore modeled of electron scavenger for photocatalysis of anatase (101). The consequence of photo-oxidation and reduction processes due to UV excitation of electron-hole pairs of anatase TiO_2 in the presence of N_2O acceptor and CO donor molecules in the vicinity of the surface can be represented by the diagram shown in Figure 6.3. The optimized structure of photo-oxidation and reduction of CO and N_2O to CO_2 and N_2 , respectively, are shown in Figure 6.4.

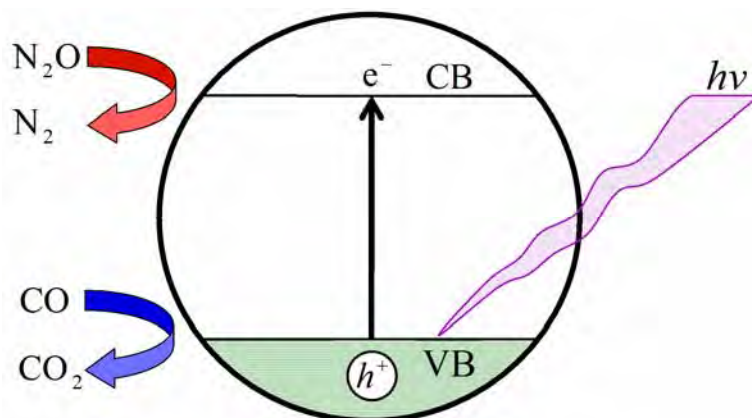


Figure 6.3 Scheme of photo-oxidation and reduction processes due to UV excitation of a TiO_2 crystal in the presence of N_2O acceptor and CO donor molecules in the vicinity of the surface.

The effect of CO molecule on the reduction of N_2O was studied at the initial configuration of CO_2 desorption with O atom bonded the $\text{Ti}_{5\text{C}}$ of 2.281 Å (see Figure 4 of Ref. [27]), assuming the CO molecule is oxidized by the positively charged hole in the valence band during photocatalysis. On the other hand, an electron is excited to the conduction band of the anatase (101) surface. It is seen in Figure 6.4 that CO molecule interacts via C -end with O atom (from $\text{O}_{2\text{C}}$), labeled as O1 , and then N_2O interacts via O -end toward the surface. This N_2O addition leads to the conversion of N_2 in which a $\text{N}\equiv\text{N}$ distance is 1.116 Å, CO_2 with O1-C-O2 angle of 178.14° and C=O distances are 1.17 Å. The optimized structure in this Figure shows that the N_2O directly heal O atom at vacancy site of the surface to the products N_2 and CO_2 , and also causes the anatase (101) surface with oxygen vacancy to perfect surface. These two reactions appear to be simultaneously occurring on the anatase (101) under photocatalysis.

The potential energy profile for conversion of $\text{CO} + \text{N}_2\text{O} \rightarrow \text{CO}_2 + \text{N}_2$ on the anatase TiO_2 (101) surface as photocatalytic process are shown in Figure 6.5. Considering the reaction pathway of the conversion, it is shown that the whole process could be efficient for photocatalytic process. The first step, CO adsorbed on anatase (101) surface through C atom above $\text{Ti}_{5\text{C}}$ site (as denoted, $\text{CO}/[\text{TiO}_2]^0$) with an adsorption energy of -0.26 eV [27]. For the second step, CO_2 adsorbed on the $\text{Ti}_{5\text{C}}$ site of the surface with creating an oxygen vacancy (V_{O}), (as denoted, $\text{CO}_2/[\text{TiO}_2 +$

$V_O]^+$) by overcoming the transition state (TS1). The N_2O interacts via O-end toward V_O site (as denoted, $CO_2/[TiO_2]^0/N_2$) can be occurred by overcoming the transition state (TS2) with the energy needed of -3.46 eV for the third step. The last step, CO_2 and N_2O and N_2 are released from the surface with the energy gain of -3.41 eV.

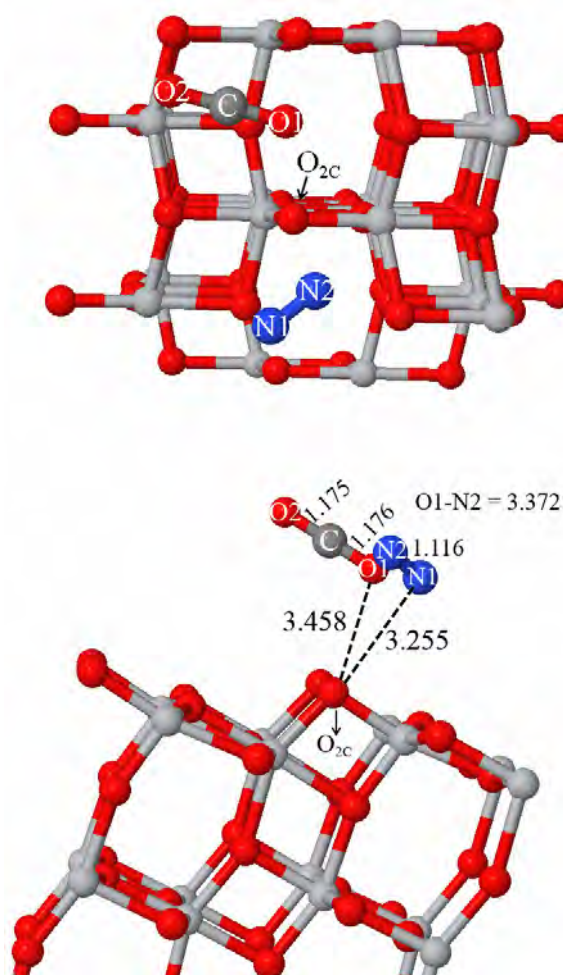


Figure 6.4 Structure for physisorptions of CO_2 and N_2 products adsorbed over the same O_{2c} atom. Top and side views are shown at above and below pictures, respectively. Bond distances are in Å.

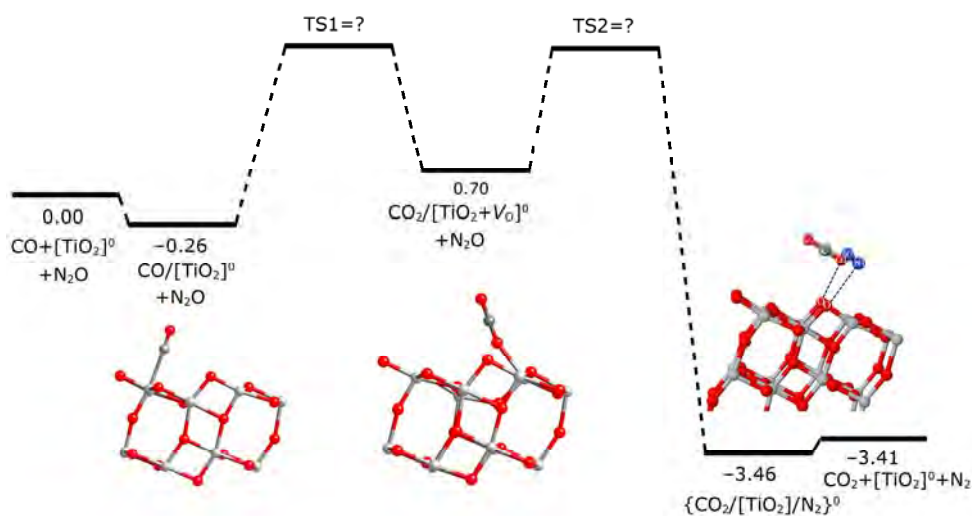


Figure 6.5 Potential energy profile (in eV) for conversion of CO + N₂O to CO₂ + N₂ on the anatase TiO₂ (101) surface. Determination of the barrier for its conversion has been not succeeded.

The reaction steps of CO and N₂O to afford CO₂ and N₂ can be proposed as shown in Figure 6.6. It shows redox process which is composed of the oxidation process of CO to CO₂ and the reduction process of N₂O to N₂. The CO/CO₂ oxidation process occurs via TS1 and follows the Mar–van Krevelen mechanism; the CO reacts with O_{2C} on the anatase (101) surface to form CO adsorption state. The N₂O/ N₂ reduction process occurs via TS2. The N₂O points its O–end toward Ti_{4C} (Ti³⁺) which its oxygen is at the position of oxygen vacancy and the Ti_{4C} (Ti³⁺) is oxidized to Ti_{5C} (Ti⁴⁺), at the same time. Therefore, the over all reactions result the CO₂ and N₂ adsorbed on the anatase TiO₂ (101) surface.

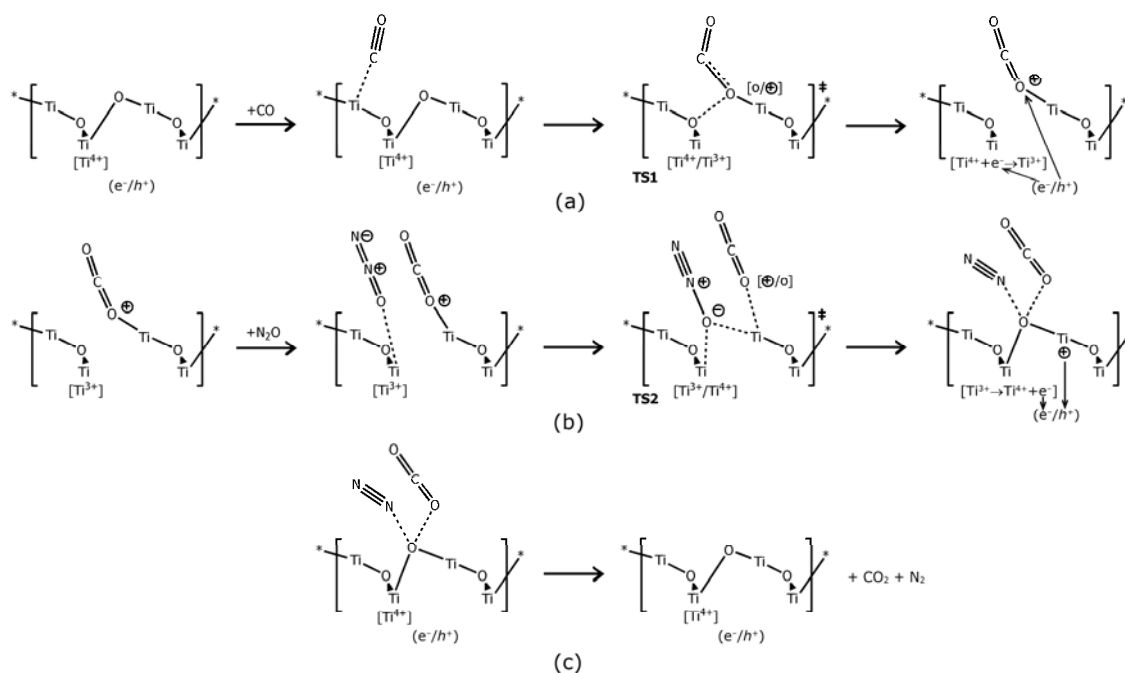


Figure 6.6 The proposed mechanism for conversion of CO + N₂O to CO₂ + N₂ on the spin-polarized anatase TiO₂ (101) surface as (a) the oxidation process of CO to the adsorption-state CO₂, via the proposed barrier state 1 (TS1), (b) the reduction process of N₂O to N₂ on the CO₂/[TiO₂+VO]⁺ via the proposed barrier state 2 (TS2) and (c) the desorption step.

6.5 CONCLUSION

The adsorption of N₂O molecule on the neutral and negative surfaces of the anatase TiO₂ (101) modeled as the photocatalysis were investigated using spin polarized periodic plane wave DFT with GGA-PBE functional calculations. We have identified several possible adsorption configurations of N₂O, linear and also bent structures. Among these configurations the most stable have been found a symmetric bridge configuration when the N atom of N₂O molecule bonded to Ti_{5C}, while O atom bonded to O_{2C} of the surface. Nevertheless, the dissociated N₂O molecule on negative surface of anatase (101) being thermodynamically favored, remarkably, the presence of electron implies that the adsorbed N₂O is dissociated. The presence of an electron acceptor of N₂O on the anatase (101) surface causes enhanced the photo-oxidation of CO to CO₂, allows its conversion to N₂.

CHAPTER VII

FIRST-PRINCIPLES THEORETICAL STUDY OF Pt ATOM SUPPORTED ON ANATASE TiO₂ (101) SURFACE AND ITS INTERACTION WITH CO, N₂, CO₂ AND N₂O

Raina Wanbayor,^{1,2} Peter Deák,² Thomas Frauenheim,² and Vithaya Ruangpornvisuti¹

¹*Department of Chemistry, Faculty of Science, Chulalongkorn University, Bangkok
10330, Thailand*

²*Bremen Center for Computational Material Science, University Bremen, 28359
Bremen, Germany*

This article is in preparation for publication (2011).

7.1 ABSTRACT

The adsorption of CO, N₂, CO₂ and N₂O on the clean TiO₂ and TiO₂-supported Pt (Pt/TiO₂) surfaces of anatase (101) have been investigated by means of density functional theory calculations in generalized gradient approximation. The strong interaction between Pt and anatase TiO₂ (101) surface was shown to be responsible for the enhanced reactivity of gases adsorption. We found the adsorption of CO, CO₂ and bridge structure of N₂O molecules adsorbed on clean TiO₂ (101) surface is energetically less stable than on the Pt/TiO₂ (101) surface. The calculations results clearly favor adsorption of CO in C-end configuration to the Ti_{5C} atom of both clean TiO₂ (101) and Pt/TiO₂ (101) surfaces and highest adsorption energy of -2.55 eV. The adsorption energies increase significantly in the presence of Pt atom. On the other hand, the adsorption of N₂, N-end and O-end of N₂O was weakly adsorbed on the both surfaces.

7.2 INTRODUCTION

Titanium dioxide (TiO₂) is an intensively studied transition metal oxide materials that is used in photocatalysis [2], heterogeneous catalysis [1] and gas-sensor [7] applications, its structures and surfaces have been widely studied [19, 20]. The two most common TiO₂ phases, rutile and anatase are extremely investigated for their potential applications in photocatalysis. However, anatase is advantageous over rutile for photocatalysis [40] and the most stable surface of anatase is the (101) surface [21]. Moreover, the transition metal-support interaction in TiO₂ catalysts has been investigated. The addition of transition metals to a TiO₂ surface can modify its chemical reactivity and therefore enhance its catalytic performance [24, 177, 140]. The electron energy loss spectroscopy (EELS) in the scanning transmission electron microscope studies reported evidence of a strong interaction between the Pt particles and the support is found to be dependent on the Pt cluster size [22]. Pt grows in three-dimensional island on the TiO₂ (110) surface in the temperature range between 160 and 420 K [178]. The interaction of CO molecule on clean TiO₂ [25, 26, 42, 120] as well as TiO₂-supported metal surfaces [16, 23] has also been investigated. The adsorption of a single Pt adatom on perfect anatase TiO₂ (101) surface has been

studied using total energy pseudopotential calculations based on density functional theory (DFT). The most stable configuration takes place a bridge site between two edge O_{2C} atoms. The binding of Pt to the surface is clearly much stronger than that of Au [179]. Molecular structures and vibrational spectra of the CO species adsorbed on the Pt/TiO₂ has been investigated by cluster models and diffuse reflectance infrared fourier transform spectroscopy (DRIFTS). The CO adsorbed on the Pt/TiO₂ gave two intense peaks at 2116 and 2073 cm⁻¹ and two weak peaks at 1857 and 1809 cm⁻¹ [180]. DFT results shown that the stretching vibration mode of the bridging adsorption of CO on the Pt–Pt and Pt–Ti site of Pt/TiO₂, respectively [23]. The Pt/TiO₂ was active for the oxidation of CO to CO₂ in the dark in ambient temperature after UV irradiation, pure TiO₂ was inactive [180]. In addition, the theoretical studies have been also reported. The comparison of the adsorption energies for the three transition metal atoms (Pt, Pd, and Au) adsorbed on anatase (101) surface indicates that the order of the activity for these atoms is Pt > Pd > Au [24]. Periodic DFT investigated the adsorption and dissociation of H₂O on clean TiO₂ (110) and metal-deposited (Pt and Au) TiO₂ (110) surfaces. The results indicate that metal-deposited TiO₂ (110) surfaces catalytically decompose H₂O with barriers much smaller than for their clean TiO₂ (110) surface [181].

In this work, we examine first principle DFT calculations on the adsorption of a Pt atom supported on anatase TiO₂ (101) surface and its interaction with CO, N₂, CO₂ and N₂O molecules. The optimized geometries and adsorption energies are reported.

7.3 COMPUTATIONAL METHODS

The DFT calculations are performed including spin-polarization and using standard plane wave expansions within the generalized gradient approximation (GGA) [82, 175] parameterized with the Perdew–Burke–Emzerho (PBE) [144] for the exchange–correlation potential. The electron–ion interactions were described by the projector augmented–wave (PAW) method [145, 176] with the Vienna ab initio simulation package (VASP) [146, 147, 182, 183] have been used, excluding also the 3*p* shell of Ti from the core. The Brillouin–zone was sampled with the (2×2×1) Monkhorst–Pack k–point set [111] including the *Γ*–point and a planewave cutoff

energy of 420 eV is used. The anatase TiO₂(101) surface slab was represented by a six TiO₂ layers and periodically repeated slabs are separated by about 15 Å thick vacuum layer above it as shown in Figure 7.1, which was used in our previous work [27]. By optimizing the bulk of anatase TiO₂, we obtained the lattice parameters are $a = 3.789$ Å, and $c = 9.607$ Å, to be compared to the experimental results of 3.782 and 9.502 Å, respectively [31]. The result implies that our calculation methods are reasonable. During structural optimization of the system with an adsorbent, the atoms in the two lowest TiO₂ layers were fixed at their bulk geometry whereas the atoms of upper three TiO₂ layers altogether with adsorbate were allowed to relax. Geometry optimizations were stopped when all the forces were smaller than 0.025 eV/Å. In the case of adsorption of single Pt adsorbed on the TiO₂ (101) surface (Pt/TiO₂), to estimate the adsorption energy, we used

$$\Delta E_{\text{ads}} = E_{\text{Pt/surface}} - (E_{\text{Pt}} + E_{\text{surface}}) \quad (7.1)$$

where $E_{\text{Pt/surface}}$ represents the total energy of the Pt/surface system, E_{Pt} is the total energy of the isolated Pt atom, and E_{surface} is the total energy of the clean surface.

The adsorptions of CO, N₂, CO₂ and N₂O on clean anatase (101) surface initiated from several starting positions over the surface were investigated. The adsorption energy (ΔE_{ads}) of adsorbates on the TiO₂ (101) surface was calculated according to the expression

$$\Delta E_{\text{ads}} = E_{\text{adsorbate/surface}} - (E_{\text{adsorbate}} + E_{\text{surface}}) \quad (7.2)$$

where $E_{\text{adsorbate/surface}}$ represents the total energy of the adsorbate/surface system, $E_{\text{adsorbate}}$ is the total energy of the isolated adsorbate in the gas phase, and E_{surface} is the total energy of the clean surface.

In addition, the case of adsorption of an adsorbates with single Pt adsorbed on the TiO₂ (101) surface, to estimate the adsorption energy, we used

$$\Delta E_{\text{ads}} = E_{\text{adsorbate/Pt-surface}} - (E_{\text{adsorbate}} + E_{\text{Pt-surface}}) \quad (7.3)$$

where $E_{\text{adsorbate/Pt-surface}}$ represents the total energy of the adsorbate/Pt-surface system and $E_{\text{adsorbate}}$ is the total energy of the isolated adsorbate in the gas phase, and $E_{\text{Pt/surface}}$ represents the total energy of the Pt/surface system. Closed-shell CO, N₂, CO₂ and N₂O molecules were optimized by spin-unpolarized calculations on a $10 \times 10 \times 10 \text{ \AA}^3$ cubic unit cell.

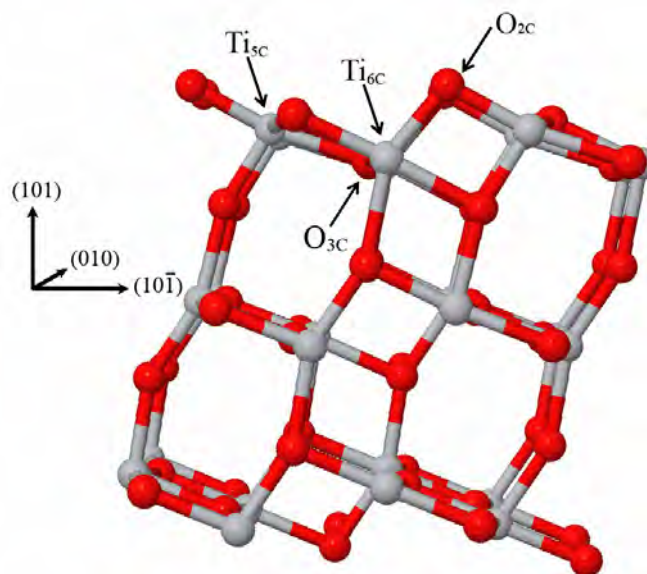


Figure 7.1 The optimized structure of the (1×2) slab model for the anatase TiO₂ (101) surface. Five- and sixfold-coordinated titanium, and two- and threefold-coordinated oxygen surface atoms are labeled as Ti_{5c}, Ti_{6c}, O_{2c}, and O_{3c}, respectively [27].

7.4 RESULTS AND DISCUSSION

We first investigated the equilibrium position of a single Pt atom adsorption on the anatase TiO₂ (101) surface. The Pt atom was placed above two O_{2c} atoms that similar to the most stable configuration of Pt adsorption on anatase TiO₂ (101) surface from the DFT study by Han *et al.* [179] It can be seen from Figure 7.2, we find the most stable configuration of a Pt atom on anatase (101) directly bound to a bridging O_{2c} and in plane O_{3c} atoms, two Ti_{6c} neighbor atoms at the bottom of the step, and the two Ti_{5c} neighbor atoms of the step. This finding is in agreement with the experimental study, which suggests that Pt atoms at low coverage adsorb preferentially at the top of Ti_{5c} site of rutile (110) surface [184]. The adsorption

surface for both configurations. In the C–end case the CO molecule is adsorbed at a distance of 2.531 Å above the Ti_{5C} site, while in the O–end case the distance is larger to 2.784 Å. In the first case the adsorption energy of –0.26 eV is higher than the latter case of –0.2 eV. There is a clear preference for the C–end configuration compared to the O–end configuration.

The interaction of CO with Pt/TiO₂ (101) surface was calculated by heading C atom and O atom of CO molecule toward the supported Pt atom. The calculated adsorption energies with the two configurations are given in Table 7.1. The adsorption of CO molecule significantly affects the bonding geometry of the supported Pt atom. The CO displaces Pt atom from the O_{2C} site and causes its migration to above of the Ti_{5C} and Ti_{6C} atoms. In the case of O atom toward the supported Pt (see Figure 7.2 (c)), the configuration after relaxation is still pointing the C atom to supported Pt atom. The adsorption energy for this system of –2.54 eV is similar to the case of C atom, in agreement with the experiment result of CO linearly adsorbed on Pt particles. [186]. It is confirmed that the C–end configuration of CO preferentially adsorbed on Pt/TiO₂ (101) surface.

Table 7.1 Adsorption energies and geometrical parameters for CO, N₂, CO₂ and N₂O adsorption on the Pt/TiO₂ (101) and TiO₂ (101) surfaces.

configuration	ΔE_{ads} (eV)	
	Pt/TiO ₂ (101)	TiO ₂ (101)
<i>C–end of CO</i>	–2.55	–0.26 ^a
<i>O–end of CO</i>	–2.54	–0.06 ^a
N ₂	–0.04	–0.10
CO ₂	–2.30	–0.17
N ₂ O with N	–0.02	–0.17
N ₂ O with O	–0.03	–0.13
N ₂ O with bend	–2.64	–2.24

^a Ref. [27]

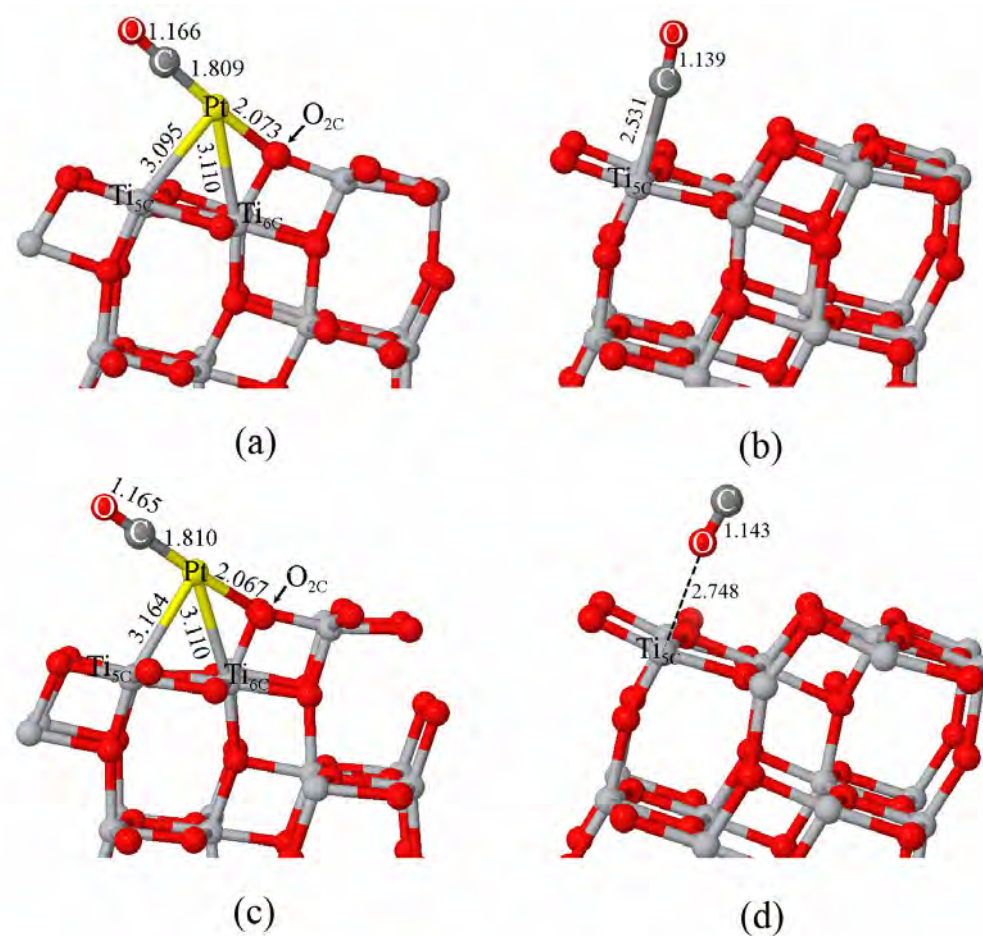


Figure 7.3 Optimized geometries of CO adsorbed on the surface of (a) Pt/TiO₂ (101) and (b) clean TiO₂ (101) with C-end, (c) Pt/TiO₂ (101) and (b) clean TiO₂ (101) with O-end. Bond distances are in Å.

7.4.2 Adsorption of N₂

Based on TPD result reported that the N₂ molecules bind head-on to Ti_{5C} atoms. The adsorption occurs preferentially on the Ti_{5C} atoms of rutile TiO₂ (110) surface [42] and also the *ab initio* SCF cluster calculation using Monte Carlo (MC) simulations [187]. Therefore, the adsorption of N₂ molecule was investigated by pointing N atom toward Ti_{5C} atom of the clean TiO₂ (101) and above Pt atom of Pt/TiO₂ (101) surface. The calculated geometries and bond distances are shown in Figure 7.4. The adsorption energies are shown in Table 7.1. As can be seen in Figure 7.4, the optimized structure gives rise to distances between N₂ molecule and Ti_{5C} atom

of Pt/TiO₂ surface that are about 3.273 Å, longer than the corresponding to the adsorption for the clean surface of 0.602 Å. Our results show N₂ molecule is weakly adsorbed on both clean TiO₂ (101) and Pt/TiO₂ (101) surfaces in tilted configuration is only a rather weak physisorption. The adsorption energies are much smaller –0.10 for clean TiO₂ surface, in agree quite well with recent experimental study of –0.14 eV for N₂O adsorption on rutile (110) [42] and –0.04 eV for Pt/TiO₂ surface. The calculated N≡N bond distances of N₂ adsorbed on clean TiO₂ and Pt/TiO₂ surfaces are 1.113 and 1.116 Å, respectively, that corresponding to the theoretical study [188]. It appears that the adsorption of N₂ at Pt/TiO₂ (101) surface is not affected. However, because of the repulsive interaction between Pt atom and N₂ molecule, N₂ moves from the Ti_{5C} site to 3.013 Å compared to 2.660 Å of clean TiO₂.

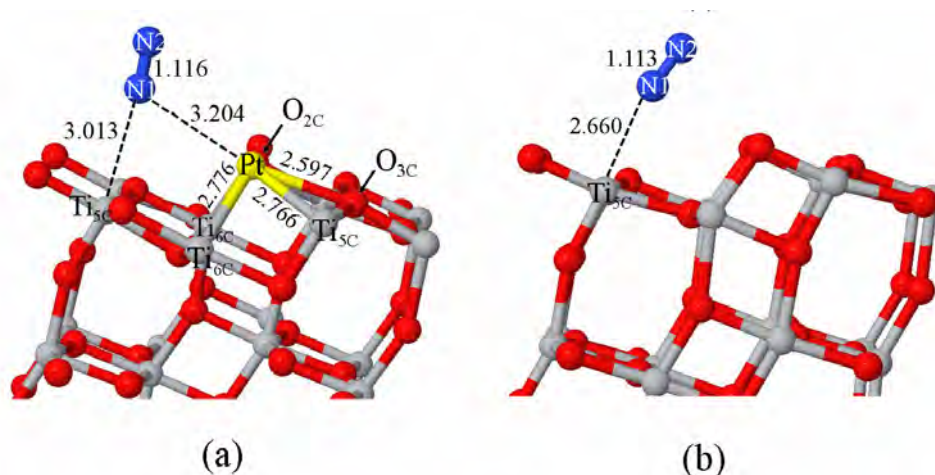


Figure 7.4 The optimized geometries of the adsorption of N₂ molecule on the surface of (a) Pt/TiO₂ (101) and (b) clean TiO₂ (101). Bond distances are in Å.

7.4.3 Adsorption of CO₂

From the temperature-programmed desorption has been reported the CO₂ bound to regular Ti_{5C} atoms on TiO₂ (110) surface [188]. Therefore, CO₂ adsorption was investigated by performing calculations with the CO₂ molecule is vertically and parallel adsorbed on the clean TiO₂ (101) surface at the Ti_{5C} site. For CO₂ adsorption on the clean TiO₂ (101), it is observed that the CO₂ molecule remain vertical to the Ti_{5C} site in slightly tilted configuration with O atom toward Ti_{5C} site as shown in

Figure 7.5 (b). The adsorption energy for vertical orientation of -0.17 eV is favored by about 0.13 eV compared to the parallel configuration. Therefore, the most stable geometry corresponds to the case when the O atom of CO_2 molecule is oriented toward the $\text{Ti}_{5\text{C}}$ site of the clean TiO_2 (101) surface. Therefore, the adsorption of CO_2 on Pt/TiO_2 (101) was calculated by using the vertical orientation of O atom toward Pt atom. The CO_2 molecule can bond to the Pt/TiO_2 (101) surface via its C–Pt bond in the length of 2.043 Å and one O– $\text{Ti}_{5\text{C}}$ bond; its adsorption energy is -2.3 eV, see Figure 7.5 (a). The strong interaction between C atom of CO_2 and supported Pt atom leads to bridging configuration of CO_2 to 130.70° comparative to 177.75° in the case of clean TiO_2 (101) surface.

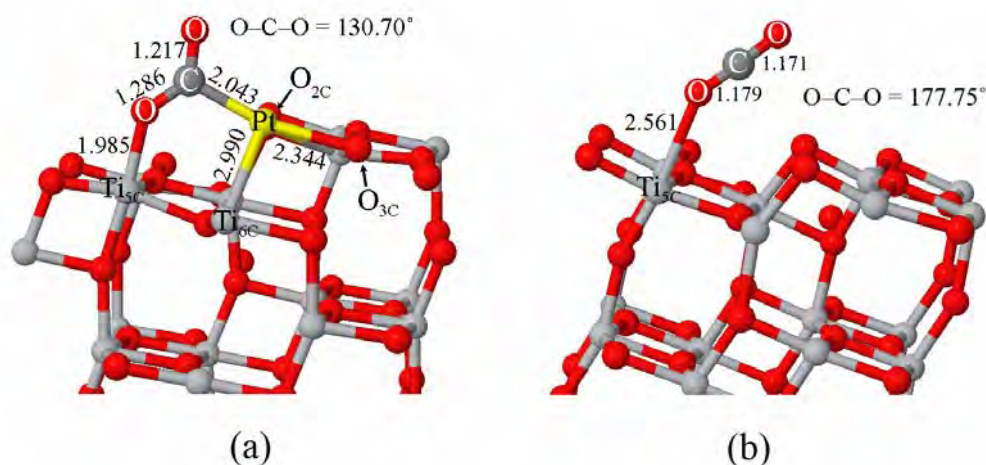


Figure 7.5 The optimized geometries of the adsorption of CO_2 molecule on the surface of (a) Pt/TiO_2 (101) and (b) clean TiO_2 (101). Bond distances are in Å.

7.4.4 Adsorption of N_2O

We determined several possible adsorption configurations for the N_2O molecule on the both clean TiO_2 (101) and Pt/TiO_2 (101) surfaces. In agreement with theoretical results, which show that the N_2O can bound via the N–end and O–end of the molecule to the $\text{Ti}_{5\text{C}}$ site as linear structure [49] and also bridge structures [130]. Therefore, three different configurations have been employed, namely, N–end, O–end and bridge bending. The optimized geometries and bond distances are shown in Figure 7.6. The calculated adsorption energies of molecularly adsorbed N_2O are

shown in Table 7.1. We start by investigating the adsorption of molecular N_2O with N-end and O-end configurations toward Ti_{5C} atom of the clean TiO_2 (101) surface. The calculated N_2O adsorption energies on both configurations are -0.17 and -0.13 eV, respectively. The optimized structures of N-end and O-end configuration adsorbed on the clean TiO_2 (101) are shown in Figures 7.6 (b) and (d), respectively. In the first case, a $N1-Ti_{5C}$ bond is a little bit shorter than $O-Ti_{5C}$ bond of 0.076 Å. There is a clear preference for the N-end configuration compared to the O-end configuration, in good agreement with the theoretical studies [41, 50,130]. For N_2O adsorption of both configurations on the Pt/TiO_2 (101) surface, adsorption energies are much smaller -0.02 and -0.03 eV, respectively. It was found that the supported Pt is reduced the adsorption energies of N_2O for both N-end and O-end configurations. This behavior is due this result suggests that the repulsion interactions between N_2O molecule with Pt atom. The relaxation of the system made the N_2O molecule leading to desorption from the Pt/TiO_2 (101) surface.

Next, we investigated the bridge N_2O configuration adsorbed on clean TiO_2 (101), see Figure 7.6 (f) where N_2O interacts with $N1$ to O_{2C} atom and an O to Ti_{5C} atom. The calculated adsorption energy is -2.24 eV. This configuration was found to be more stable than both N-end and O-end configurations. For the N_2O bridge bending adsorbed on Pt/TiO_2 (101) surface, one N atom ($N1$) is bound to Pt atom and O_{2C} atom of the surface while it one O atom is bound to Ti_{5C} atom, $N1-Pt$, $N2-Pt$ distances are 2.035 and 2.013 Å, respectively, and allowing the Pt atom closest to the O_{3C} surface of $Pt-O_{3C}$ distance is 2.227 Å. The calculated adsorption energy of this configuration is -2.64 eV, which stronger than of 0.4 eV comparative to clean TiO_2 surface.

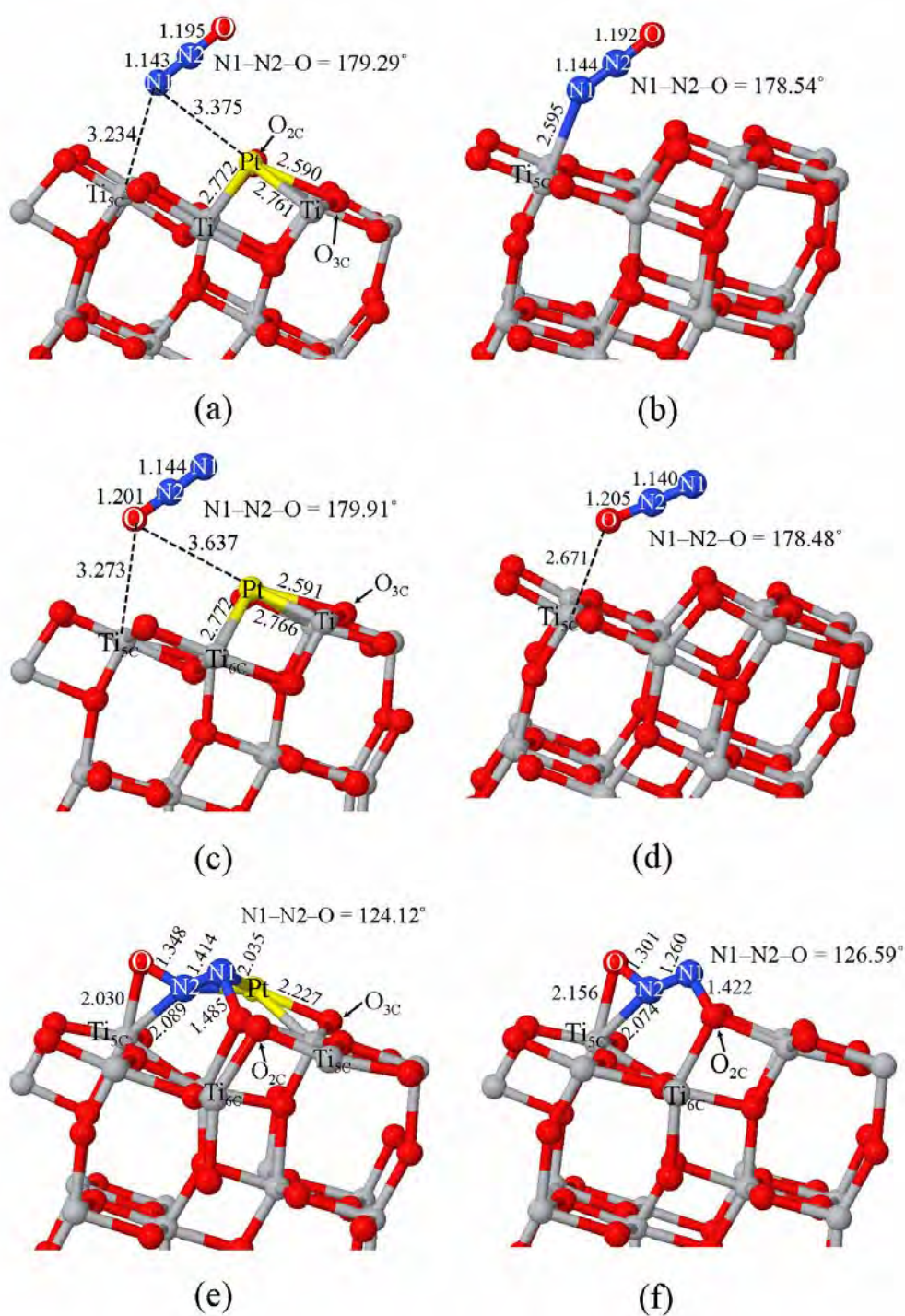


Figure 7.6 The optimized geometries of the adsorption of N_2O molecule on the surface of (a) Pt/TiO_2 (101) and (b) clean TiO_2 (101), with N-end (c) Pt/TiO_2 (101) and (b) clean TiO_2 (101), with O-end and (e) Pt/TiO_2 (101) and (f) clean TiO_2 (101), with bridge configuration. Bond distances are in \AA .

7.5 CONCLUSION

The adsorption of CO, N₂, CO₂, and N₂O on the clean TiO₂ (101) and Pt/TiO₂ surfaces of anatase (101) have been studied by a periodic approach using density functional theory. The presence of the Pt atom supported on anatase TiO₂ (101) strongly stabilizes the adsorption of CO and CO₂ molecules. Adsorption of N₂O in N-end, O-end and bridge configurations has been studied. We found that the bridge configuration to be favorable for both clean TiO₂ (101) and Pt/TiO₂ (101) surfaces. On the contrary, adsorption of N₂, N-end and O-end of N₂O on Pt/TiO₂ (101) are energetically less stable than on the clean TiO₂ (101) surface.

CHAPTER VIII

CONCLUSIONS

8.1 CONCLUSIONS

In this work we report the theoretical study based on DFT within B3LYP and GGA calculations on the adsorption of molecular gases on anatase TiO₂ (001) and (101) as well as on rutile TiO₂ (001) and (110) surfaces. In addition, the adsorption of a single Pt atom on anatase (101) surface was examined. The model clusters and periodic boundary conditions were employed. The conclusions can be summarized as follows.

Firstly, we have systematically studied the adsorption of diatomic (O₂, N₂, H₂, CO and NO), triatomic (H₂O, H₂S, N₂O, CO₂, NO₂ and SO₂) and polyatomic (NH₃, C₂H₂, C₂H₄ and CH₄) gases on Ti₉O₃₃H₃₀ and Ti₉O₃₃H₄₂ model clusters of the anatase TiO₂ (001) and (101) surfaces, respectively, by using the B3LYP/6-31G(d), B3LYP/6-311G(d,p)//B3LYP/6-31G(d) and BSSE corrected B3LYP/6-31G(d) calculations. The adsorptions of all studied gases on the anatase TiO₂ can be summarized that the TiO₂ (001) surface greatly prefers to adsorb NH₃ and H₂O, and the TiO₂ (101) surface prefers to adsorb NO and O₂. The TiO₂ (101) surface can be used a catalyst for NO_x conversion reaction.

We have used the periodic slab calculations with DFT at the B3LYP level in order to study the adsorption of CO, H₂, N₂O, NH₃ and CH₄ on the anatase TiO₂ (001) and (101) surfaces and have investigated the optimized geometries and adsorption energies. The relative adsorption energies of these gases on the TiO₂ (001) and (101) surfaces are in orders: NH₃ >> CO >> H₂ ≈ CH₄ ≈ N₂O and NH₃ >> CO ≈ N₂O > CH₄, respectively. The co-adsorption configuration of N₂O and CO on the TiO₂ (001) surface to form products CO₂ and N₂ *via* the transition-state was proposed.

The adsorption energies of CO, H₂, N₂O, NH₃ and CH₄ on the rutile TiO₂ (001) and (110) surfaces were also obtained using periodic first-principles calculations based on DFT/B3LYP theory. All the studied gases can adsorb on the rutile TiO₂ (001) and (110) surfaces, except methane cannot adsorb on the (110) surface. The relative adsorption energies of these gases on the rutile TiO₂ (001) and

(110) surfaces are in orders: $\text{NH}_3 > \text{H}_2\text{O} \gg \text{N}_2\text{O} > \text{CO} \gg \text{H}_2 > \text{CH}_4$ and $\text{NH}_3 \approx \text{H}_2\text{O} > \text{N}_2\text{O} \approx \text{CO} \gg \text{H}_2$, respectively.

We have found that the adsorption of these adsorbed gases on rutile surfaces are much stronger than on anatase surfaces. The strong adsorption of molecular gases on TiO_2 can be used for designing new catalytic processes.

To understand the photocatalytic oxidation process of CO, the neutrally and positively charged anatase (101) surfaces have been determined. By first principles spin polarized GGA calculations we have shown that positive charge on the anatase (101) surface increases the adsorption energy of CO, allowing the spontaneous conversion of CO to CO_2 , and the desorption of CO_2 creation of a surface oxygen vacancy. In this three-step process the adsorption energy, the activation energy for conversion, and the energy of dissociation was calculated to be -0.45 , $+0.4$ and $+0.42$ eV, respectively, with a total energy gain of -1.59 eV. Holes on anatase can be produced by UV excitation. The photocatalytic oxidation of CO to CO_2 can be spontaneous at room temperature.

In addition, we have investigated the reduction of N_2O into N_2 on anatase (101) surface after photocatalytic oxidation of CO. The reaction proceeds *via* the oxidation of CO by hole-assisted to produce CO_2 leaving the surface, and therefore facilitates the reduction of N_2O . The photocatalytic redox mechanism is proposed for CO + N_2O reaction, which is subsequently provided to CO_2 and N_2 . According to our calculations, the oxidation of CO and reduction of N_2O on the anatase (101) surface can be an efficient photocatalytic process.

Finally, we have studied the TiO_2 -supported Pt on anatase (101) surface and its interaction with CO, N_2 , CO_2 and N_2O molecules using periodic approach. Our calculations thus reveal that TiO_2 -supported Pt on the anatase (101) surface might exhibit a catalytic activity toward the adsorption of CO and CO_2 .

8.2 RESEARCH LIMITATIONS

Although, first-principles calculation in computational chemistry is a powerful tool to provide information for solid state physics development, the understanding of the mechanistic details of the reaction process under chemically reactive conditions is still far from complete. In particular the interaction between gases–TiO₂ surfaces would greatly enhance the computational work. Due to the limitation of computer facilities, time-consuming calculations could not be performed to obtain the dynamical and electrical properties of the molecular gases adsorption on TiO₂ and Pt/TiO₂ surfaces over longer time periods. Moreover, the use of molecular dynamic (MD) simulations for reaction path ways may be required.

8.3 SUGGESTIONS FOR FUTURE WORK

Titanium dioxide (TiO₂) is still an important material for gas sensors and photocatalysis applications. Due to the knowledge of the molecular gases adsorption on TiO₂ lead to find efficient and economical way to convert toxic gas into non-toxic gas. Thus, this important aspect of catalytic reactions occurring with participation of adsorbed molecule remains open for further experimental and theoretical studies. In this dissertation, the obtained results could provide the knowledge for molecular gases adsorption on both anatase and rutile surfaces of TiO₂ as well as TiO₂–supported metals.

Moreover, the transition calculations need to be described in order to get higher accurate prediction of chemical reaction. To improve the research, there are many interesting projects to provide the information for discovering and designing the new photocatalyst. In a future study we will address the more general case when molecular gases adsorption take place on the defective TiO₂ surfaces and TiO₂–supported metals. The comprehensive theoretical studies are still desirable in view of the potential applications of the system in a considerably wide range.

REFERENCES

- [1] Han, F., Kambala, V. S. R., Srinivasan, M., Rajarathnam, D., and Naidu R. Tailored titanium dioxide photocatalysts for the degradation of organic dyes in wastewater treatment: A review. Appl. Catal. A: Gen. 359 (2009): 25–40.
- [2] Fujishima, A., Zhang, X., and Tryk, D. A. TiO₂ photocatalysis and related surface phenomena. Surf. Sci. Rep. 63 (2008): 515–582.
- [3] Diebold, U. The surface science of titanium dioxide. Surf. Sci. Rep. 48 (2003): 53–229.
- [4] Hoffman, M. R., Martin, S. T., Choi, W., and Bahnemannt, D. W. Environmental applications of semiconductor photocatalysis. Chem. Rev. 95 (1995): 69–96.
- [5] Thompson, T. L., and Yates, J. T. Surface science studies of the photoactivation of TiO₂—new photochemical processes. Chem. Rev. 106 (2006): 4428–4453.
- [6] Ohtani, B., Ogawa, Y., and Nishimoto, S. Photocatalytic activity of amorphous–anatase mixture of titanium (IV) oxide particles suspended in aqueous solutions. J. Phys. Chem. B 101 (1997): 3746–3752.
- [7] Tang, J. H., Prasad, K., Sanjinés, R., and Lévy, F. TiO₂ anatase thin films as gas sensors. Sens. Actuators B: Chem. 26 (1995): 71–75.
- [8] Guidi, V., Carotta, M. C., Ferroni, M., Martinelli, G., Paglialonga, L., Comini, E., et al. Preparation of nanosized titania thick and thin films as gas–sensors. Sens. Actuators B: Chem. 57 (1999): 197–200.
- [9] Mather, G. C., Marques, F. M. B., and Frade, J. R. Detection mechanism of TiO₂–based ceramic H₂ sensors. J. Eur. Ceram. Soc. 19 (1999): 887–891.
- [10] Mor, G. K., Varghese, O. K., Paulose, M., Ong, K. G., and Grimes, C. A. Fabrication of hydrogen sensors with transparent titanium oxidenanotube–array thin films as sensing elements. Thin Solid Films 496 (2006): 42–48.
- [11] Savage, N. O., Akbar, S. A., and Dutta, P. K. Titanium dioxide based high temperature carbon monoxide selective sensor. Sens. Actuators B 72 (2001): 239–248.
- [12] Oregan, B., and Gratzel, M. A low–cost, high–efficiency solar cell based on dye–sensitized colloidal TiO₂ films. Nature 353 (1991): 737–740.

- [13] Bach, U., Lupo, D., Comte, P., Moser, J. E., Weissortel, F., Salbeck, J., et al. Solid-state dye-sensitized mesoporous TiO₂ solar cells with high photon-to-electron conversion efficiencies. Nature 395 (1998): 583–585.
- [14] Macak, J. M., Tsuchiya, H., Ghicov, A., and Schmuki, P. Dye-sensitized anodic TiO₂ nanotubes. Electrochem. Commun. 7 (2005): 1133–1137.
- [15] Shankar, K., Bandara, J., Paulose, M., Wietasch, H., Varghese, O. K., Mor, G. K., et al. Highly efficient solar cells using TiO₂ nanotube arrays sensitized with a donor-antenna dye. Nano Lett. 8 (2008): 1654–1659.
- [16] Bredow, T., and Pacchioni G. A quantum-chemical study of Pd atoms and dimmers supported on TiO₂ (110) and their interaction with CO. Surf. Sci. 426 (1999): 106–122.
- [17] Di Valentin, C., Finazzi, E., Pacchioni, G., and Selloni, A. Density functional theory and electron paramagnetic resonance study on the effect of N-F codoping of TiO₂. Chem. Mater. 20 (2008): 3706–3714.
- [18] Wold, A. Photocatalytic properties of TiO₂. Chem. Mater. 5 (1993): 280–283.
- [19] Hsiung, T. L., Wang, H. P., and Lin, H. P. Chemical structure of photocatalytic active sites in nanosize TiO₂. J. Phys. Chem. Solids 69 (2008): 383–385.
- [20] Ariga, H., Taniike, T., Morikawa, H., Tero R., Kondoh, H., and Iwasawa, Y. Lattice-work structure of a TiO₂ (001) surface studied by STM. Chem. Phys. Lett. 454 (2008): 350–354.
- [21] Diebold, U., Ruzycki, N., Hermanb, G. S., and Selloni, A. One step towards bridging the materials gap: surface studies of TiO₂ anatase. Catal. Today 85 (2003): 93–100.
- [22] Iddir, H., Disko, M. M., Ogut, S., and Browning, N. D. Atomic scale characterization of the Pt/TiO₂ interface. Micron 36 (2005): 233–241.
- [23] Gao, H., Xu, W., Hea, H., Shi, X., Zhang, X., and Tanaka, K. -I. DRIFTS investigation and DFT calculation of the adsorption of CO on Pt/TiO₂, Pt/CeO₂ and FeO_x/Pt/CeO₂. Spectro. Acta Part A 71 (2008): 1193.
- [24] Zhang, J., Zhang, M., Han, Y., Li, W., Meng, X., and Zong, B. Nucleation and growth of palladium clusters on anatase TiO₂ (101) surface: A first principle study. J. Phys. Chem. C 112 (2008): 19506–19515.
- [25] Wanbayor, R., and Ruangpornvisuti, V. Adsorption of di-, tri- and polyatomic gases on the anatase TiO₂ (001) and (101) surfaces and their adsorption abilities. J. Mol. Struct. (theochem) 952 (2010) 103–108.

- [26] Wanbayor, R., and Ruangpornvisuti, V. Adsorption of CO, H₂, N₂O, NH₃ and CH₄ on the anatase TiO₂ (001) and (101) surfaces and their competitive adsorption predicted by periodic DFT calculations. *Mat. Chem. Phys.* 124 (2010): 720–725.
- [27] Wanbayor, R., Deák, P., Frauenheim, T., and Ruangpornvisuti, V. First-principles theoretical study of the hole-assisted conversion of CO to CO₂ on the anatase TiO₂ (101) surface. *J. Chem. Phys.* 134 (2011): 104701-1–104701-6.
- [28] Wanbayor, R., and Ruangpornvisuti, V. Periodic density-functional theory study of CO, H₂, N₂O, H₂O, NH₃ and CH₄ adsorbed on the rutile TiO₂ (001) and (110) surface. (2011) *Submitted*.
- [29] Pyrgiotakis, G., Ph.D. Thesis. Titania carbon nanotube composites for enhanced photocatalysis. University of Florida, 2006.
- [30] Linsebigler, A. L., Lu, G., and Yates, J. T., Jr. Photocatalysis on TiO₂ surfaces: Principles, mechanism, and selected results. *Chem. Rev.* 95 (1995): 735–758.
- [31] Burdett, J. K., Hughbanks, T., Miller, G. J., Richardson, J. W., Yates, J. T., Jr. and Smith, J. V. Structural–electronic relationships in inorganic solids: powder neutron diffraction studies of the rutile and anatase polymorphs of titanium dioxide at 15 and 295 K. *J. Am. Chem. Soc.* 109 (1987): 3639–3646.
- [32] Sclafani, A., and Herrman, J. M. Comparison of the photoelectronic and photocatalytic activities of various anatase and rutile forms of titania in pure liquid organic phases and in aqueous solutions. *J. Phys. Chem.* 100 (1996): 13655–13661.
- [33] Kormann, C., Bahnemann, D. W., and Hoffmann, M. R. Preparation and characterization of quantum-size titanium dioxide. *J. Phys. Chem.* 92 (1988): 5196–5210.
- [34] Zhang, H., and Banfield, J. F. Thermodynamic analysis of phase stability of nanocrystalline titania. *J. Mater. Chem.* 8 (1998): 2073–2076.
- [35] Herman, G. S., Sievers, M. R., and Gao, Y. Structure determination of the two-domain (1×4) anatase TiO₂ (001) surface. *Phys. Rev. Lett.* 84 (2000) 3354–3357.

- [36] Nörenberg, H., Dinelli, F., Briggs, G. A. D. Network-like ($7\sqrt{2} \times \sqrt{2}$) $R45^\circ$ surface reconstruction on rutile TiO_2 (001) by non-equilibrium self-organization. Surf. Sci. 436 (1999) L635–L640
- [37] Hussain, A., Gracia, J., Nieuwenhuys, B. E., and Niemantsverdriet, J. W. Chemistry of O- and H-containing species on the (001) surface of anatase TiO_2 : A DFT study. Chemphyschem 11 (2010): 2375–82.
- [38] Barteau, M. A. Organic reactions at well-defined oxide surfaces. Chem. Rev. 96 (1996): 1413–1430.
- [39] Hadjiivanov, K. FTIR study of CO and NH_3 co-adsorption on TiO_2 rutile. Appl. Surf. Sci. 135 (1998): 331–338.
- [40] Sumita, T., Yamaki, T., Yamamoto, S., and Miyashita, A. Photo-induced surface charge separation of highly oriented TiO_2 anatase and rutile thin films. App. Surf. Sci. 200 (2002): 21–26.
- [41] Tamaki, Y., Furube, A., and Murai, M. Direct observation of reactive trapped holes in TiO_2 undergoing photocatalytic oxidation of adsorbed alcohols: Evaluation of the reaction rates and yields. J. Am. Chem. Soc. 128 (2006): 416–417.
- [42] Dohnálek, Z., Kim, J., Bondarchuk, O., White, J. M., and Kay, B. D. Physisorption of N_2 , O_2 , and CO on fully oxidized TiO_2 (110). J. Phys. Chem. B 110 (2006): 6229–6235.
- [43] Rauppt, G. B., and Dumesic, J. A. Adsorption of CO, CO_2 , H_2 , and H_2O on titania surfaces with different oxidation states. J. Phys. Chem. 89 (1985): 5240–5246.
- [44] Pang, C. L., Sasahara, A., and Onishi, H. Scanning tunnelling microscopy study of ammonia adsorption on TiO_2 (110). Nanotechnology 18 (2007): 1–4.
- [45] Yamazoe, S., Okumura, T., Teramura, K., and Tanaka, T. Development of the efficient TiO_2 photocatalyst in photoassisted selective catalytic reduction of NO with NH_3 . Catal. Today 111 (2006): 266–270.
- [46] Abad, J., Böhme, O., and Román, E. Dissociative adsorption of NO on TiO_2 (110)–(1×2) surface: Ti_2O_3 rows as active sites for the adsorption. Langmuir 23 (2007): 7583–7586.

- [47] Sorescu, D. C., Rusu, C. N., and Yates, J. T. Adsorption of NO on the TiO₂ (110) surface: An experimental and theoretical study. J. Phys. Chem. B 104 (2000): 4408–4417.
- [48] Rodriguez, J. A., Jirsak, T., Liu, G., Hrbek, J., Dvorak, J., and Maiti, A. Chemistry of NO₂ on oxide surfaces: formation of NO₃ on TiO₂ (110) and NO₂↔O vacancy interactions. J. Am. Chem. Soc. 123 (2001): 9597–9605.
- [49] Rusu, C. N., Yates, J. T., Jr. N₂O Adsorption and photochemistry on high area TiO₂ powder. J. Phys. Chem. B 105 (2001): 2596–2603.
- [50] Gratzel, M. Photoelectrochemical cells. Nature 414 (2001): 338–344.
- [51] Zhang, Z. B., Wang, C. C., Zakaria, R., and Ying, J. Y. Role of particle size in nanocrystalline TiO₂-based photocatalysts. J. Phys. Chem. B 102 (52) (1998) 10871–10878.
- [52] Paulose, M., Varghese, O. K., Mor, G. K., Grimes, C. A., and Ong, K. G. Unprecedented ultra-high hydrogen gas sensitivity in undoped titania nanotubes. Nanotechnology 17 (2006): 398–402.
- [53] Varghese, O. K., Gong, D. W., Paulose, M., Ong, K. G., Dickey, E. C., and Grimes, C. A. Extreme changes in the electrical resistance of titania nanotubes with hydrogen exposure. Adv. Mater. 15 (2003): 624–627.
- [54] Varghese, O. K., Mor, G. K., Grimes, C. A., Paulose, M., and Mukherjee, N. A titania nanotube-array room-temperature sensor for selective detection of hydrogen at low concentrations. J. Nanosci. Nanotechnol. 4 (2004): 733–737.
- [55] Yoriya, S., Prakasam, H. E., Varghese, O. K., Shankar, K., Paulose, M., Mor, G. K., et al. Initial studies on the hydrogen gas sensing properties of highly-ordered high aspect ratio TiO₂ nanotube-arrays 20 μm to 222 μm. Sensor Lett. 4 (2006): 334–339.
- [56] Mor, G. K., Carvalho, M. A., Varghese, O. K., Pishko, M. V., and Grimes, C. A. A room-temperature TiO₂-nanotube hydrogen sensor able to self-clean photoactively from environmental contamination. J. Mater. Res. 19 (2004): 628–634.
- [57] Mor, G. K., Varghese, O. K., Paulose, M., and Grimes, C. A. A Self-cleaning, room-temperature titania-nanotube hydrogen gas sensor. Sensor Lett. 1 (2003): 42–46.

- [58] Oregan, B., and Gratzel, M. A low-cost, high-efficiency solar cell based on dye-sensitized colloidal TiO₂ films. Nature 353 (1991): 737–740.
- [59] Bach, U., Lupo, D., Comte, P., Moser, J. E., Weissortel, F., Salbeck, J., et al. Solid-state dye-sensitized mesoporous TiO₂ solar cells with high photon-to-electron conversion efficiencies. Nature 395 (1998): 583–585.
- [60] Macak, J. M., Tsuchiya, H., Ghicov, A., and Schmuki, P. Dye-sensitized anodic TiO₂ nanotubes. Electrochem. Commun. 7 (2005): 1133–1137.
- [61] Mor, G. K., Varghese, O. K., Paulose, M., Shankar, K., and Grimes, C. A. A review on highly ordered, vertically oriented TiO₂ nanotube arrays: Fabrication, material properties, and solar energy applications. Solar Energ. Mater. Solar Cell 90 (2006): 2011–2075.
- [62] Mor, G. K., Shankar, K., Paulose, M., Varghese, O. K., and Grimes, C. A. Use of highly-ordered TiO₂ nanotube arrays in dye-sensitized solar cells. Nano Lett. 6 (2006): 215–218.
- [63] Bechinger, C., Ferrer, S., Zaban, A., Sprague, J., Gregg, B. A. Photoelectrochromic windows and displays. Nature 383 (1996): 608–610.
- [64] Allam, N. K., Shankar, K., and Grimes, C. A. Photoelectrochemical and water photoelectrolysis properties of ordered TiO₂ nanotubes fabricated by Ti anodization in fluoride-free HCl electrolytes. J. Mater. Chem. 18 (2008): 2341–2348.
- [65] Beranek, R., Tsuchiya, H., Sugishima, T., Macak, J. M., Taveira, L., Fujimoto, S., Kisch, et al. Enhancement and limits of the photoelectrochemical response from anodic TiO₂ nanotubes. Appl. Phys. Lett. 87 (2005): 243114-1–243114-3.
- [66] Mor, G. K., Shankar, K., Varghese, O. K., and Grimes, C. A. Photoelectrochemical properties of titania nanotubes. J. Mater. Res. 19 (2004): 2989–2996.
- [67] Yamashita, H., Kamada, N., He, H., Tanaka, K., Ehara, S., and Anpo, M. Reduction of CO₂ with H₂O on TiO₂ (100) and TiO₂ (110) single crystals under UV-irradiation. Chem. Lett. 5 (1994) 855–858.
- [68] Onal, I., Soyer, S., and Senkan, S. Adsorption of water and ammonia on TiO₂-anatase cluster models. Surf. Sci. 600 (2006): 2457–2469.
- [69] Mguig, B., Calatayud, M., and Minot, C. CO oxidation over anatase TiO₂-(001). J. Mol. Struct. (Theochem) 709 (2004): 73–78.

- [70] Wahab, H. S., Bredow, T., and Aliwi, S. M. Computational investigation of water and oxygen adsorption on the anatase TiO₂ (100) surface. J. Mol. Struct. (Theochem) 868 (2008): 101–108.
- [71] Wahab, H. S., Bredow, T., M., and Aliwi, S. MSINDO quantum chemical modeling study of water molecule adsorption. Chem. Phys. 354 (2008): 50–57.
- [72] Redfern, P. C., Zapol, P., Curtiss, L. A., Rajh, T., and Thurnauer, M. C. Computational studies of catechol and water interactions with titanium oxide nanoparticles. J. Phys. Chem. B 107 (2003): 11419–11427.
- [73] Indrakanti, V. P, Kubicki, J. D., and Schobert, H. H. Quantum chemical modeling of ground states of CO₂ chemisorbed on anatase (001), (101), and (010) TiO₂ surfaces. Energy Fuels 22 (2008): 2611–2618.
- [74] Mattioli, G., Filippone, F., and Bonapasta, A. A. Reaction intermediates in the photoreduction of oxygen Molecules at the (101) TiO₂ (anatase) surface. J. Am. Chem. Soc. 128 (2006): 13772–13780.
- [75] Mattioli, G., Filippone, F., Caminiti, R., and Bonapasta, A. A. Short hydrogen bonds at the water/TiO₂ (anatase) interface. J. Phys. Chem. C 112 (2008): 13579–13586.
- [76] Tilocca, A., and Selloni, A. Structure and reactivity of water layers on defect-free and defective anatase TiO₂ (101) surfaces. J. Phys. Chem. B 108 (2004): 4743–4751.
- [77] Tilocca, A., and Selloni, A. Vertical and lateral order in adsorbed water layers on anatase TiO₂ (101). Langmuir 20 (2004): 8379–8384.
- [78] Blomquist, J., Walle, L. E., Uvdal, P., Borg, A., and Sandell, A. Water dissociation on single crystalline anatase TiO₂ (001) studied by photoelectron spectroscopy. J. Phys. Chem. C 112 (2008): 16616–16621.
- [79] Went, G. T., and Bell, A. T. Laser Raman spectroscopy of NH₃ and ND₃ adsorbed on TiO₂ (anatase). Catal. Lett. 11 (1991): 111–117.
- [80] Primet, M., Pichat, P., and Mathieu, M. V. Infrared study of the surface of titanium dioxides. II. Acidic and basic properties. J. Phys. Chem. 75 (1971): 1221–1226.
- [81] Herman, G. S., Dohnálek, Z., Ruzycki, N., and Diebold, U. Experimental investigation of the interaction of water and methanol with anatase–TiO₂ (101). J. Phys. Chem. B 107 (2003): 2788–2795.

- [82] Kohn, W., and Sham, L. J. Self-consistent equations including exchange and correlation effects. Phys. Rev. 140 (1965): A1133–A1138.
- [83] Becke, A. D. Density-functional thermochemistry. III. The role of exact exchange. J. Chem. Phys. 98 (1993): 5648–5652.
- [84] Lee, C., Yang, W., and Parr, R. G. Development of the Colle–Salvetti correlation–energy formula into a functional of the electron density. Phys. Rev. B 37 (1988): 785–789.
- [85] Hehre, W. J., Ditchfield, R., and Pople, J. A. Self-consistent molecular orbital methods. XII. Further extensions of Gaussian-type basis sets for use in molecular orbital studies of organic molecules. J. Chem. Phys. 56 (1972) 2257–2261.
- [86] Gordon, M. S. The isomers of silacyclopropane. Chem. Phys. Lett. 76 (1980) 163–168.
- [87] Frisch, M. J., Trucks, G. W., Schlegel, H. B., Scuseria, G. E., Robb, M. A., Cheeseman, J. R., et al. Gaussian 03; Revision C.02; Gaussian, Inc., Wallingford, CT, 2006.
- [88] Horn, M., Schwerdtfeger, C. F., and Meagher, E. P. Refinement of the structure of anatase at several temperatures. Z. Kristallogr. 136 (1972) 273–281.
- [89] Boys, S. F., and Bernadi, F. The calculation of small molecular interactions by the differences of separate total energies. Some procedures with reduced errors. Mol. Phys. 19 (1970): 553–565.
- [90] Rasmussen, M. D., Molina, L. M., and Hammer, B. Adsorption, diffusion, and dissociation of molecular oxygen at defected TiO₂ (110): A density functional theory study. J. Chem. Phys. 120 (2004): 988–997.
- [91] Liu, L. M., McAllister, B., Ye, H. Q., and Hu, P. Identifying an O₂ supply pathway in CO oxidation on Au/TiO₂ (110): A density functional theory Study on the intrinsic role of water. J. Am. Chem. Soc. 128 (2006): 4017–4022.
- [92] Onda, K., Li, B., and Petek, H. Two-photon photoemission spectroscopy of TiO₂ (110) surfaces modified by defects and O₂ or H₂O adsorbates. Phys. Rev. B 70 (2004): 045415–045426.
- [93] Thomas, B., and Karl, J. Theoretical investigation of water adsorption at rutile and anatase surfaces. Surf. Sci. 327 (1995): 398–408.

- [94] Vittadini, A., Selloni, A., Rotzinger, F. P., and Grätzel, M. Structure and energetics of water adsorbed at TiO₂ anatase (101) and (001) surfaces. Phys. Rev. Lett. 81 (1998): 2954–2957.
- [95] Kachurovskaya, N. A., Mikheeva, E. P., Zhidomirov, G. M. Cluster molecular modeling of strong interaction for VO_x/TiO₂ supported catalyst. J. Mol. Catal. A: Chem. 178 (2002): 191–198.
- [96] Selloni, A., Vittadini, A., and Grätzel, M. The adsorption of small molecules on the TiO₂ anatase (101) surface by first-principles molecular dynamics. Surf. Sci. 402–404 (1998): 219–222.
- [97] Arrouvel, C., Digne, M., Breyse, M., Toulhoat, H., and Raybaud, P. Effects of morphology on surface hydroxyl concentration: A DFT comparison of anatase–TiO₂ and γ -alumina catalytic supports. J. Catal. 222 (2004) 152–166.
- [98] Czekaj, I., Kröcher, O., and Piazzesi, G. DFT calculations, DRIFT spectroscopy and kinetic studies on the hydrolysis of isocyanic acid on the TiO₂–anatase (101) surface. J. Mol. Catal. A: Chemical 280 (2008): 68–80.
- [99] Li, W. K., Gong, X. Q., Lu, G., and Selloni, A. Different reactivities of TiO₂ polymorphs: Comparative DFT calculations of water and formic acid adsorption at anatase and brookite TiO₂ surface. J. Phys. Chem. C 112 (2008): 6594–6596.
- [100] Varghese, O. K., and Grimes, C. A. Metal oxide nanoarchitectures for environmental sensing. J. Nanosci. Nanotechnol. 3 (2003): 277–293.
- [101] Nilsing, M., Lunell, S., Persson, P., and Ojamäe, L. Phosphonic acid adsorption at the TiO₂ anatase (101) surface investigated by periodic hybrid HF–DFT computations. Surf. Sci. 582 (2005): 49–60.
- [102] Lushtinetz, R., Frenzel, J., Milek, T., and Seifert, G. Adsorption of phosphonic acid at the TiO₂ anatase (101) and rutile (110) surface. J. Phys. Chem. C 113 (2009) 5730–5740.
- [103] Raghunath, P., Lin, M. C. A Computational study on the adsorption configurations and reactions of phosphorous acid on TiO₂ anatase (101) and rutile (110) surfaces. J. Phys. Chem. C 113 (2009): 8394–8406.
- [104] Dovesi, R., Saunders, V. R., Roetti, C., Orlando, R., Zicovich–Wilson, C. M., Pascale, F., et al. CRYSTAL06 User’s Manual, University of Torino, Torino, 2006.

- [105] Muscat, J., Ph.D. thesis. The phase stability, surface structure and defect chemistry of titanium dioxide from first principles techniques. University of Manchester (1999).
- [106] Towler, M. D., Allan, N. L., Harrison, N. M., Saunders, V. R., Mackrodt, W. C., and Aprà, E. *Ab initio* study of MnO and NiO. Phys. Rev. B 50 (1994): 5041–5054.
- [107] Catti, M., Pavese, A., Dovesi, R., and Saunders, V. C. Static lattice and electron properties of MgCO₃ (magnesite) calculated by *ab initio* periodic Hartree–Fock methods. J. Phys. Rev. B 47 (1993): 9189–9198.
- [108] Valenzano, L., Torres, F. J., Doll, K., Pascale, F., Zicovich–Wilson, C. M., and Dovesi, R. Z. *Ab initio* study of the vibrational spectrum and related properties of crystalline compounds; the case of CaCO₃ calcite. Phys. Chem. 220 (2006): 893–912.
- [109] Gatti, C., Saunders, V. R., and Roetti C. Crystal field effects on the topological properties of the electron density in molecular crystals. The case of urea. J. Chem. Phys. 101 (1994): 10686–10696.
- [110] Cromer, D. T., and Herrington, K. The Structures of anatase and rutile. J. Am. Chem. Soc. 77 (1955): 4708–4709.
- [111] Monkhorst, H. J., and Pack, J. D. Special points for Brillouin–zone integrations. Phys. Rev. B 13 (1976): 5188–5192.
- [112] Scaranto, J., and Giorgianni, S. A quantum–mechanical study of CO adsorbed on TiO₂: A comparison of the Lewis acidity of the rutile (110) and the anatase (101) surfaces. J. Mol. Struct. (Theochem.) 858 (2008): 72–76.
- [113] Bruska, M. K., Szaciowski, K., and Piechota, J. Adsorption of selected ions on the anatase TiO₂ (101) surface: A density–functional study. Mol. Sim. 35 (2009) 567–576.
- [114] Howard, C. J., Sabine, T. M., and Dickson, F. Structural and thermal parameters for rutile and anatase. Acta Crystallogr. B 47 (1991): 462–468.
- [115] Weirich, T. E., Winterer, M., Seifried, S., and Mayer, J. Structure of nanocrystalline anatase solved and refined from electron powder data. Acta Crystallogr. A 58 (2002): 308–315.
- [116] Swamy, V., Dubrovinsky, L. S., Dubrovinskaia, N. A., Simionovici, A. S., Drakopoulos, M., Dmitriev, V., et al. Compression behavior of

- nanocrystalline anatase TiO₂. Solid State Commun. 125 (2003): 111–115.
- [117] Asahi, R., Taga, Y., Mannstadt, W., and Freeman, A. J. Electronic and optical properties of anatase TiO₂. Phys. Rev. B 61(2000): 7459–7465.
- [118] Chang, J. –G, Ju, S. –P., Chang, C. –S., and Chen, H. –T. Adsorption configuration and dissociative reaction of NH₃ on anatase (101) surface with and without hydroxyl groups. J. Phys. Chem. C 113 (2009): 6663–6672.
- [119] Yang, D., Liu, H., Zheng, Z., Yuan, Y., Zhao, J. C., Waclawik, E. R., et al. An efficient photocatalyst structure: TiO₂(B) nanofibers with a shell of anatase nanocrystals. J. Am. Chem. Soc 131 (2009): 17885–17893.
- [120] Göpel, W., and Rocker, G. Intrinsic defects of TiO₂ (110): Interaction with chemisorbed O₂, H₂, CO, and CO₂. Phys. Rev. B 28 (1983): 3427–3438.
- [121] Pang, C. L., Sasahara, A., and Onishi, H. Scanning tunnelling microscopy study of ammonia adsorption on TiO₂ (110). Nanotechnology 18 (2007): 1–4.
- [122] Yamazoe, S., Okumura, T., Hitomi, Y., Shishido, T., and Tanaka, T. Mechanism of photo-oxidation of NH₃ over TiO₂: Fourier transform infrared study of the intermediate species. J. Phys. Chem. C 111 (2007): 11077–11085.
- [123] Peng, H., and Li, J. Quantum confinement and electronic properties of rutile TiO₂ nanowires. J. Phys. Chem. C 112 (2008): 20241–20245.
- [124] Zeng, Z. –L., Zheng, G., Wang, X. –C., He, K. –H., Chen, Q. –L., Yu, L., et al. First-principles study on the structural and electronic properties of double N atoms doped-rutile TiO₂. J. At. Mol. Sci. 1 (2010): 177–184.
- [125] Von Oertzen, G. U., and Gerson, A. R. O deficiency in the rutile TiO₂ (110) surface: *Ab initio* quantum chemical investigation of the electronic properties. Int. J. Quan. Chem. 106 (2006): 2054–2064.
- [126] He, J., Liu, Q., Sun, Z., Yan, W., Zhang, G., Qi, Z., et al. High photocatalytic activity of rutile TiO₂ induced by iodine doping. J. Phys. Chem. C 114 (2010) 6035–6038.
- [127] Traylor, J. G., Smith, H. G., and Nicklow, R. M. Lattice dynamics of rutile. Phys. Rev. B 3 (1971): 3457–3472.

- [128] Kang, S. H., Kang, M. -S., Kim, H. -S., Kim, J. -Y., Chung, Y. -H., Smyrl, W. H., et al. Columnar rutile TiO₂ based dye-sensitized solar cells by radio-frequency magnetron sputtering. J. Power Sources 184 (2008): 331–335.
- [129] Scaranto, J., and Giorgianni, S. A DFT study of CO adsorbed on clean and hydroxylated anatase TiO₂ (001) surfaces. Chem. Phys. Lett. 473 (2009): 179–183.
- [130] Sorescu, D. C., and Yates, J. T. First principles calculations of the adsorption properties of CO and NO on the defective TiO₂ (110) surface. J. Phys. Chem. B 106 (2002): 6184–6199.
- [131] Tanaka, K., Capule, M. F. V., and Hisanaga, T. Effect of crystallinity of TiO₂ on its photo-catalytic action. Chem. Phys. Lett. 187 (1991): 73–76.
- [132] Yanagisawa, K., and Ovenstone, J. Crystallization of anatase from material and temperature. J. Phys. Chem. B 103 (1999): 7781–7787.
- [133] Linsebigler, A., Lu, G., and Yates, J. T. CO chemisorption on TiO₂ (110): Oxygen vacancy site influence on CO adsorption. J. Chem. Phys. 103 (1995): 9438–9443.
- [134] Kunat, M., Traeger, F., Silber, D., Qiu, H., Wang, Y., van Veen, A. C., et al. Formation of weakly bound, ordered adlayers of CO on rutile TiO₂(110): A combined experimental and theoretical study. J. Chem. Phys. 130 (2009): 144703–144714.
- [135] Linsebigler, A., Lu, G., and Yates, J. T. CO Photooxidation on TiO₂ (110). J. Phys. Chem. 100 (1996): 6631–6636.
- [136] Zhang, Z., and Yates, J. T., Jr. Electron-mediated CO oxidation on the TiO₂ (110) surface during electronic excitation. J. Am. Chem. Soc. 132 (2010) 12084–12091.
- [137] Pillay, D., and Hwang, G. S. O₂-coverage-dependent CO oxidation on reduced TiO₂ (110): A first principles study. J. Chem. Phys. 125 (2006): 144706–144712.
- [138] Wu, X., Selloni, A., and Nayak, S. K. First principles study of CO oxidation on TiO₂ (110): The role of surface oxygen vacancies. J. Chem. Phys. 120 (2004): 4512–4516.
- [139] Yang, Z., Wu, R., Zhang, Q., and Goodman, D. W. First-principles study of the adsorption of CO on TiO₂ (110). Phys. Rev. B 63 (2001): 454191–494196.

- [140] Gong, X. -Q., Selloni, A., Dulub, O., Jacobson, P., and Diebold, U. Small Au and Pt clusters at the anatase TiO₂ (101) surface: behavior at terraces, steps, and surface oxygen vacancies. J. Am. Chem. Soc. 130 (2008): 370–381.
- [141] Scaranto, J., and Giorgianni, S. A DFT study of CO adsorbed on clean and hydroxylated anatase TiO₂ (001) surfaces. Mol. Phys. 107 (2009) 1997–2003.
- [142] Kočí, K., Obalová, L., and Lacný, Z. Photocatalytic reduction of CO₂, chemical papers. Chem. Papers 62 (2008): 1–9.
- [143] Tamaki, Y., Furube, A., Murai, M., Hara, K., Katoh, R., and Tachiya, M. Direct observation of reactive trapped holes in TiO₂ undergoing photocatalytic oxidation of adsorbed alcohols: Evaluation of the reaction rates and yields. J. Am. Chem. Soc. 128 (2006): 416–417.
- [144] Perdew, J. P., Burke, K., and Ernzerhof, M. Generalized gradient approximation made simple. Phys. Rev. Lett. 77 (1996): 3865–386.
- [145] Kresse, G., and Joubert, D. From ultrasoft pseudopotentials to the projector augmented-wave method. Phys. Rev. B 59 (1999): 1758–1775.
- [146] Kresse, G., and Furthmüller, J. Efficient iterative schemes for *ab initio* total-energy calculations using a plane-wave basis set. Phys. Rev. B 54 (1996): 11169–1118.
- [147] Kresse, G., and Hafner, J. *Ab initio* molecular-dynamics simulation of the liquid-metal–amorphous–semiconductor transition in germanium. Phys. Rev. B 49 (1994): 14251–14269.
- [148] Lany, S., and Zunger, A. Assessment of correction methods for the band-gap problem and for finite-size effects in supercell defect calculations: Case studies for ZnO and GaAs. Phys. Rev. B 78 (2008): 235104–235129.
- [149] Mills, G., Jonsson, H., and Schenter, G. K. Reversible work transition state theory: application to dissociative adsorption of hydrogen. Surf. Sci. 324 (1995) 305–337.
- [150] Deák, P., Aradi, B., Frauenheim, Th. Polaronic effects in TiO₂ calculated by the HSE06 hybrid functional: dopant passivation by carrier selftrapping. Phys. Rev. B *Submitted*.
- [151] Morgan, B. J., and Watson, G. W. Polaronic trapping of electrons and holes by native defects in anatase TiO₂. Phys. Rev. B 80 (2009): 233102–233105.

- [152] Lany, S., and Zunger, A. Polaronic hole localization and multiple hole binding of acceptors in oxide wide-gap semiconductors. Phys. Rev. B 80 (2009): 085202–085207.
- [153] Alkauskas, A., Broquist, P., and Pasquarello, A. Defect energy levels in density functional calculations: Alignment and band gap problem. Phys. Rev. Lett. 101 (2008): 046405–046408.
- [154] Henderson, M. A., Epling, W. S., Peden, C. H. F., and Perkins, C. L. Insights into photoexcited electron scavenging processes on TiO₂ obtained from studies of the reaction of O₂ with OH Groups adsorbed at electronic defects on TiO₂ (110). J. Phys. Chem. B 107 (2003): 534–545.
- [155] Tilocca, A., Di valentin, C., and Selloni, A. O₂ interaction and reactivity on a model hydroxylated rutile (110) surface. J. Phys. Chem. B 109 (2005): 20963–20967.
- [156] Oviedo, J., and Sanz, J. F. N₂O Decomposition on TiO₂ (110) from Dynamic First-Principles Calculations. J. Phys. Chem. B 109 (2005): 16223–16226.
- [157] Shultz, A. N., Hetherington III, W. M., Baer, D. R., Wang, L. Q., and Engelhard, M. H. Comparative SHG and XPS studies of interactions between defects and N₂O on rutile TiO₂ (110) surfaces. Surf. Sci. 392 (1997): 1–7.
- [158] Henderson, M. A., Szanyi, J., and Peden, C. H. F. Conversion of N₂O to N₂ on TiO₂ (110). Catal. Today 85 (2003): 251–257.
- [159] Tanaka¹, K. I., and Blyholder, G. Photocatalytic reactions on semiconductor surfaces. I. Decomposition of nitrous oxide on zinc oxide. J. Phy. Chem. 75 (1971): 1037–1043.
- [160] Miller, T. M., Grassian, V. H. Environmental catalysis: Adsorption and decomposition of nitrous oxide on zirconia. J. Am. Chem. Soc. 117 (1995): 10969–10975.
- [161] Lian, J. C., Kieseritzky, E., Gonchar, A., Sterrer, M., Rocker, J., Gao, H. J., et al. N₂O adsorption on the surface of MgO (001) thin films: An infrared and TPD study. J. Phys. Chem. C 114 (2010): 3148–3151.
- [162] Sun, B. Z., Chen, W. K., Wang, X., and Lu, C. –H. A density functional theory study on the adsorption and dissociation of N₂O on Cu₂O (111) surface. App. Surf. Sci. 253 (2007): 7501–7505.

- [163] Solkan, V. N., Zhidomirov, G. M., and Kazansky, V. B. Density functional theory studies of nitrous oxide adsorption and decomposition on Ga-ZSM-5. Int. J. Quan. Chem. 107 (2007): 2417–2425
- [164] Hu, C. L., Chen, Y., Li, J. Q., and Zhang, Y. F. First-principles calculations of N₂O adsorption and decomposition on GaN (0001) surface. Chem. Phys. Lett. 438 (2007): 213–217.
- [165] Kubo, T., Ema, T., Atli, A., Aruga, T., Takagi, N., and Nishijima, M. Adsorption and thermal decomposition of N₂O on Si (100): Electron energy loss spectroscopy and thermal desorption studies. Surf. Sci. 382 (1997): 214–220.
- [166] Kokalj, A., Kobal, I., Horino, H., Ohno, Y., and Matsushima, T. Orientation of N₂O molecule on Pd (110) surface. Surf. Sci. 506, (2002): 196–202.
- [167] Matsushima, T., and Kokalj, A. Angular distributions of desorbing N₂ in thermal N₂O decomposition on Rh (100). Surf. Sci. 601 (2007): 3996–4000.
- [168] Manzhos, S., Yamashita, K. A model for the dissociative adsorption of N₂O on Cu (100) using a continuous potential energy surface. Surf. Sci. 604 (2010): 555–561.
- [169] Orita, H., and Itoh, N. Adsorption of N₂ and N₂O on Ni (755) surface: *Ab Initio* periodic density functional study. Surf. Sci. 550 (2004): 166–176.
- [170] Paul, J. F., Pérez-Ramírez, J., Ample, F., and Ricart, J. M. Theoretical studies of N₂O adsorption and reactivity to N₂ and NO on Rh(111). J. Phys. Chem. B 108 (2004): 17921–17927.
- [171] Kudo, A., and Nagayoshi, H. Photocatalytic reduction of N₂O. Catal. Lett. 52 (1998): 109–111.
- [172] Zhdanov, V. P., Ma, Y., and Matsushima, T. Analysis of the kinetics of N₂O–CO reaction on Pd (110). Surf. Sci. 583 (2005): 36–45.
- [173] Zhdanov, V. P., Nakagoe, O., and Matsushima, T. Kinetics of the N₂O–CO reaction on Rh (110). Surf. Sci. 601 (2007): L49–L54.
- [174] Gluhoi, A. C., Dekkers, M. A. P., and Nieuwenhuys, B. E. Comparative studies of the N₂O/H₂, N₂O/CO, H₂/O₂ and CO/O₂ reactions on supported gold catalysts: effect of the addition of various oxides. J. Catal. 219 (2003): 197–205.

- [175] Car, R., and Parrinello, M. Unified approach for molecular dynamics and density–functional theory. Phys. Rev. Lett. 55 (1985): 2471–2474.
- [176] Blochl, P. E. Projector augmented–wave method. Phys. Rev. B 50 (1994): 17953–17979.
- [177] Liang, H., Zhang, Y., and Liu, Y. Three–dimensionally ordered macro–porous Pt/TiO₂ catalyst used for water–gas shift reaction. J. Nat. Gas Chem. 17 (2008): 403–408.
- [178] Steinrück, H. –P, Pesty, F., Zhang, L., and Madey, T. E. Ultrathin Film of Pt on TiO₂ (110): Grows and chemisorptions–induces surfactant effects. Phys. Rev. B 51 (1995): 2427–2439.
- [179] Han, Y., Liu, C. –J, and Ge, Q. Interaction of Pt clusters with the anatase TiO₂ (101) surface: A first principles study. J. Phys. Chem. B 110 (2006): 7463–7472.
- [180] Einaga, H., Ogata, A., Futamura, S., and Ibusuki, T. The stabilization of active oxygen species by Pt supported on TiO₂. Chem. Phys. Lett. 338 (2001): 303–307.
- [181] Peng, S. –F., and Ho, J. –J. The adsorption and dissociation of H₂O on TiO₂ (110) and M/TiO₂ (110) (M = Pt, Au) surfaces: A computational investigation. Inter. J. Hydro. Energy 35 (2010): 1530–1536.
- [182] Kresse, G., Furthmüller, J. Efficiency of *ab initio* total energy calculations for metals and semiconductors using a plane–wave basis set. Comput. Mater. Sci. 6 (1996): 15–50.
- [183] Kresse, G., and Hafner, J. *Ab initio* molecular dynamics for liquid metals. Phys. Rev. B 47 (1993): 558–561.
- [184] Schierbaum, K. D., Fischer, S., Torquemada, M. C., de Segovia, J. L., Romám, E., and Martín–Gago, J. A. The interaction of Pt with TiO₂ (110) surfaces: A comparative XPS, UPS, ISS, and ESD study. Surf. Sci. 345 (1996): 261–273.
- [185] Vittadini, A., and Selloni, A. Small gold clusters on stoichiometric and defected TiO₂ anatase (101) and their interaction with CO: A density functional study. J. Chem. Phys. 117 (2002): 353–364.
- [186] Benvenuti, E. V., Franken, L., and Moro, C. C. FTIR study of hydrogen and carbon monoxide adsorption on Pt/TiO₂, Pt/ZrO₂, and Pt/Al₂O₃. Langmuir 15 (1999): 8140–8146.

- [187] Rittner, F., Boddenberg, B., Fink, R. F., and Staemmler, V. Adsorption of nitrogen on rutile (110). 2. Construction of a full five-dimensional potential energy surface. Langmuir 15 (1999): 1449–1455.
- [188] Thompson, T. L., Diwald, O., and Yates, J. T., Jr. CO₂ as a probe for monitoring the surface defects on TiO₂ (110) temperature-programmed desorption. J. Phys. Chem. B 107 (2003): 11700–11704.

APPENDIX

UNIT CONVERSION FACTORS

1 unit =	Hartree	kJ mol^{-1}	kcal mol^{-1}	eV
Hartree	1	2.6255×10^3	6.2751×10^2	2.7212×10
kJ mol^{-1}	3.8088×10^{-4}	1	2.3901×10^{-1}	1.0364×10^{-2}
kcal mol^{-1}	1.5936×10^{-3}	0.4184×10	1	4.3363×10^{-2}
eV	3.6749×10^{-2}	9.6485×10	2.3061×10	1

VITAE

PERSONAL DATA

Name	Raina Wanbayor
Nationality	Thai
Date of Birth	17 June 1979
Religion	Muslim
E-mail	wanbayor_r@hotmail.com

EDUCATION

1999–2002	B.Sc. in Chemistry, Department of Chemistry, Faculty of Science, Rajamangala University, Pathumthani, Thailand.
2005– 2007	M.Sc. in chemistry, Department of Chemistry, Faculty of Science, Chulalongkorn University, Bangkok, Thailand.
2007–2010	Ph.D. in chemistry, Department of Chemistry, Faculty of Science, Chulalongkorn University, Bangkok, Thailand.

PUBLICATIONS IN THIS DESSERTATION

- [1] Wanbayor, R., and Ruangpornvisuti, V. Adsorption of di-, tri- and polyatomic gases on the anatase TiO₂ (001) and (101) surfaces and their adsorption abilities. *J. Mol. Struct. (theochem)* 952 (2010): 103–108.
- [2] Wanbayor, R., and Ruangpornvisuti, V. Adsorption of CO, H₂, N₂O, NH₃ and CH₄ on the anatase TiO₂ (001) and (101) surfaces and their competitive adsorption predicted by periodic DFT calculations. *Mat. Chem. Phys.* 124 (2010): 720–725.
- [3] Wanbayor, R., Deák, P., Frauenheim, T., and Ruangpornvisuti, V. First-principles theoretical study of the hole-assisted conversion of CO to CO₂ on the anatase TiO₂ (101) surface. *J. Chem. Phys.* 134 (2011): 104701–104706.
- [4] Wanbayor, R., and Ruangpornvisuti, V. Periodic density–functional theory study of CO, H₂, N₂O, H₂O, NH₃ and CH₄ adsorbed on the rutile TiO₂ (001) and (110) surfaces. *Submitted*.